SELENOLOGY TODAY

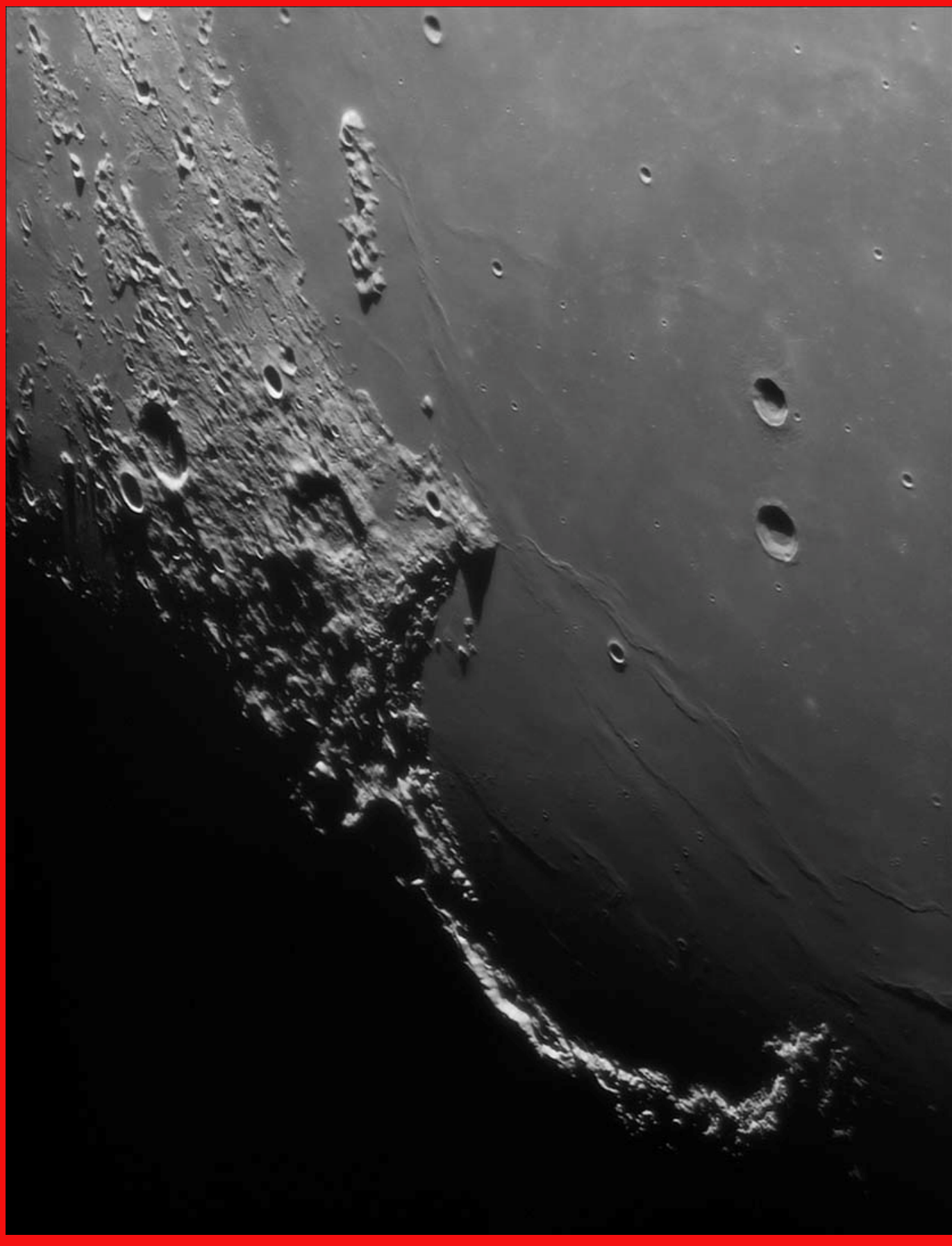

SELENOLOGY TODAY # 16
October 2009

http://www.glrgroup.eu/old/

Selenology Today is devoted to the publication of contributions in the field of lunar studies.

Manuscripts reporting the results of new research concerning the astronomy, geology, physics, chemistry and other scientific aspects of Earth's Moon are welcome.

Selenology Today publishes papers devoted exclusively to the Moon.

Reviews, historical papers and manuscripts describing observing or spacecraft instrumentation are considered.

The Selenology Today

Editorial Office

selenology_today@christian-woehler.de

Cover

Stefan Lammel

SELENOLOGY TODAY #16
October 2009

GLR group
http://www.glrgroup.eu/old/

Selenology Today website
http://digilander.libero.it/glrgroup/

Three unusual flashes: detection of the military US satellite USA 142

By Stefano Sposetti, Gnosca Observatory, Switzerland
http://web.ticino.com/sposetti/

Abstract
What was first supposed to be a lunar meteor impact during our earthlit-lunar-surface monitoring of 2009 April 30th, later revealed as a slow moving satellite. An interesting analysis for future candidate impacts.

Observational equipment

I became interested in lunar impact monitoring about 4 years ago when I heard about this NASA observing project and their need of (also amateur) observers. Last year I decided to buy the necessary hardware to equip my 8-inch Schmidt-Cassegrain telescope. I contacted a friend of mine, Marco Iten, to help in this project. He lives 13km away from me. We shared the initial difficulties of hardware and software choice.

We live in the southern part of Switzerland. From a meteorological point of view this region offer clearer nights than the regions placed in the northern part of the nation. But, because of the nature of the alpine territory, my observatory suffer from a high western horizon.

Both observatories own a small size telescope, equatorial mounted and equipped for auto guiding.

Both instruments have a focal length of about 600mm and are equipped with Watec 902H ultimate ½ inch videocameras. The field of view is wide enough to image the Moonhalf. Precise time is assured with KIWI-OSD II RTG time inserters coupled with KIWI-GPS Garmin 18LVC. The avi-movies are stored directly into HD thru Virtualdub. We use also the software Nudger for autoguiding on Moon's bright features. At the end of the software chain we use Lunarscan for detecting possible impacts

The April 30th unusual flashes

During the monitoring of the earthlit Moon surface in the evening of April 30th, Marco Iten and me detected a first unusual flash. Both avi files showed up an evident simultaneous flash of light (less than a second) located on the moon surface (Fig.1 and 2). We thought we had captured our first meteor impact. But the two simultaneous flashes weren't located at the same moon's feature.

We checked the frames further. A second flash of light, stronger that the precedent, was detected outside the Moon disk some 23s after the first. This one behaved as a typical meteor, lasted about one second, and left a very small trail, probably because of a nearly head-on hit. The direction of this suspected meteor seemed to come from the location of the first flash. An unusual behaviour, indeed. Also this second flash of light was not detected in the same sky position from the two locations. Because the two observatories are located about 13km apart, the tiny displacement of the two flashes was surely caused by the (small) parallax angle (Fig. 3).

But it's not finished. What was more unusual is that a third flash of light, fainter than the two preceding ones, about

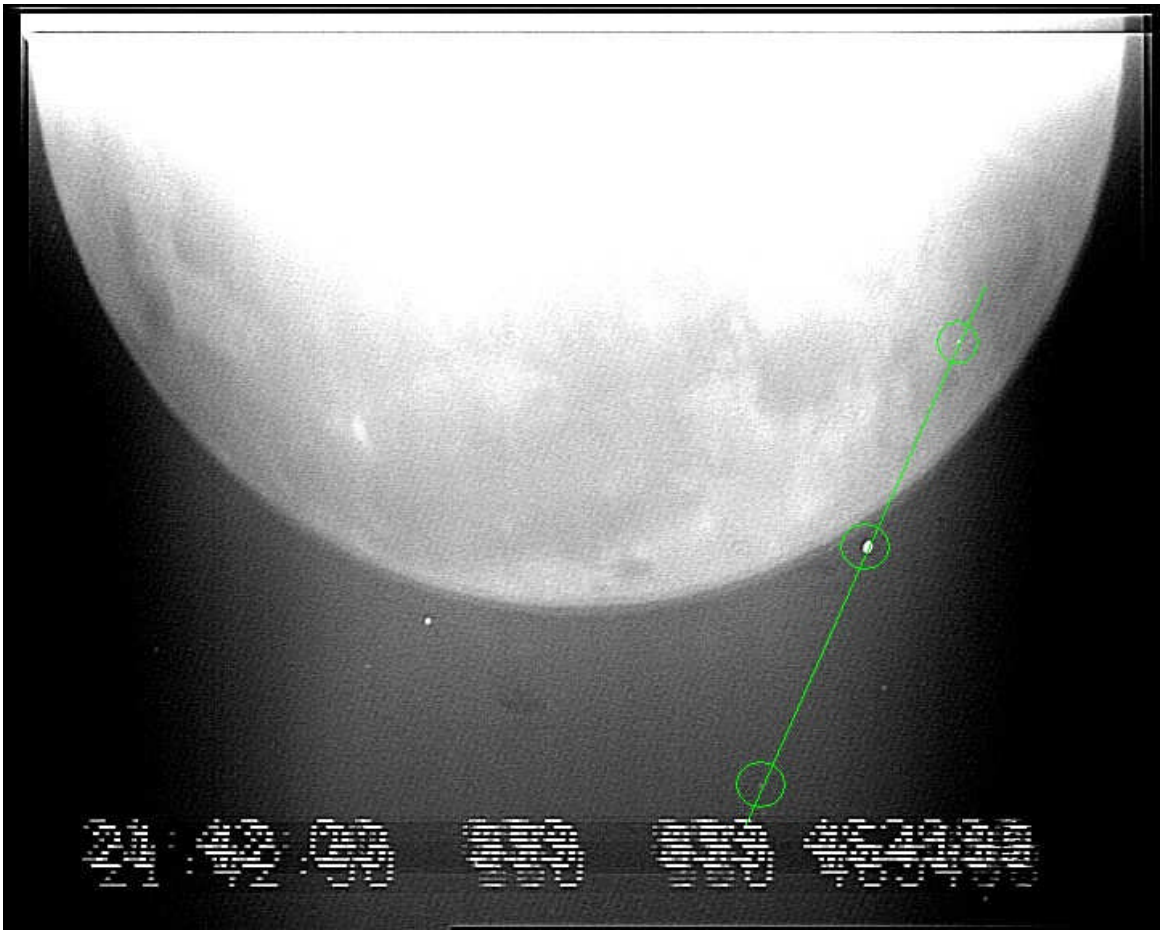

Figure 1. The superposition of the three events, registered on the background stars, as seen from the observatory of Marco Iten.

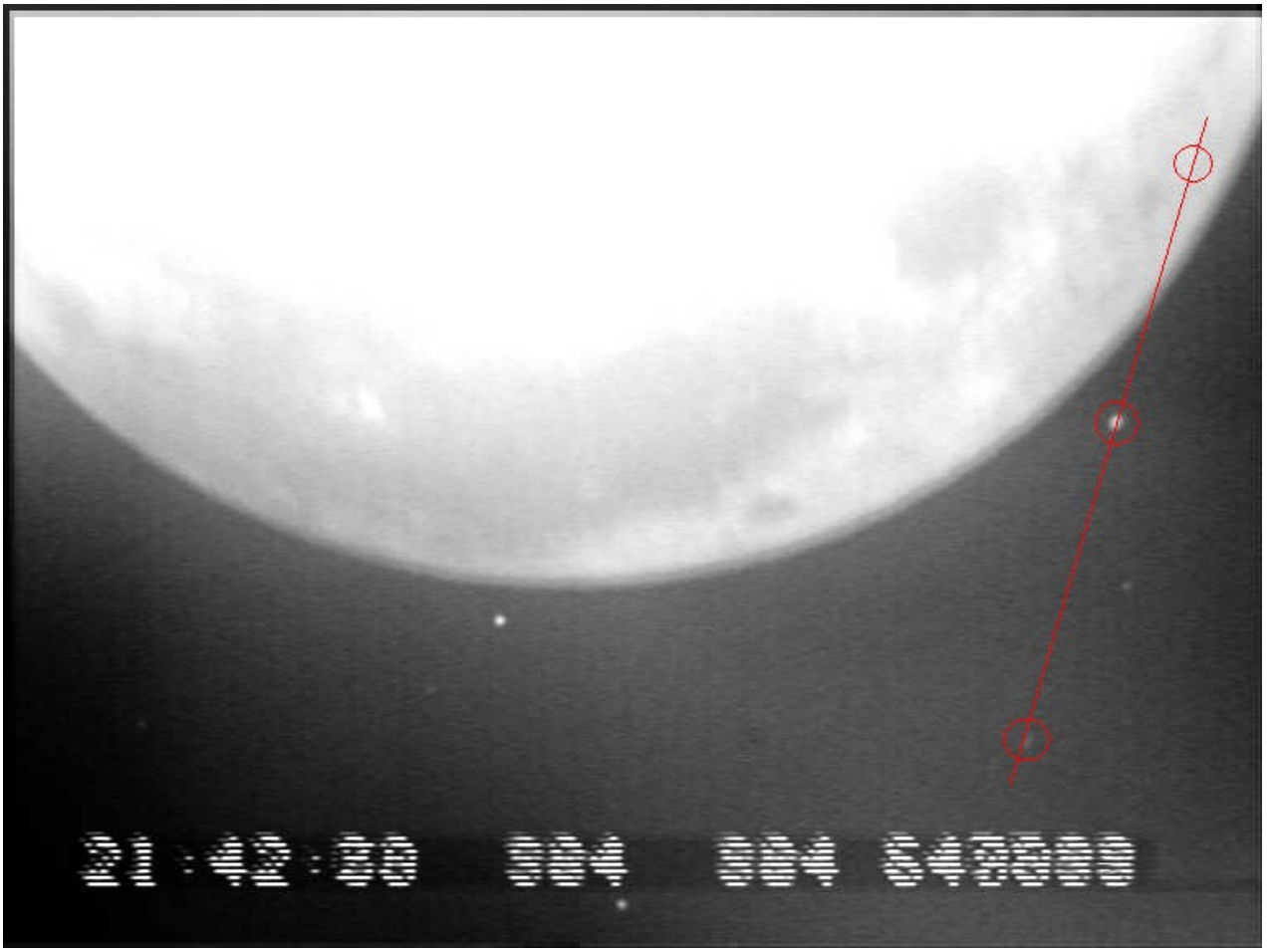

Figure 2. The superposition of the three events, registered on the background stars, as seen from the observatory of Stefano Sposetti.

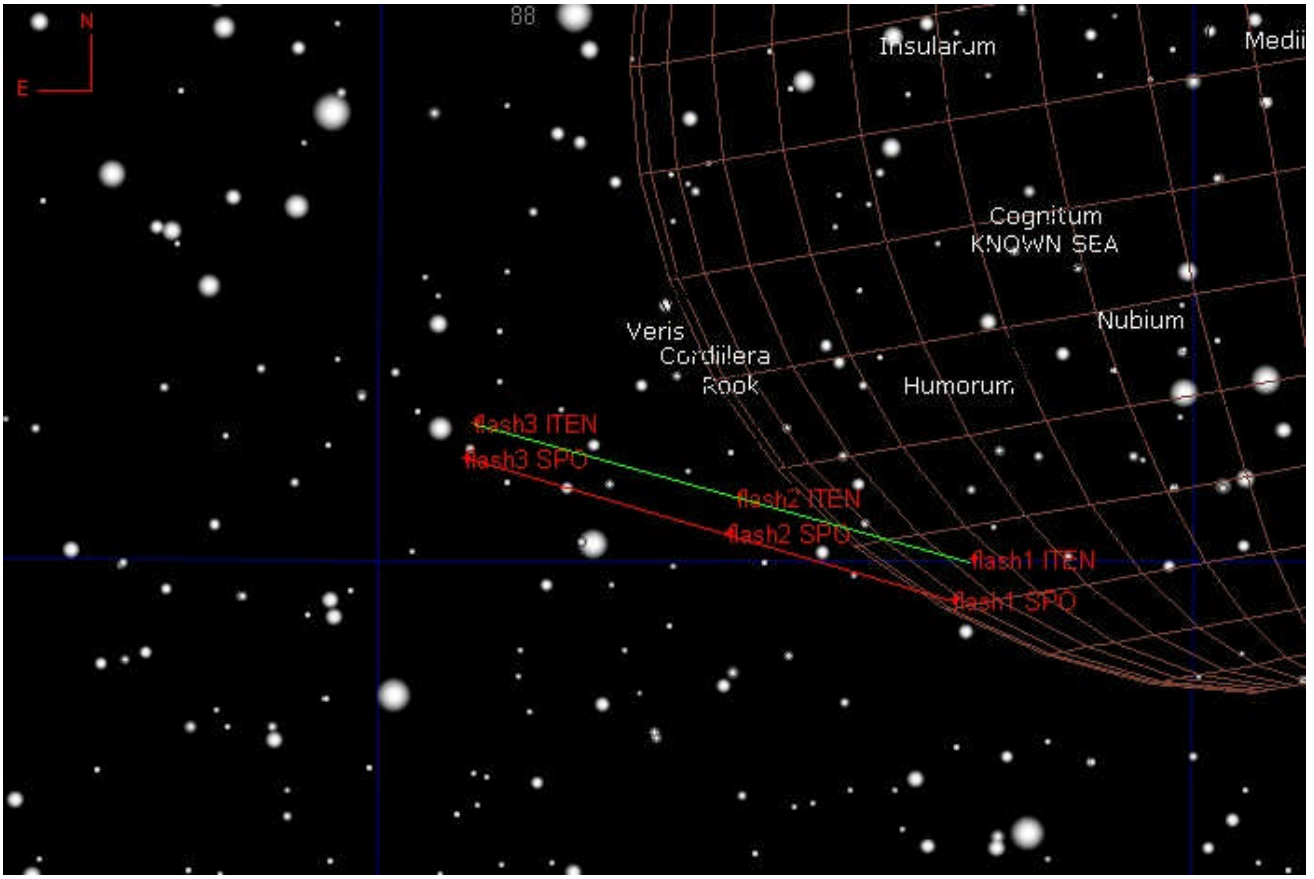

Figure 3. The three events and their parallax from the two observatories.

27s after the second, was detected simultaneously on the two movies. All the three flashes were placed on a straight line. The angular distance of them was almost exactly proportional to their time interval. What was first suspected an earth meteor, was now a very unusual phenomenon. Three meteors hitting our atmosphere almost head-on with the same direction? Suspicious. We analysed further our frames and calculated the parallax. The resulted angle was about 1.0arcmin for all the three flashes. Hence, they happened to locate between 30'000 and 40'000km, the height of a typical distant satellite.

Arnold Barmettler, from Calsky, identified the object as the military US satellite USA 142 / (DSP 19) launched on 09. Apr. 1999. At the time of the observation it was at an altitude of 28'900km.

Conclusion

What was firstly identified as a possible impact on the moon disk, was secondly looked out as a typical head-on meteor hitting our atmosphere and finally recognised as a US military satellite. In our past observational runs, the movies showed up frequent satellite passes. They were normally fast and evident. The April 30th flashes were intriguing and misleading because they were slow.

A Shape-from-Shading Refined method for Lunar Domes Heights derived from Carlotto Algorithm: application of an empirical formula

by Raffaello Lena

Geological Lunar Research (GLR) Group

Abstract

A new approach for recovering a 3D shape of a lunar dome, using a preceding algorithm described by Evans (2006), is proposed. The DEM obtained from the Carlotto method is corrected with an empirical formula. The Algorithm described in this article is tested for lunar dome images and compared with the results obtained with the full lunar-Lambert method and Carlotto algorithm. The proposed new method is found to perform accurate and efficient results.

1.Introduction

Digital elevation maps (DEMs) are an important information source for many applications in planetary and lunar sciences, such as the description of local and regional topographic features, slopes and height of lunar domes. For solving the DEM reconstruction problem by shape from shading (SFS) a variety of algorithms have been described in literature. Information about the theory of the application of SFS can be found in, e.g, Horn (1989), Hapke (1993).

SFS is based on the fact that surfaces patches, having different inclination relative to a light source, are imaged with different brightness. SFS uses these variations in the grey values of digital image to reconstruct the topography of the observed surface.

Many SFS assume that the albedo of a surface is constant, becausebased on a single image it is not possible to distinguish between albedo and topographic variations causing grey value changes in the image.
The Lambert law is one of the simplest reflectance models. It assumes perfectly diffuse scattering, implying an intensity R_L of scattered light according to:

$$RL(\rho, \theta i) = \rho \cos \theta i \qquad (1)$$

with ρ as the surface albedo and θi as the angle between the surface normal and the direction of incident light. But the Lambert model does not correspond very well to the true scattering behaviour of the lunar surface.

n many astrogeologic applications the simple empirical lunar-Lambert law is used:

$$R_{LL}(\rho, \theta_i, \theta_e, \alpha) = \rho\,[2\,L(\alpha)\cos\theta_i / (\cos\theta_i + \cos\theta_e) + (1 - L(\alpha))\cos\theta_i] \qquad (2)$$

with θ_e as the angle between the surface normal and the viewing direction and the lunar-Lambert parameter $L(\alpha)$ as an empirical value depending on the phase angle α. This model is a weighted sum of the Lommel-Seeliger (the first term in the sum) and the Lambert reflectance (the second term in the sum), which is proportional to $\cos\theta_i$ and describes perfectly diffuse scattering.

McEwen (1991) tabulates the phase angle dependent weight parameter $L(\alpha)$ over the complete range of phase angles between 0° and 180° by fitting Eq. (2) to the Hapke model (cf. Fig.1).

Evans (2006) developed a technique that made practical use of Carlotto algorithm, and it was later refined by Fisher (2007). This method makes use of separate software including Microsoft Excel (Evans, 2006; Fisher, 2007). Surfaces with perfectly matte properties typically reflect incident light according to Lambert's cosine law which states that the intensity of reflected or transmitted light on such a surface will vary as the cosine of the angle between the direction of illumination and the vector normal to (i.e. perpendicular to) the surface. For the moon, therefore, intensity varies with the cosine of the zenith angle of the sun, which is given by subtracting the local solar elevation from 90°. In the Carlotto method, SFS computation is reduced to a minimum by using astrophotography software to rotate a lunar dome such that the apparent solar azimuth incidence is 270º (Carlotto 1996).
Evans recommends that the method only be used for features between 30º lunar latitude and longitude. In fact the lunar-Lambert model behaves very similar to the simple Lambert model near the centre of the lunar disk but strongly deviates from the Lambert model near the limb.

Hence, lunar reflectance can be approximated by Lambert's law when:
1) the lunar surface under study is within the area bounded approximately by the 30° longitude and latitude lines (not too close to the lunar limb);
2) solar lighting of the lunar surface is oblique (solar elevation should not exceed 20°-30°);
3) reflectance properties are uniform across the surface (the surface should not vary excessively in albedo).
In contrast, under oblique view and illumination angles and/or low phase angles the reflectance behaviour of the lunar surface largely obeys the Lommel-Seeliger law, i. e. the dependence of the surface reflectance on the incidence angle: as a consequence, the heights of some domes obtained assuming the method based on Carlotto algorithm are too low compared to the values derived with the lunar-Lambert reflectance law (cf. section 3). The height of lunar domes reported in the Consolidated Lunar Dome Catalogue *CLDC* (Lena and Wöhler, 2008) were derived by a combined photoclinometry

and shape from shading analysis based on the full lunar-Lambert law (cf. Horn, 1989; Wöhler et al, 2006; Lena et al., 2006, and references therein). The Consolidated Lunar Dome Catalogue contains all lunar domes which have been studied in detail by the GLR group and for which reasonably accurate morphometric properties could be determined.

This paper includes an analysis of the effect of increasing angular distance from the centre of the moon and the effect of phase angles on dome height measurements obtained by the Carlotto algorithm.

A new algorithm, based on empirical formula, is introduced. Finally the article compares the accuracy and the convergence of the new technique to previous use of Carlotto algorithm (Evans, 2006).

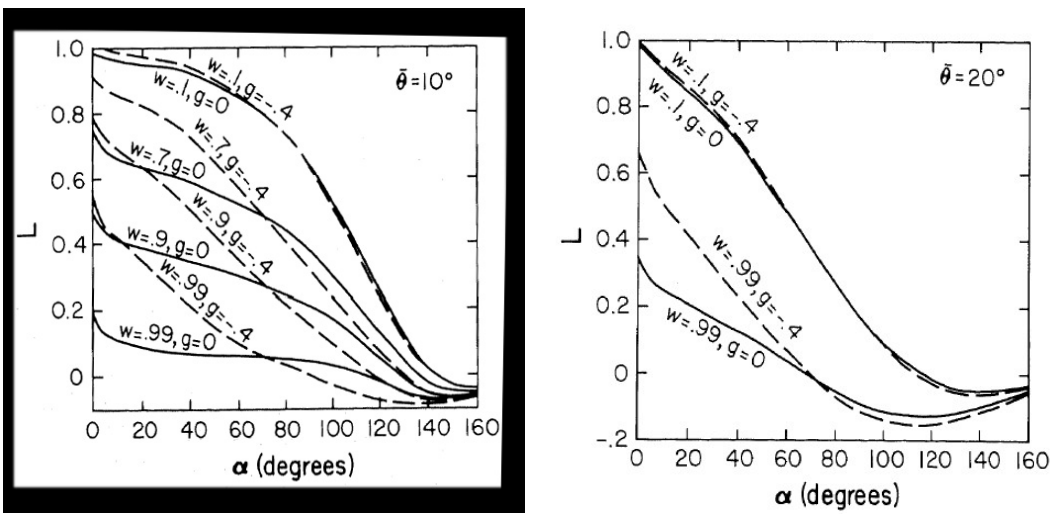

Figure 1 by McEwen (1991). The curve relevant for the Moon is the uppermost one with w = 0.1 (w denoted the so-called single-scattering albedo in the Hapke reflectance model). The curve depends on the macroscopic roughness theta-bar of the surface (to the left theta-bar of 10°, to the right theta-bar of 20°). Reprinted from Icarus, August 1991, Vol 92 (2), McEwen, A. S., Photometric functions for photoclinometry and other applications, with permission from Elsevier.

2.Method

The image scale, the selenographic coordinates and the solar altitude for each examined dome was computed using the LTVT software package by Mosher and Bondo (2006) which requires a calibration of the images by identifying the precise selenographic coordinates of some landmarks on the image. This calibration was performed based on the UCLN 1994 list of control points. For the evaluation of the results I derived values for the offset of the analyzed images so that the average grey level for the shadows is

zero. The "shadow offset" is definitely a critical point for all photoclinometric approaches, independent of the specific reflectance model used, and must always be taken into account carefully. Usual telescopic optics often produce some scattered light, which becomes especially important when regarding objects near the terminator, where the surface brightness is low. The images, transformed in rectified view, were then processed using the math and image calculator features under the Process menu of Image J: thus the corresponding "shadow offset" was subtracted. The resulting images were saved as image txt format and then imported into Excel. According to Evans (2006) and Fisher (2007) a DEM was obtained taking into account the effect of the lunar curvature, which was then subtracted using Image J math option.

The procedure described above was automated.

3.Height analysis

For solving the DEM reconstruction problem by SFS, the image process for domes close to the limb and/or imaged under low phase angle, has to be corrected when regarding the computation obtained with Carlotto method. Hence, the heights of several domes computed with the full lunar–Lambert law are compared with the heights obtained, for the same image data, with the Carlotto algorithm used by Evans (2006). Consequently the correction factor C_f is computed for each examined dome (Fig.2, and Table 1).

$$C_f = (H_{lunarLambert}) / (H_{Carlotto}) \quad (3)$$

Refers to the *CLDC* for the images and label of the domes according to the scheme used in the articles published by the GLR group (Lena and Wöhler, 2008 and references therein).

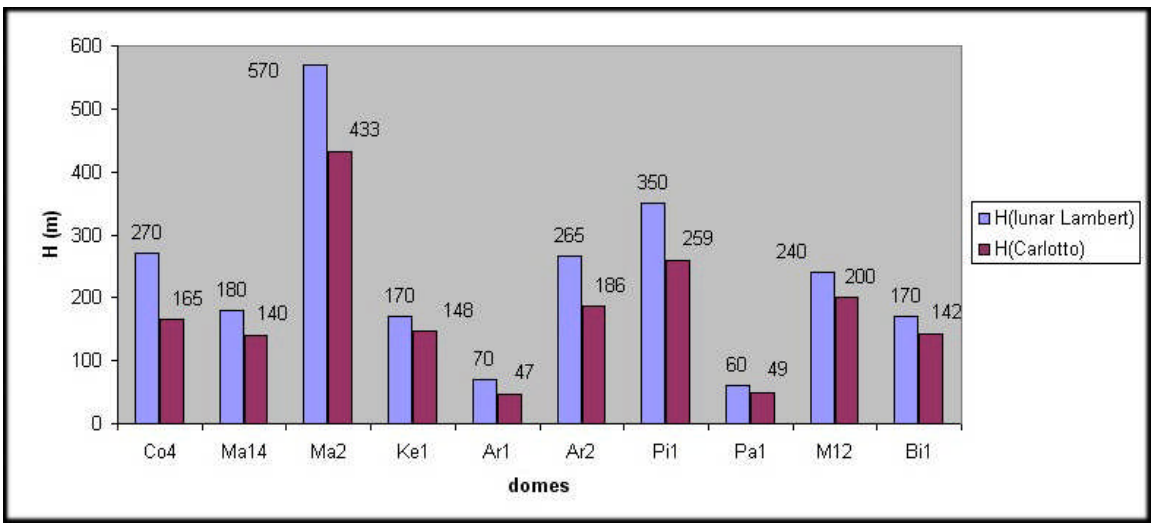

Figure 2. The dome heights derived from the full lunar Lambert law (blue bars) and Carlotto algorithm (red bars).

Dome	Longitude [°]	Latitude [°]	H (lunarLambert)	H (Carlotto)	Cf	name
Co4	70.93	6.67	270	165	1.6363	Condorcet 4
Ma14	-53.73	11.02	180	140	1.2857	Marius 14
Ma2	-55.26	10.32	570	433	1.3164	Marius 2
Ke1	-39.53	8.88	170	148	1.1486	Kepler 1
Ar1	0.71	55.71	70	47	1.4894	Archytas 1
Ar2	-2.71	56.52	265	186	1.4247	Archytas 2
Pi1	28.56	-27.46	350	259	1.3513	Piccolomini 1
Pa1	-47.88	-26.63	60	49	1.2245	Palmieri 1
M12	-31.2	10.08	240	200	1.2000	Milichius 12
Bi1	-9.66	-20.73	170	142	1.1972	Birt 1

Table 1. The heights (in meters) derived from the full lunar Lambert law and Carlotto algorithm with the corresponding C_f and labels for the examined domes. The contribution of the lunar curvature is taken into account and it was subtracted.

Figure 2, and Table 1, show that some domes such as Co4, Ar1 and Ar2, with high values of the correction factor C_f, are associated with higher deviation ($\geq$ 20 %) of the computed heights using the simple Carlotto method. The deviation is related to combined effects of two variables: the distance from the lunar centre and the phase angle, as shown in Figs. 3 and 4.

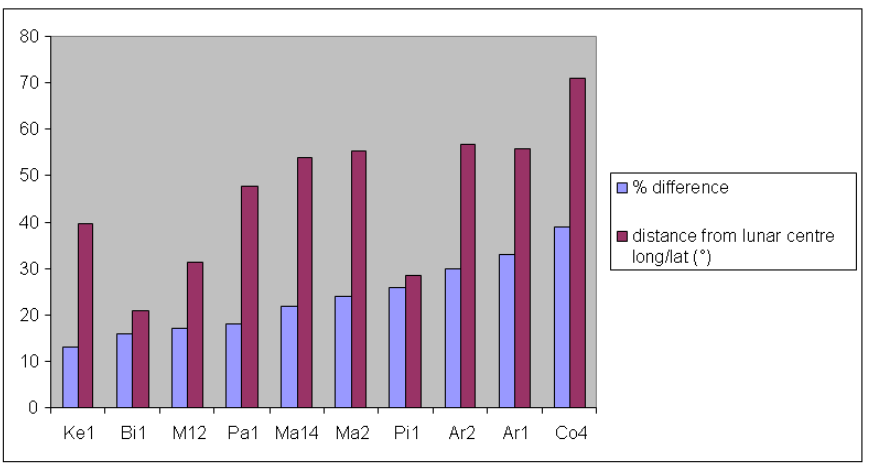

Figure 3.The diagram shows the % difference (blue bars) of the heights derived from the full lunar Lambert law and Carlotto algorithm, along with the corresponding distance from lunar centre as longitude-latitude (red bars). The diagram in Fig.5 shows the angular distance Δ.

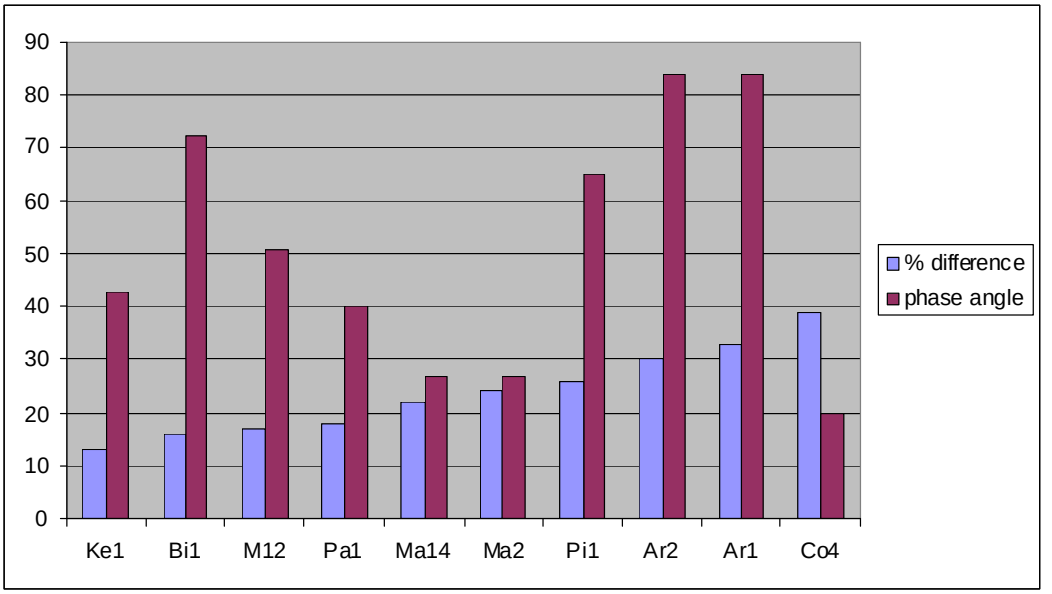

Figure 4.The diagram shows the % difference (blue bars) of the heights derived from the full lunar- Lambert law and Carlotto algorithm, along with the different phase angle when the images were taken (red bars).

Some conclusions can be drawn.

a) Phase angle: the difference between the Carlotto algorithm and the full lunar-Lambert law is evident especially for high values of L(α), i. e. low phase angles (cf. Fig.1). For high phase angles, L(α) obtains near-zero values, which means that the reflectance function becomes purely Lambertian. The parameter L(α) is known as the limb darkening parameter and controls the influence of the Lambert term relative to the Lommel-Seeliger term. Furthermore L(α) influences the contrast of shading on topographic slopes and, to a lesser extent, the direction relative to the sun and the observers, in which slopes have the maximum contrast (Lohse et al., 2006). Values of L (α) may be interpolated from the curve shown in Fig.1 (McEwen, 1991). The L(α) curve depends on the macroscopic roughness theta-bar of the surface.

Note that for theta-bar = 20°, L(α) is significantly lower (cf. Fig.1). For the Moon we have values between about 10° (mostly) and 15°. The correct value of theta-bar is very difficult to determine since it requires accurate absolute photometry at high phase angles larger than 140° or 150°, which is just difficult from the practical point of view. Furthermore, it is terrain-dependent. Whatever, if one assumes an inaccuracy of theta-bar of ± 0.1°, the influence of this error on the dome height is only a few percent for the full Lunar-Lambert method.

b) Distance from the lunar centre: the difference between the Carlotto algorithm and the full lunar- Lambert law is also related to the longitude and latitude of a lunar dome (cf. Fig. 3), which means that the reflectance function is also depending from an angular distance Δ.

The cosine law of spherical trigonometry yields:

$$\cos(\Delta) = \cos(\text{long})\cos(\text{lat}) \qquad (4)$$

This is exactly true for zero libration; including non zero libration, equation (4) is to be considered as a good approximation.

The diagrams (Figs. 3 and 4) show a weak dependence of the correction factor on L(α) (which is not surprising, since for the high regarded phase angles, L(α) only covers the range between about 0.7 and 0.95) but a strong correlation with the distance Δ from the centre of the lunar disk (cf. Fig.5).

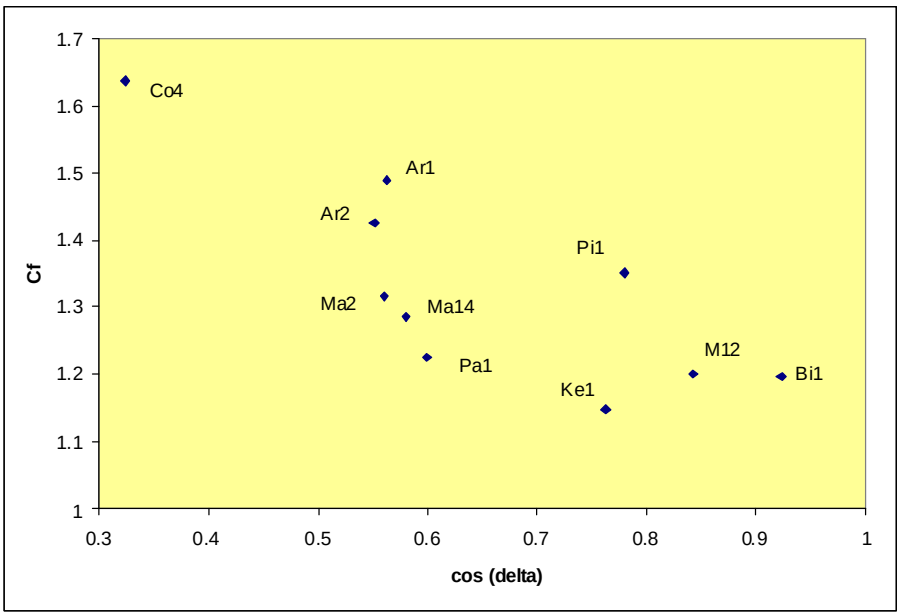

Figure 5. The diagram displays the correlation between the angular distance and the correction factor $C_f = (H_{lunarLambert}) / (H_{Carlotto})$

4.Empirical formula for height correction

In a refinement stage, the estimates obtained using the Carlotto algorithm are optimized, minimizing the differences, by using a correction factor F :

$$F = [2^* (1/1+\cos(\Delta)) + \lambda] \qquad (5)$$

The second summand in equation (5) will provide the best fit to the available dome heights. The value of λ then has to be adjusted until the corrected values correspond to the solutions of the full lunar-Lambert law.

The diagram of Fig.6 shows the variation of the term λ versus L(α), for some empirical equations. For L(α) ≤0.6, λ is set at zero, thus there is only a correction by the first summand in equation (5), becoming 1 for Δ=0.

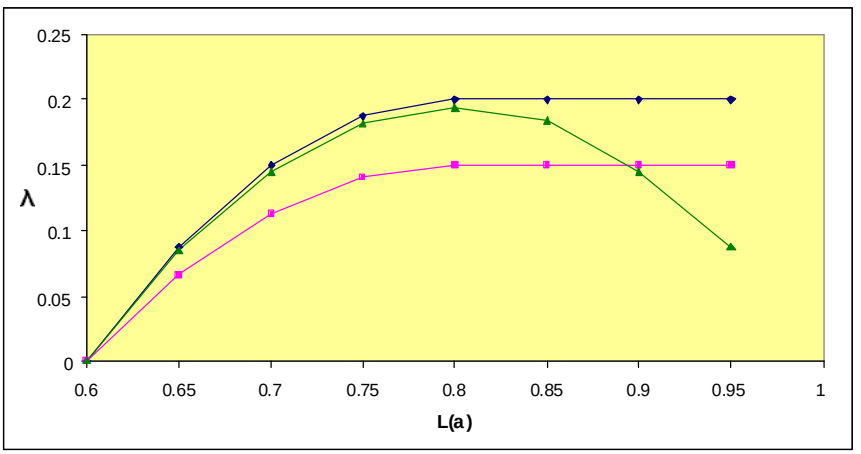

Figure 6. The variation of λ versus L(α), for several empirical equations.

The heights derived from Carlotto algorithm are then multiplied for the correction factor F yielding

$$H_{corrected} = (H_{Carlotto}) * [2* (1/(1+\cos(long)*\cos(lat)) + \lambda] \qquad (6)$$

Fig.7 shows the heights derived from the application of the full lunar-Lambert method, and the values computed from three different empirical equations.

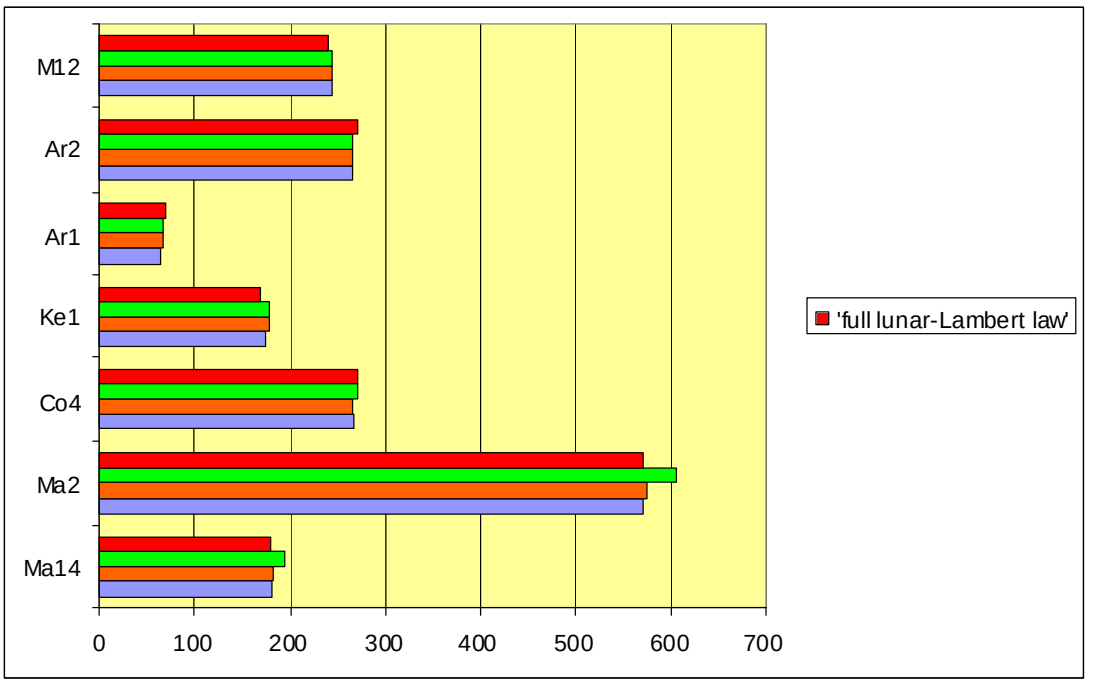

Figure 7. The dome heights derived from the full lunar Lambert model (red bars) and the use of the empirical formula for different correction factor (λ_1 green bars, λ_2 orange bars and λ_3 blue bars).

Equation 6 is solved for :

- λ_1 (green bars in Fig.7) where

$\lambda_1 = 0$ if $L(\alpha) < 0.60$; $\lambda_1 = [1 - L(\alpha)]\,[(L(\alpha) - 0.6)/0.2]$ if $0.60 < L(\alpha) \leq 0.80$ and

$\lambda_1 = 0.2$ (0.75) if $L(\alpha) > 0.80$

- λ_2 (orange bars in Fig.7) where

$\lambda_1 = 0$ if $L(\alpha) < 0.60$; $\lambda_1 = [1 - L(\alpha)]\,[(L(\alpha) - 0.6)/0.2]$ if $L(\alpha) > 0.60$

- λ_3 (blue bars in Fig.7) where

$\lambda_1 = 0$ if $L(\alpha) < 0.60$; $\lambda_1 = [1 - L(\alpha)]\,[(L(\alpha) - 0.6)/0.2]$ (0.97) if $L(\alpha) > 0.60$

For two domes (Ma14, Ma2) the solution of the method with the terms λ_2 and λ_3 is clearly better, while for Co4 dome the method with the term λ_1 is better, according to the full lunar Lambert function.

However all deviations are lower than 6%, and the full lunar-Lambert has error of as much as 10%, which is of the same order as the derived deviations. Moreover the best fit using the terms λ_2 and λ_3 for some domes is justified because the phase angle is very low for $L(\alpha) > 0.8$ and the object is thus very far from the centre of the lunar disk: the first summand in equation (5) depending on cos (Δ) lead to an overcompensation which has to be de-compensated by a decreasing second summand for L(alpha)>0.8.

In order to prove the efficiency and accuracy of this approach, the values $H_{Carlotto}$, reported in Table 1, are corrected with the application of the empirical formula (equation 6). The resulting heights $H_{corrected}$ may be compared with the heights derived from full lunar-Lambert model (Table 2, and derived heights obtained with the term λ_3).

Dome	H (Carlotto)	H (correction formula)	H (lunarLambert)
Co4	165	271	270
Ma14	140	181	180
Ma2	433	573	570
Ke1	148	175	170
Ar1	47	67	70
Ar2	186	267	265
Pi1	259	350	350
Pa1	49	65	60
M12	200	245	240
Bi1	142	170	170

Table 2. The heights (in meters) derived from the Carlotto algorithm, the empirical formula with the term λ_3 and the full lunar- Lambert model for the examined domes. The contribution of the lunar curvature is taken into account and it was subtracted.

Consequently the conversion factor P_c is derived for each dome

$$P_c = (H_{correction\ formula} / H_{Carlotto}) \qquad (7)$$

Fig. 8 illustrates the relation between the conversion factor P_c and the correction factor C_f based on Eqs. (7) and (3). Fitting power laws to the data points representing the factors P_c and C_f yields:

$$P_c = 1.0479\, C_f - 0.0612 \quad (R^2 = 0.9915) \qquad (8)$$

with R^2 as the squared correlation coefficient in the respective diagram.

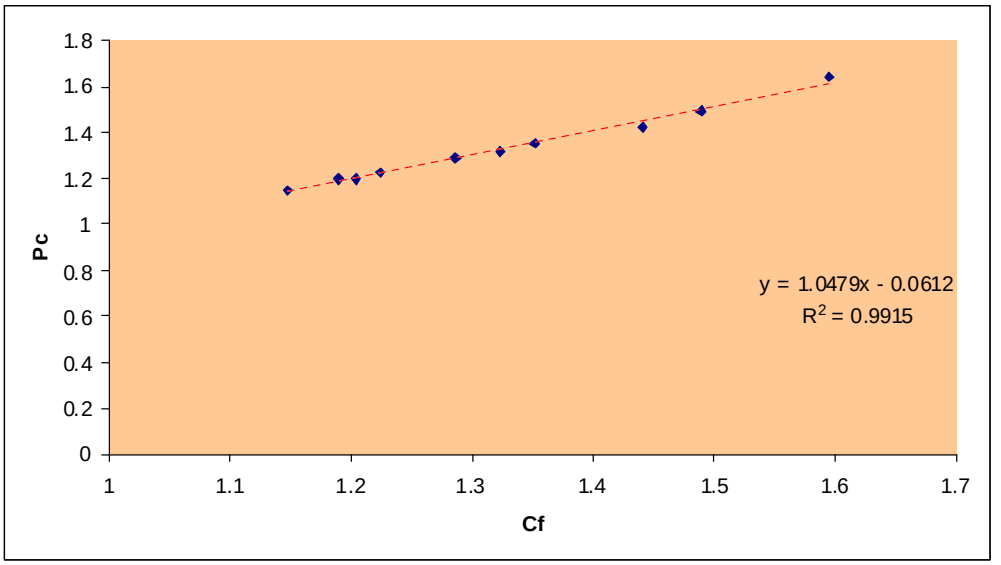

Figure 8. The squared correlation coefficient in the diagram showing the fit between the factor P_c =($H_{correction\ formula}$)/($H_{Carlotto}$) and C_f= ($H_{lunarLambert}$)/ ($H_{Carlotto}$)

The results of surface reconstruction, shown in Table 2, demonstrate the applicability of the empirical formula.

5.Generating a DEM Image from empirical formula (Co4 dome)

In Fig.9 it is shown the effect of the angular distance for Condorcet 4, a lunar dome distant from the lunar centre (longitude 70.93° and latitude 6.67°). The computed height of the Co4, initially calculated with the Carlotto method (Table 1), increases with the increased distance in longitude, and thus with the angular distance Δ. The computation is obtained with the empirical algorithm described in equation (6).

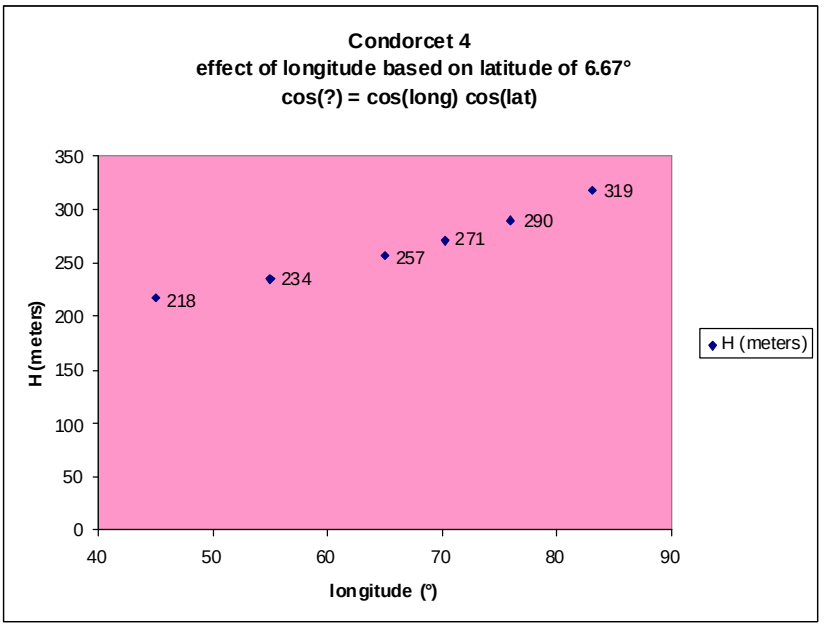

Figure 9. The height of Co4 obtained with the empirical algorithm described in equation (6) and the term λ_1. The height will increase with increased angular distance derived from equation (4).

A DEM is particularly useful for dome height computation. In this section I describe the corresponding DEM when the empirical formula is applied to Co4 dome. Running the Macros in Excel described by Evans (2006) yields Transform summation and DEM greyscale data maps for each row ($DEM_{carlotto}$). The original $DEM_{carlotto}$ of the dome Co4, subtracted for the lunar curvature, is thus transformed in the final corrected DEM as follows.

The conversion factor P_c is derived from the computed heights :

$P_c = (H_{correction\ formula} / H_{Carlotto})$

The original Carlotto DEM, saved as a txt file, is imported in Image J and then multiplied with the resulting factor P_c, using the math and image calculator features under the Process menu of Image J.

This procedure yields a new DEM, which is compared to initial $DEM_{carlotto}$ in Fig.10.

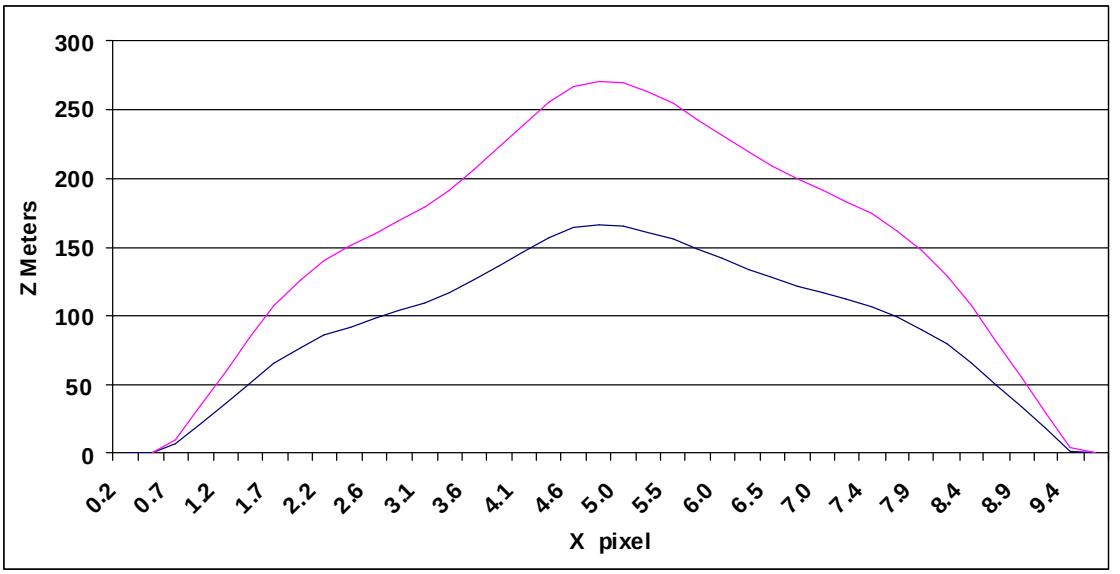

Figure 10. The DEMs of Co4 derived from Carlotto algorithm (blue curve) and the empirical formula (red curve). The contribution of the lunar curvature is taken into account and it was subtracted. The profile of the red curve was obtained using the term λ_1 ***which yields the same result of the term*** λ_3.

For surface reconstruction the final DEM image, as txt file format, can be imported into Image J as a height field map and utilized to generate a three dimensional map of the dome or part of its surface (cf. Fig 11).

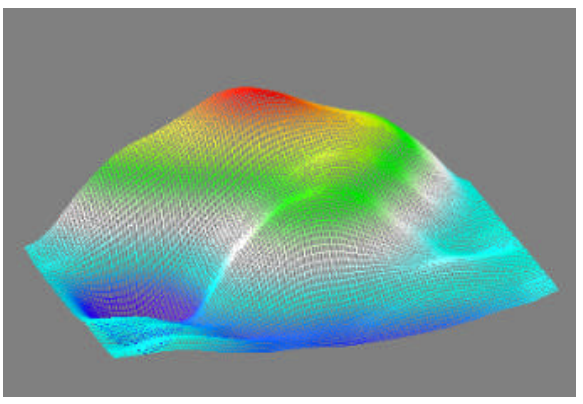

Figure 11.Three dimensional map of Co4 dome.

6. Error estimation

In the context of image-based 3D reconstruction several sources of error can be found.

-L(α): the parameter L(α) of the reflectance function is not exactly known and may show variations over the surface for different terrain types. I assume a standard error of L(α) of ± 0.10, an error range that also includes larger values of the macroscopic surface roughness of theta-bar up to 20° (McEwen, 1991). The uncertainties in L(α) affects the measured height values no more than 20 meters.

- Offset: the offset is another source of error, because if shadows are not black in the image the corresponding slope is always underestimated. The uncertainty of the determined offset (e.g from 31 to 34 grey levels for Marius 27 dome, see Appendix 1) approximately amounts to ±5% .

-Reflectance: the algorithms described in section 4 yield some solutions for λ_1- λ_3. For Condorcet 4 (Co4) dome, the height is comprised from 265 and 273 m, and the mean is calculated as 271 m. Since the standard deviation amounts to σ= 4.7, the true height is comprised at a probability of 95% between the mean value ± 2σ, i. e. in the interval between 261 m and 280 m. Hence the uncertainties in height using the three methods, with the term λ_1- λ_3, are clearly smaller than 10%.

7. Empirical algorithms, description of the results and comparison

As described in section 4, three solutions are derived when regarding the use of the three proposed terms, λ_1- λ_3.

In a refinement stage, it can be adopted the following procedures for computation of dome height :

Procedure (a). For L(α) =0.9 the same results is obtained using the term λ_1 and λ_2. Hence the height can be computed using the mean value of the heights calculated with the terms λ_1 and λ_3. Consequently the standard deviation σ is computed and the interval of confidence is then derived: the true height of the examined dome will be comprised, at a probability of 95% , between the mean value ± 2σ.

Procedure (b). For L(α) =0.95 three results are obtained using the terms λ_1–λ_3. Hence the height can be computed using the mean value of the three heights calculated with the terms λ_1-λ_3. Consequently the standard deviation σ is computed and the interval of confidence is then derived: the true height of the examined dome will be comprised, at a probability of 95% , between the mean value ± 2σ.

Procedure (c). For $0.60<L(\alpha)\leq 0.80$ the height can be computed using the mean value of

the heights calculated with the terms λ_1 -λ_3. Consequently the standard deviation σ is computed and the interval of confidence is then derived: the true height of the examined dome will be comprised, at a probability of 95% , between the mean value ± 2σ.

8. Tests

In this section are described some examples of numerical results obtained on real images. These tests were carried out in order to study the applicability of this method to further images of lunar domes reported in the Consolidated Lunar Dome Catalogue *CLDC* (Lena and Wöhler, 2008) or recently analyzed by GLR group. Further data are reported in Appendix.

Marius30 dome: The empirical formula was applied to Marius 30 (Ma30) dome (Lena et al, 2009). It is located at longitude -52.9° and latitude 13.5°. The image was taken by Phillips on April 18, 2008 at 02:05 UT. The diameter amounts to 7.4 km and the solar altitude was of 6.28°. Image scale was determined as 0.270 km per pixel. The rectified image, after the shadow offset subtraction of 18 grey levels, was imported into Excel according to Evans (2006). Zenith angle is 83.72°.

The Excel computation, based on Carlotto algorithm, yields H=397 m, after correcting for lunar curvature.

Assuming L(α)=0.95 for a phase angle of about 26.9°, the empirical formula yields :

$H_{corrected}$= 535m (for λ_2). The derived heights using the term λ_1 and λ_3 amount to 560 m and 519 m respectively. Using the **Procedure (b),** described in section 7**, the mean is computed as H=538 m**.

The height measurements derived from the full lunar-Lambert algorithm (540 m) and the empirical correction are similar. Fig. 12 displays the resulting DEM obtained for Ma30 dome as described in section 5.

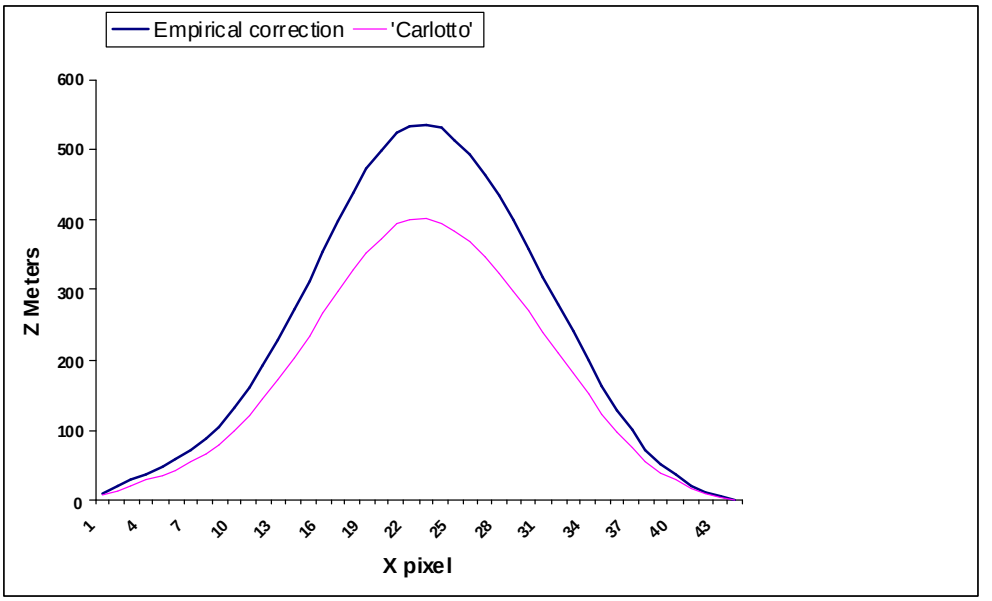

Figure 12. The DEMs of Ma30 derived from Carlotto algorithm (red curve) and the empirical formula (blue curve). The contribution of the lunar curvature is taken into account and it was subtracted.

For surface reconstruction the final DEM image, as txt file format, can be imported into Image J as a height field map and utilized to generate a three dimensional map of the dome surface (cf. Fig 13 a and b).

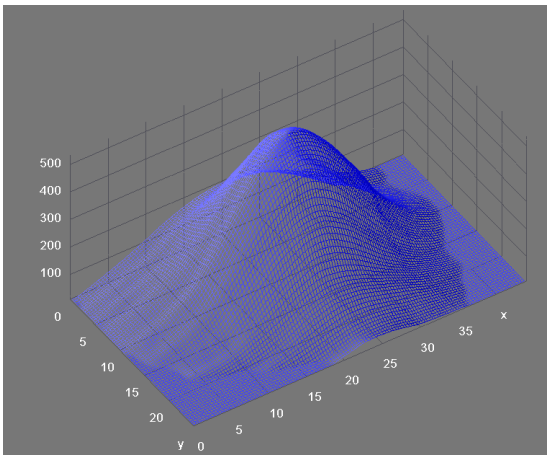

Figure 13a.Three dimensional maps of Ma30 dome.

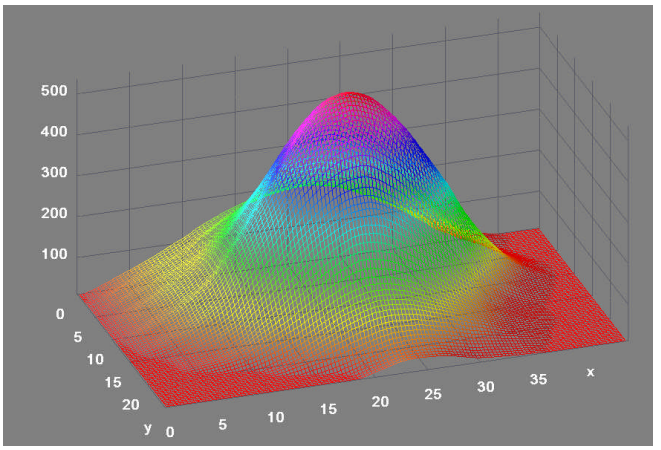

Figure 13b.Three dimensional maps of Ma30 dome.

Mee1 dome: The empirical formula was applied to Mee 1 dome. It is located at longitude -42.9° and latitude -43.5°. The image was taken by Sellini and Zompatori, on December 20, 2007 at 18:25 UT. The diameter amounts to 25 km and the solar altitude was of 3.7°. Image scale was determined as 0.280 km per pixel. The rectified image, after the shadow offset subtraction, was imported into Excel according to Evans (2006). Zenith angle is 86.3°.

The Excel computation, based on Carlotto algorithm, yields H=165 m after correcting for lunar curvature.

Assuming L(α)=0.80 for a phase angle of about 42°, the empirical formula **using the procedure (c)** described in section 7, yields, as mean value, $\mathbf{H_{corrected}}$**= 245 m.**

Fig. 14 shows the result obtained using the full lunar-Lambert model, the empirical correction described in this article, and the simple Carlotto method. The height measurements derived from the full lunar-Lambert algorithm and the empirical correction, are similar. It is not the case for the simple Carlotto method, due to the fact that the corresponding error interval does not overlap.

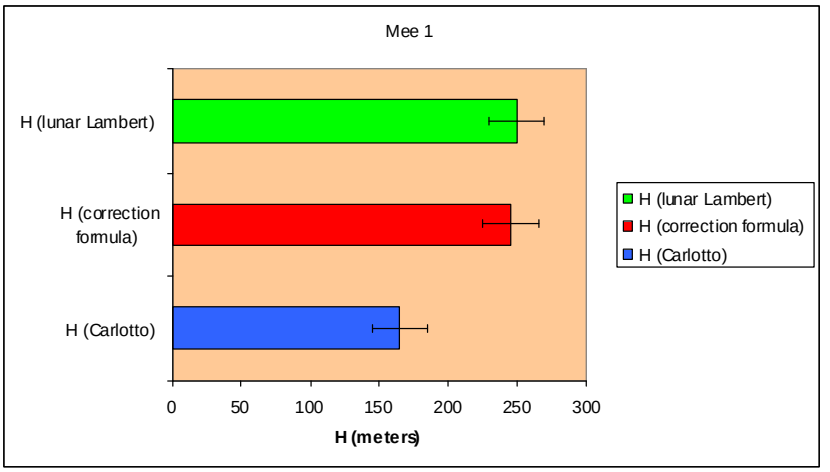

Figure 14. Heights of the Mee1 dome derived from the full LunarLambert law (green bar), the Carlotto algorithm (blue bar) and the empirical formula (red bar).

Finally, Fig. 15 displays the resulting DEM of Mee1 obtained as described in section 5, for Co4 dome.

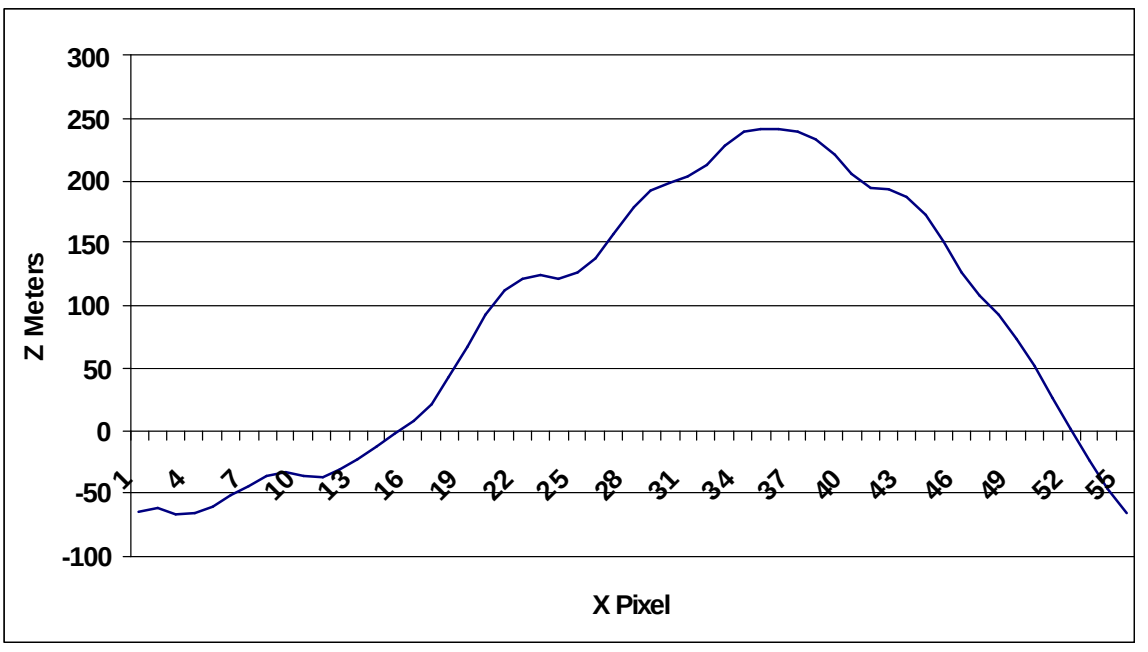

Figure 15. The DEM of Mee 1 derived from the empirical formula

Grimaldi 1 dome: The empirical formula was applied to Grimaldi 1 dome, image taken by Pau on November 11, 2008 at 13:23 UT. The dome is located at longitude -68.70° and latitude -4.51°. The diameter amounts to 29.7 km and the solar altitude was of 2.98°. Image scale was determined as 0.410 km per pixel. The rectified image, after the shadow offset subtraction of 10 grey levels, was imported into Excel according to Evans (2006). Zenith angle is 87.02°. The Excel computation, based on Carlotto algorithm, yields H=94.5 m after correcting for lunar curvature. Assuming L(α)=0.90 for a phase angle of about 23°, and using the **Procedure (a),** described in section 7**,** the empirical formula yields a computed **height of 150 m.** The analysis was performed using half dome surface.

Palus Putredinis 1 dome: The empirical formula was applied to a dome located in Palus Putredinis, recently imaged by the author on April 2, 2009 at 19:42 UT. The dome is located at longitude 1.44° and latitude 26.32°. The diameter amounts to 7 km and the solar altitude was of 4.2°. Image scale was determined as 0.430 km per pixel. The rectified image, after the shadow offset subtraction of 4 grey levels, was imported into Excel according to Evans (2006). Zenith angle is 85.8°. The Excel computation, based on Carlotto algorithm, yields H=79 m after correcting for lunar curvature. Assuming L(α) =0.70 for a phase angle of about 88°, and using the **Procedure (c),** described in section 7**,** the empirical formula yields a computed **height of 90 m.**

Arago α dome: The empirical formula was applied to Arago α dome, image taken by Lazzarotti on January 1, 2005 at 01:49 UT. The dome is located at longitude 21.7° and latitude 7.6°. The diameter amounts to 25.4 km and the solar altitude was of 2.96°. Image scale was determined as 0.330 km per pixel. The rectified image, after the shadow offset subtraction of 22 grey levels, was imported into Excel according to Evans (2006). Zenith angle is 87.05°. The Excel computation, based on Carlotto algorithm, yields H=280 m after correcting for lunar curvature. Assuming L(α)=0.80 for a phase angle of about 60°, and using the **Procedure (c),** described in section 7**,** the empirical formula yields a computed **height of 339 m**. The estimated height derived in preceding paper by the full lunar Lambert law yields 330 m.

Arago β dome: The empirical formula was applied to Arago β dome, image taken by Lazzarotti on January 1, 2005 at 01:49 UT. The dome is located at longitude 19.9° and latitude 6.1°. The diameter amounts to 23.6 km and the solar altitude was of 4.60°. Image scale was determined as 0.330 km per pixel. The rectified image, after the shadow offset subtraction of 20 grey levels, was imported into Excel according to Evans (2006). Zenith angle is 85.4°. The Excel computation, based on Carlotto algorithm, yields H=223 m after correcting for lunar curvature. Assuming L(α)=0.80 for a phase angle of about 60°, using the **Procedure (c),** described in section 7**,** the empirical formula yields **a computed height of 269 m.** The estimated height derived in preceding paper by the full lunar Lambert law yields 270 m.

9. Results

In this paper, I have described an empirical algorithm for shape-from-shading, minimizing the dome height differences computed using the simple Carlotto algorithm. The optimized results are obtained from the equation (6) described in section 4. I have compared the empirical correction proposed in this paper with two alternatives. The first of these is the shape-from-shading height by using the full lunar Lambert law. The second method used in this comparison is the simple Carlotto algorithm. The heights measurements computed with the empirical formula agree well with the results of the lunar Lambert method, used as comparison. The estimated heights obtained with the Carlotto method tend to be systematically lower. The observed deviation is higher for domes far from the lunar centre, as is shown in the diagram of Fig. 16. On the contrary the results derived by the application of the empirical algorithm are similar to those computed with the classic lunar Lambert method, and no systematic deviations occur. The proposed new method is found to perform efficient results.

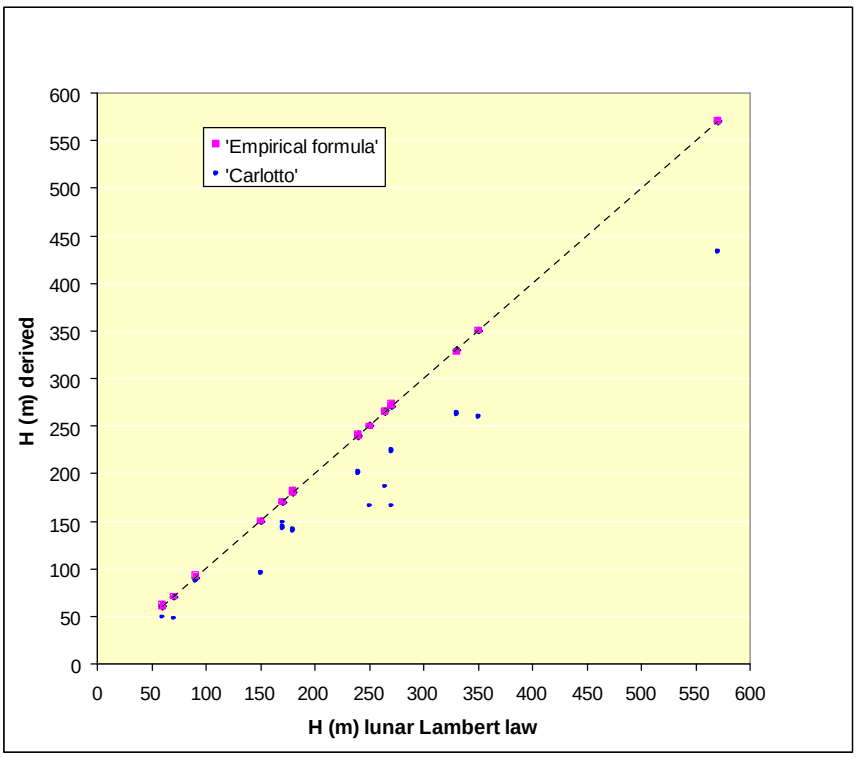

Figure 16. Results derived by the application of the empirical algorithm (red squares) and Carlotto method (blue circles).

10. Algorithm description

Having described the different steps of the surface reconstruction process, in this section I summarise how the steps are combined together in an algorithm. The sequence of processing steps is as follows:

Step 0: From the initial image, the image scale, the solar altitude and the selenographic coordinates are computed using the LTVT software package by Mosher and Bondo (2006) which requires a calibration of the images by identifying the precise selenographic coordinates of some landmarks on the image. This calibration is performed based on the UCLN 1994 list of control points. Moreover the dome diameter is computed. The image is transformed in rectified view and saved as BMP image.

Step 1: An estimate of the shadow offset is made. The "shadow offset" is definitely a critical point for all photoclinometric approaches. Thus the image is imported into Image J and the corresponding "shadow offset" is subtracted using the math option. The resulting image is saved as image txt format and then imported into Excel.

Step 2: An automated Excel spreadsheet is used for the computation. According to Evans (2006), SFS computation is made by using astrophotography software to rotate a lunar dome so the apparent solar azimuth incidence is 270º. Thus, use the Image pixel values to compute the surface gradient, including for the computation the image scale and the zenith angle of the sun, which is obtained by subtracting the local solar altitude from 90°. According with the method described in detail by Evans (2006) and Fisher (2007) the computation yields the gradient elevation and the DEM. The graphing function in Excel can be used to generate x, z plots along any desired y row. The contribution to dome height caused by lunar curvature is taken into account and is subtracted yielding height of a dome corrected for lunar curvature =>$H_{carlotto}$

Step 3: The phase angle is obtained using a lunar program. The resulting value of L(α) is interpolated from the curve shown in Fig.1 (McEwen, 1991). The angular distance is computed from the longitude and latitude of a lunar dome.

Step 4: The correction factor F is computed in Excel by using

$$F= [2* (1/1+\cos(\Delta)) + \lambda] \quad (5)$$

The height, derived from Carlotto algorithm $H_{carlotto}$, is then multiplied for the correction factor F yielding :

$$H_{corrected}= (H_{Carlotto}) * [2* (1/1+\cos(\Delta)) + \lambda] \quad (6)$$

with $\cos(\Delta)=\cos(long)\cos(lat)$

Equation 6 is solved for three different terms λ, introduced in section 4, as follows:

- λ_1 where

$\lambda_1 = 0$ if $L(\alpha) < 0.60$; $\lambda_1 = [1 - L(\alpha)]\,[(L(\alpha) - 0.6)/0.2]$ if $0.60 < L(\alpha) \leq 0.80$ and

$\lambda_1 = 0.2\ (0.75)$ if $L(\alpha) > 0.80$

- λ_2 where

$\lambda_1 = 0$ if $L(\alpha) < 0.60$; $\lambda_1 = [1 - L(\alpha)]\,[(L(\alpha) - 0.6)/0.2]$ if $L(\alpha) > 0.60$

- λ_3 where

$\lambda_1 = 0$ if $L(\alpha) < 0.60$; $\lambda_1 = [1 - L(\alpha)]\,[(L(\alpha) - 0.6)/0.2]\ (0.97)$ if $L(\alpha) > 0.60$

The computation is automated using a spreadsheet in Excel. It yields the value of heights for the three equations => $H_{\lambda 1}$, $H_{\lambda 2}$ and $H_{\lambda 3}$

Step 5: The corrected Height is assessed for the three cases with the following procedures:

Procedure (a). For $L(\alpha) = 0.9$ the same results is obtained using the term λ_1 and λ_2. Hence the height can be computed using the mean value of the heights calculated with the terms λ_1 and λ_3, as reported in section 7. Consequently the standard deviation σ is computed and the interval of confidence is then derived: the true height of the examined dome will be comprised, at a probability of 95% , between the mean value $\pm 2\sigma$.

Procedure (b). For $L(\alpha) = 0.95$ three results are obtained using the terms $\lambda_1 - \lambda_3$. Hence the height can be computed using the mean value of the three heights calculated with the terms λ_1-λ_3.

Procedure (c). For $0.60 < L(\alpha) \leq 0.85$ the height can be computed using the mean value of the heights calculated with the terms λ_1 -λ_3. Consequently the standard deviation σ is computed and the interval of confidence is then derived: the true height of the examined dome will be comprised, at a probability of 95% , between the mean value $\pm 2\sigma$.

***Step 6*:** To compute $P_c = (H_{correction\ formula} / H_{Carlotto})$ and then multiply the original Carlotto DEM values with P_c using the math option of Image J. The DEM is saved as a txt file format and as TIFF 32 bit, which is used for a 3D reconstruction==>Image J plug-in interactive 3D surface plot.

A complete description of the different steps is reported in Appendix 1-3.

10. Conclusion

I hope that these comparisons of three methods will help practitioners to make their choices when dealing with SFS analysis. From the tests reported in this work an empirical formula is proposed and discussed. The analysis contained in this paper could give rise to several interesting developments and improvements, such as the extension of this method based on the simple SFS model described by Evans (2006) to further lunar domes and new investigation.

Of course, I also plan to increase the automated version in Excel and, possibly, to create a lunar program. Therefore, I hope that many other researchers will make available their own codes and images.

Acknowledgements: I wish to thank C. Wöhler for the stimulating discussion about this study and his suggestions. I thank also R. Evans and K. Fisher for their preceding works about the application of the Carlotto method using Excel. Fig.1 was reprinted with permission from Elsevier.

References

[1] Carlotto, M.J., 1996. Shape From Shading. http://www.newfrontiersinscience.com/martianenigmas/Articles/SFS/sfs.html

[2] Evans, R., 2006. The Moon on a Spreadsheet: Photoclinometry using Excel.

Selenology Today 1 pp. 21-59.

[3] Fisher, K.A., 1997. An Excel Spreadsheet Implementing Shape-for-Shading (SFS) per Carlotto 1996. http://members.csolutions.net/fisherka/astronote/Photometry/sfs/SFS.html

[4] Hapke, B., 1993. Theory of reflectance and emittance spectroscopy, Cambridge University Press, Cambridge, UK.

[5] Horn, B. K. P., 1989. Height and Gradient from Shading, MIT technical report, AI memo no. 1105A. http://people.csail.mit.edu/people/bkph/AIM/AIM-1105A-TEX.pdf

[6] Lena, R., Wöhler, C., Bregante, M. T., Fattinnanzi, C., 2006. A combined morphometric and spectrophotometric study of the complex lunar volcanic region in the south of Petavius.
Journal of the Royal Astronomical Society of Canada 100(1), pp. 14-25.

[7] Lena, R., Wöhler, C., 2008. Consolidated Lunar Dome Catalogue (CLDC).

http://digilander.libero.it/glrgroup/consolidatedlunardomecatalogue.htm

[8] Lena, R., Wöhler, C., Phillips, J., 2009. Marius Hills: Morphometry, Rheology, and Mode of Emplacement. European Planetary Science Congress, Vol.4, EPSC 2009-262.

[9] Lohse, V., Heipke, C., Kirk, R.L., 2006. Derivation of Planetary topography using multi-image-shape-from-shading. Planetary and Space Science, 54. pp. 661-674.

[10] McEwen, A. S., 1991. Photometric Functions for Photoclinometry and Other Applications. Icarus, 92 (2), pp. 298-311.

[11] Mosher, J., Bondo, H., 2006. Lunar Termination Visualization Tool (LTVT).

http://inet.uni2.dk/ d120588/henrik/jim ltvt.html

[12] Wöhler, C., Lena, R., Lazzarotti, P., Phillips, J., Wirths, M., Pujic, Z., 2006. A combined spectrophotometric and morphometric study of the lunar mare dome fields near Cauchy, Arago, Hortensius, and Milichius. Icarus 183(2), pp. 237-264.

APPENDIX 1

Analysis of Marius 27 (Ma 27) dome (cf. Lena et al., 2009)

1) Starting from the lunar image to rectified view

The image was taken by Phillips on April 18, 2008 at 02:05 UT. The image scale, the solar altitude and the selenographic coordinates are computed using the LTVT software package by Mosher and Bondo (2006) which requires a calibration of the images by identifying the precise selenographic coordinates of some landmarks on the image. This calibration is performed based on the UCLN 1994 list of control points. The dome is located at longitude -53.65° and latitude 15.26°. The diameter amounts to 6.5 km and the solar altitude was of 5.6°. Image scale was determined, using LTVT, as 0.270 km per pixel. The Image is thus transformed in rectified view (Fig A1).

In Carlotto method, SFS computation is reduced to a minimum by using astrophotography software to rotate a lunar dome so the apparent solar azimuth incidence is 270º (Carlotto 1996), as shown in Fig. A2.

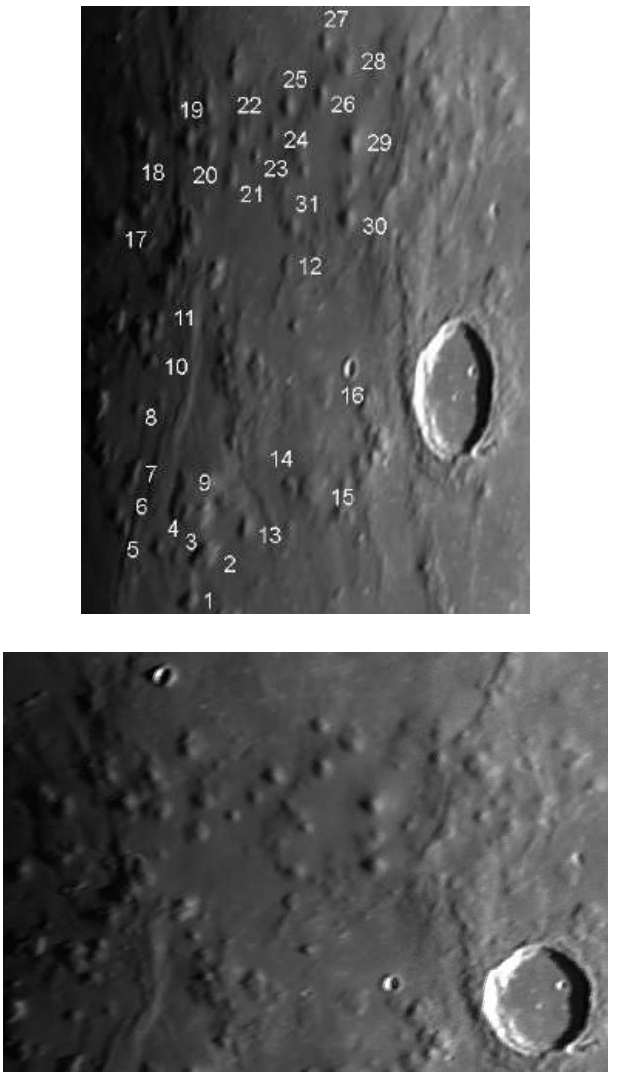

Figure A1. The image taken by Phillips on April 18, 2008 at 02:05 UT. The examined dome is termed as Marius 27 in the above image. To the top the calibrated image based on the UCLN 1994 list of control points. To the bottom the rectified view obtained using LTVT software package (the dome is the uppermost one).

Figure A2. To the top the rectified view of Marius Hills which is rotated so that the apparent solar azimuth incidence is 270º, according to Carlotto. The dome Ma27 is the uppermost one. To the bottom the ROI of Ma27, here enlarged.

2) Shadow offset

The rectified image, was analyzed for the offset subtraction. The offset problem is also important but completely independent of the reflectance function used. If the shadows are not black in the image, the corresponding slope is always underestimated. Our ground-based images can be affected by scattered light (cf. section 2). The offset can be determined from the intensity profile of shadows cast by steep mountains and/or crater rims, where an abrupt transition from illuminated surface to darkness is expected. In this case the dome cast a shadow on the soil and the intensity profile observed in the image allows for an estimation of the shadow offset, determined as 34 grey level.

The rectified image was then processed using the math and image calculator features under the Process menu of Image J: thus the corresponding “shadow offset” was subtracted. The resulting image was saved as image txt format and then imported into Excel.

3) DEM corrected for lunar curvature

An automated Excel spreadsheet is used for the computation. The corresponding Image pixel value map, as txt format, is introduced and is reported in Fig. A3.

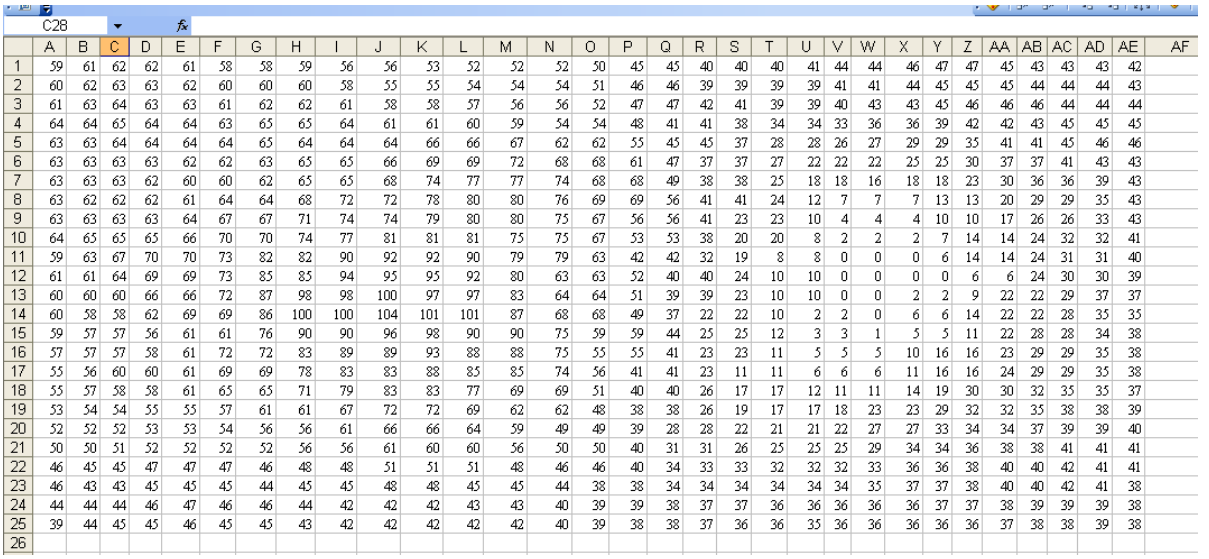

	A	B	C	D	E	F	G	H	I	J	K	L	M	N	O	P	Q	R	S	T	U	V	W	X	Y	Z	AA	AB	AC	AD	AE	AF
1	59	61	62	62	61	58	58	59	56	56	53	52	52	52	50	45	45	40	40	40	41	44	44	46	47	47	45	43	43	43	42	
2	60	62	63	63	62	60	60	60	58	55	55	54	54	54	51	46	46	39	39	39	39	41	41	44	45	45	45	44	44	44	43	
3	61	63	64	63	63	61	62	62	61	58	58	57	56	56	52	47	47	42	41	39	39	40	43	43	45	46	46	46	44	44	44	
4	64	64	65	64	64	63	65	65	64	61	61	60	59	54	54	48	41	41	38	34	34	33	36	36	39	42	42	43	45	45	45	
5	63	63	64	64	64	64	65	64	64	64	66	66	67	62	62	55	45	45	37	28	28	26	27	29	29	35	41	41	45	46	46	
6	63	63	63	63	62	62	63	65	65	66	69	69	72	68	68	61	47	37	37	27	22	22	22	25	25	30	37	37	41	43	43	
7	63	63	63	62	60	60	62	65	65	68	74	77	77	74	68	68	49	38	38	25	18	18	16	18	18	23	30	36	36	39	43	
8	63	62	62	62	61	64	64	68	72	72	78	80	80	76	69	69	56	41	41	24	12	7	7	7	13	13	20	29	29	35	43	
9	63	63	63	63	64	67	67	71	74	74	79	80	80	75	67	56	56	41	23	23	10	4	4	4	10	10	17	26	26	33	43	
10	64	65	65	65	66	70	70	74	77	81	81	81	75	75	67	53	53	38	20	20	8	2	2	2	7	14	14	24	32	32	41	
11	59	63	67	70	70	73	82	82	90	92	92	90	79	79	63	42	42	32	19	8	8	0	0	0	6	14	14	24	31	31	40	
12	61	61	64	69	69	73	85	85	94	95	95	92	80	63	63	52	40	40	24	10	10	0	0	0	0	6	6	24	30	30	39	
13	60	60	60	66	66	72	87	98	98	100	97	97	83	64	64	51	39	39	23	10	10	0	0	2	2	9	22	22	29	37	37	
14	60	58	58	62	69	69	86	100	100	104	101	101	87	68	68	49	37	22	22	10	2	2	0	6	6	14	22	22	28	35	35	
15	59	57	57	56	61	61	76	90	90	96	98	90	90	75	59	59	44	25	25	12	3	3	1	5	5	11	22	28	28	34	38	
16	57	57	57	58	61	72	72	83	89	89	93	88	88	75	55	55	41	23	23	11	5	5	5	10	16	16	23	29	29	35	38	
17	55	56	60	60	61	69	69	78	83	83	88	85	85	74	56	41	41	23	11	11	6	6	6	11	16	16	24	29	29	35	38	
18	55	57	58	58	61	65	65	71	79	83	83	77	69	69	51	40	40	26	17	17	12	11	11	14	19	30	30	32	35	35	37	
19	53	54	54	55	55	57	61	61	67	72	72	69	62	62	48	38	38	26	19	17	17	18	23	23	29	32	32	35	38	38	39	
20	52	52	52	53	53	54	56	56	61	66	66	64	59	49	49	39	28	28	22	21	21	22	27	27	33	34	34	37	39	39	40	
21	50	50	51	52	52	52	52	56	56	61	60	60	56	50	50	40	31	31	26	25	25	25	29	34	34	36	38	38	41	41	41	
22	46	45	45	47	47	47	46	48	48	51	51	51	48	46	46	40	34	33	33	32	32	32	33	36	36	38	40	40	42	41	41	
23	46	43	43	45	45	45	44	45	45	48	48	45	45	44	38	38	34	34	34	34	34	34	35	37	37	38	40	40	42	41	38	
24	44	44	44	46	47	46	46	44	42	42	42	43	43	40	39	39	38	37	37	36	36	36	36	36	37	37	38	39	39	39	38	
25	39	44	45	45	46	45	45	43	42	42	42	42	42	40	39	38	38	37	36	36	35	36	36	36	36	36	37	38	38	39	38	
26																																

Figure A3. The Image pixel value map is obtained after subtraction of shadow offset. The excel spreadsheet is shown in the figure.

The Excel computation, based on Carlotto algorithm, yields H=253 m.

Image scale:	270	meters/px		27	meter/px	uncertainty		
Solar altitude:	5.6	degrees		84.4	Zenith angle degrees			
DEM Max:	253.0	DEM Avg:	68.97381	Eleva-tions	No. rows:	25	No. cols:	31

According with the method described in detail by Evans (2006) and Fisher (2007), the computation yields the gradient elevation maps (Fig. A4) and the DEM (Fig. A5).

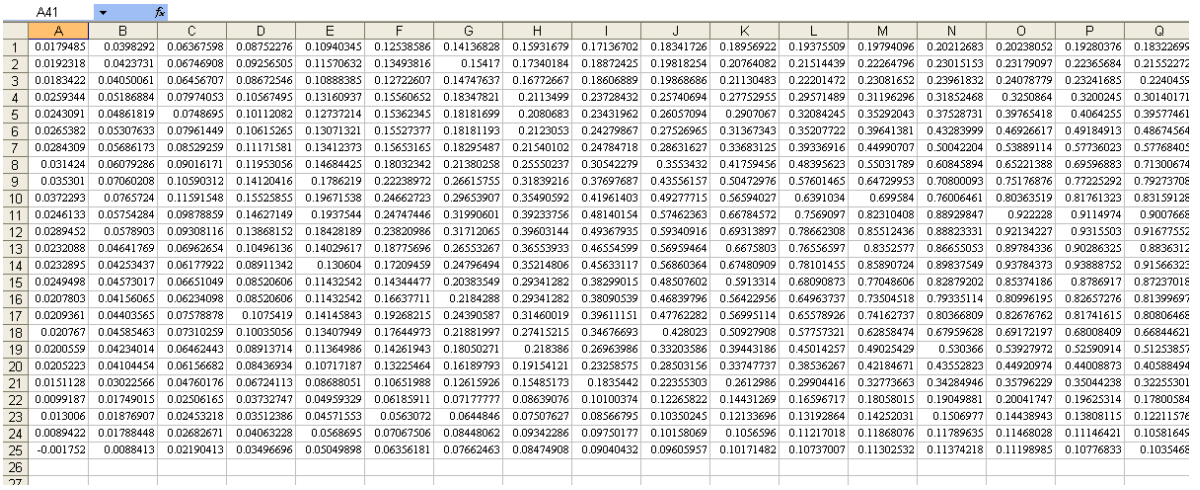

	A	B	C	D	E	F	G	H	I	J	K	L	M	N	O	P	Q
1	0.0179485	0.0398292	0.06367598	0.08752276	0.10940345	0.12538586	0.14136828	0.15931679	0.17136702	0.18341726	0.18956922	0.19375509	0.19794096	0.20212683	0.20238052	0.19280376	0.18322695
2	0.0192318	0.0423731	0.06746908	0.09256505	0.11570632	0.13493816	0.15417	0.17340184	0.18872425	0.19818254	0.20764082	0.21514439	0.22264796	0.23015153	0.23179097	0.22365684	0.21552272
3	0.0183422	0.04050061	0.06456707	0.08672546	0.10888385	0.12722607	0.14747637	0.16772667	0.18606889	0.19868686	0.21130483	0.22201472	0.23081652	0.23961832	0.24078779	0.23241685	0.2240459
4	0.0259344	0.05186884	0.07974053	0.10567495	0.13160937	0.15560652	0.18347821	0.2113499	0.23728432	0.25740694	0.27752955	0.29571489	0.31196296	0.31852468	0.3250864	0.3200245	0.30140171
5	0.0243091	0.04861819	0.0748695	0.10112082	0.12737214	0.15362345	0.18181699	0.2080683	0.23431962	0.26057094	0.2907067	0.32084245	0.35292043	0.37528731	0.39765418	0.4064255	0.39577461
6	0.0265382	0.05307633	0.07961449	0.10615265	0.13071321	0.15527377	0.18181193	0.2123053	0.24279867	0.27526965	0.31367343	0.35207722	0.39641381	0.43283999	0.46926617	0.49184913	0.48674564
7	0.0284309	0.05686173	0.08529259	0.11171581	0.13412373	0.15653165	0.18295487	0.21540102	0.24784718	0.28631627	0.33683125	0.39336916	0.44990707	0.50042204	0.53889114	0.57736023	0.57768405
8	0.031424	0.06079286	0.09016171	0.11953056	0.14684425	0.18032342	0.21380258	0.25550237	0.30542279	0.3553432	0.41759456	0.48395623	0.55031789	0.60845894	0.65221388	0.69596883	0.71300674
9	0.035301	0.07060208	0.10590312	0.14120416	0.1786219	0.22238972	0.26615755	0.31839216	0.37697687	0.43556157	0.50472976	0.57601465	0.64729953	0.70800093	0.75176876	0.77225292	0.79273708
10	0.0372293	0.0765724	0.11591548	0.15525855	0.19671538	0.24662723	0.29653907	0.35490592	0.41961403	0.49277715	0.56594027	0.6391034	0.699584	0.76006461	0.80363519	0.81761323	0.83159128
11	0.0246133	0.05754284	0.09878859	0.14627149	0.1937544	0.24747446	0.31990601	0.39233756	0.48140154	0.57462363	0.66784572	0.7569097	0.82310408	0.88929847	0.922228	0.9114974	0.9007668
12	0.0289452	0.0578903	0.09308116	0.13868152	0.18428189	0.23820986	0.31712065	0.39603144	0.49367935	0.59340916	0.69313897	0.78662308	0.85512436	0.88823331	0.92134227	0.9315503	0.91677552
13	0.0232088	0.04641769	0.06962654	0.10496136	0.14029617	0.18775696	0.26553267	0.36553933	0.46554599	0.56959464	0.6675803	0.76556597	0.8352577	0.86655053	0.89784336	0.90286325	0.8836312
14	0.0232895	0.04253437	0.06177922	0.08911342	0.130604	0.17209459	0.24796494	0.35214806	0.45633117	0.56860364	0.67480909	0.78101455	0.85890724	0.89837549	0.93784373	0.93888752	0.91566323
15	0.0249498	0.04573017	0.06651049	0.08520606	0.11432542	0.14344477	0.20383549	0.29341282	0.38299015	0.48507602	0.5913314	0.68090873	0.77048606	0.82879202	0.85374186	0.8786917	0.87237018
16	0.0207803	0.04156065	0.06234098	0.08520606	0.11432542	0.16637711	0.2184288	0.29341282	0.38090539	0.46839796	0.56422956	0.64963737	0.73504518	0.79335114	0.80996195	0.82657276	0.81399697
17	0.0209361	0.04403565	0.07578878	0.1075419	0.14145843	0.19268215	0.24390587	0.31460019	0.39611151	0.47762282	0.56995114	0.65578926	0.74162737	0.80366809	0.82676762	0.81741615	0.80806468
18	0.020767	0.04585463	0.07310259	0.10035056	0.13407949	0.17644973	0.21881997	0.27415215	0.34676693	0.428023	0.50927908	0.57757321	0.62858474	0.67959628	0.69172197	0.68008409	0.66844621
19	0.0200559	0.04234014	0.06462443	0.08913714	0.11364986	0.14261943	0.18050271	0.218386	0.26963986	0.33203586	0.39443186	0.45014257	0.49025429	0.530366	0.53927972	0.52590914	0.51253857
20	0.0205223	0.04104454	0.06156682	0.08436934	0.10717187	0.13225464	0.16189793	0.19154121	0.23258575	0.28503156	0.33747737	0.38536267	0.42184671	0.43552823	0.44920974	0.44008873	0.40588494
21	0.0151128	0.03022566	0.04760176	0.06724113	0.08688051	0.10651988	0.12615926	0.15485173	0.1835442	0.22355303	0.2612986	0.29904416	0.32773663	0.34284946	0.35796229	0.35044238	0.32255301
22	0.0099187	0.01749015	0.02506165	0.03732747	0.04959329	0.06185911	0.07177777	0.08639076	0.10100374	0.12265822	0.14431269	0.16596717	0.18058015	0.19049881	0.20041747	0.19625314	0.17800584
23	0.013006	0.01876907	0.02453218	0.03512386	0.04571553	0.0563072	0.0644846	0.07507627	0.08566795	0.10350245	0.12133696	0.13192864	0.14252031	0.1506977	0.14438943	0.13808115	0.12211576
24	0.0089422	0.01788448	0.02682671	0.04063228	0.0568695	0.07067506	0.08448062	0.09342286	0.09750177	0.10158069	0.1056596	0.11217018	0.11868076	0.11789635	0.11468028	0.11146421	0.10581645
25	-0.001752	0.0088413	0.02190413	0.03496696	0.05049898	0.06356181	0.07662463	0.08474908	0.09040432	0.09605957	0.10171482	0.10737007	0.11302532	0.11374218	0.11198985	0.10776833	0.1035468

Figure A4. The gradient elevation maps.

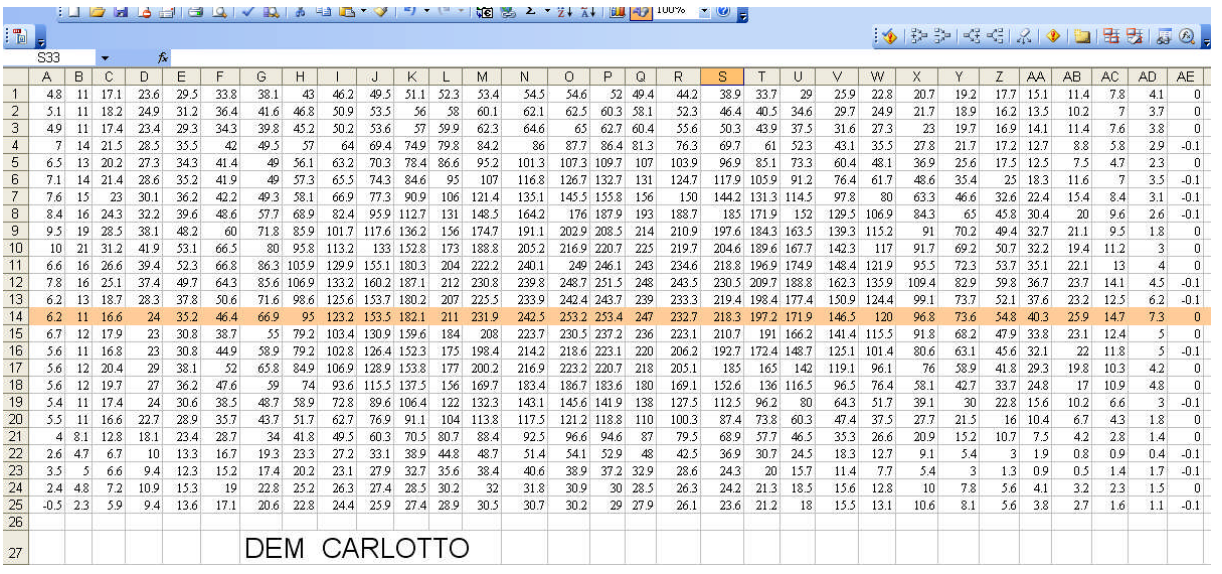

	A	B	C	D	E	F	G	H	I	J	K	L	M	N	O	P	Q	R	S	T	U	V	W	X	Y	Z	AA	AB	AC	AD	AE
1	4.8	11	17.1	23.6	29.5	33.8	38.1	43	46.2	49.5	51.1	52.3	53.4	54.5	54.6	52	49.4	44.2	38.9	33.7	29	25.9	22.8	20.7	19.2	17.7	15.1	11.4	7.8	4.1	0
2	5.1	11	18.2	24.9	31.2	36.4	41.6	46.8	50.9	53.5	56	58	60.1	62.1	62.5	60.3	58.1	52.3	46.4	40.5	34.6	29.7	24.9	21.7	18.9	16.2	13.5	10.2	7	3.7	0
3	4.9	11	17.4	23.4	29.3	34.3	39.8	45.2	50.2	53.6	57	59.9	62.3	64.6	65	62.7	60.4	55.6	50.3	43.9	37.5	31.6	27.3	23	19.7	16.9	14.1	11.4	7.6	3.8	0
4	7	14	21.5	28.5	35.5	42	49.5	57	64	69.4	74.9	79.8	84.2	86	87.7	86.4	81.3	76.3	69.7	61	52.3	43.1	35.5	27.8	21.7	17.2	12.7	8.8	5.8	2.9	-0.1
5	6.5	13	20.2	27.3	34.3	41.4	49	56.1	63.2	70.3	78.4	86.6	95.2	101.3	107.3	109.7	107	103.9	96.9	85.1	73.3	60.4	48.1	36.9	25.6	17.5	12.5	7.5	4.7	2.3	0
6	7.1	14	21.4	28.6	35.2	41.9	49	57.3	65.5	74.3	84.6	95	107	116.8	126.7	132.7	131	124.7	117.9	105.9	91.2	76.4	61.7	48.6	35.4	25	18.3	11.6	7	3.5	-0.1
7	7.6	15	23	30.1	36.2	42.2	49.3	58.1	66.9	77.3	90.9	106	121.4	135.1	145.5	155.8	156	150	144.2	131.3	114.5	97.8	80	63.3	46.6	32.6	22.4	15.4	8.4	3.1	-0.1
8	8.4	16	24.3	32.2	39.6	48.6	57.7	68.9	82.4	95.9	112.7	131	148.5	164.2	176	187.9	193	188.7	185	171.9	152	129.5	106.9	84.3	65	45.8	30.4	20	9.6	2.6	-0.1
9	9.5	19	28.5	38.1	48.2	60	71.8	85.9	101.7	117.6	136.2	156	174.7	191.1	202.9	208.5	214	210.9	197.6	184.3	163.5	139.3	115.2	91	70.2	49.4	32.7	21.1	9.5	1.8	0
10	10	21	31.2	41.9	53.1	66.5	80	95.8	113.2	133	152.8	173	188.8	205.2	216.9	220.7	225	219.7	204.6	189.6	167.7	142.3	117	91.7	69.2	50.7	32.2	19.4	11.2	3	0
11	6.6	16	26.6	39.4	52.3	66.8	86.3	105.9	129.9	155.1	180.3	204	222.2	240.1	249	246.1	243	234.6	218.8	196.9	174.9	148.4	121.9	95.5	72.3	53.7	35.1	22.1	13	4	0
12	7.8	16	25.1	37.4	49.7	64.3	85.6	106.9	133.2	160.2	187.1	212	230.8	239.8	248.7	251.5	248	243.5	230.5	209.7	188.8	162.3	135.9	109.4	82.9	59.8	36.7	23.7	14.1	4.5	-0.1
13	6.2	13	18.7	28.3	37.8	50.6	71.6	98.6	125.6	153.7	180.2	207	225.5	233.9	242.4	243.7	239	233.3	219.4	198.4	177.4	150.9	124.4	99.1	73.7	52.1	37.6	23.2	12.5	6.2	-0.1
14	6.2	11	16.6	24	35.2	46.4	66.9	95	123.2	153.5	182.1	211	231.9	242.5	253.2	253.4	247	232.7	218.3	197.2	171.9	146.5	120	96.8	73.6	54.8	40.3	25.9	14.7	7.3	0
15	6.7	12	17.9	23	30.8	38.7	55	79.2	103.4	130.9	159.6	184	208	223.7	230.5	237.2	236	223.1	210.7	191	166.2	141.4	115.5	91.8	68.2	47.9	33.8	23.1	12.4	5	0
16	5.6	11	16.8	23	30.8	44.9	58.9	79.2	102.8	126.4	152.3	175	198.4	214.2	218.6	223.1	220	206.2	192.7	172.4	148.7	125.1	101.4	80.6	63.1	45.6	32.1	22	11.8	5	-0.1
17	5.6	12	20.4	29	38.1	52	65.8	84.9	106.9	128.9	153.8	177	200.2	216.9	223.2	220.7	218	205.1	185	165	142	119.1	96.1	76	58.9	41.8	29.3	19.8	10.3	4.2	0
18	5.6	12	19.7	27	36.2	47.6	59	74	93.6	115.5	137.5	156	169.7	183.4	186.7	183.6	180	169.1	152.6	136	116.5	96.5	76.4	58.1	42.7	33.7	24.8	17	10.9	4.8	0
19	5.4	11	17.4	24	30.6	38.5	48.7	58.9	72.8	89.6	106.4	122	132.3	143.1	145.6	141.9	138	127.5	112.5	96.2	80	64.3	51.7	39.1	30	22.8	15.6	10.2	6.6	3	-0.1
20	5.5	11	16.6	22.7	28.9	35.7	43.7	51.7	62.7	76.9	91.1	104	113.8	117.5	121.2	118.8	110	100.3	87.4	73.8	60.3	47.4	37.5	27.7	21.5	16	10.4	6.7	4.3	1.8	0
21	4	8.1	12.8	18.1	23.4	28.7	34	41.8	49.5	60.3	70.5	80.7	88.4	92.5	96.6	94.6	87	79.5	68.9	57.7	46.5	35.3	26.6	20.9	15.2	10.7	7.5	4.2	2.8	1.4	0
22	2.6	4.7	6.7	10	13.3	16.7	19.3	23.3	27.2	33.1	38.9	44.8	48.7	51.4	54.1	52.9	48	42.5	36.9	30.7	24.5	18.3	12.7	9.1	5.4	3	1.9	0.8	0.9	0.4	-0.1
23	3.5	5	6.6	9.4	12.3	15.2	17.4	20.2	23.1	27.9	32.7	35.6	38.4	40.6	38.9	37.2	32.9	28.6	24.3	20	15.7	11.4	7.7	5.4	3	1.3	0.9	0.5	1.4	1.7	-0.1
24	2.4	4.8	7.2	10.9	15.3	19	22.8	25.2	26.3	27.4	28.5	30.2	32	31.8	30.9	30	28.5	26.3	24.2	21.3	18.5	15.6	12.8	10	7.8	5.6	4.1	3.2	2.3	1.5	0
25	-0.5	2.3	5.9	9.4	13.6	17.1	20.6	22.8	24.4	25.9	27.4	28.9	30.5	30.7	30.2	29	27.9	26.1	23.6	21.2	18	15.5	13.1	10.6	8.1	5.6	3.8	2.7	1.6	1.1	-0.1
26																															
27							DEM CARLOTTO																								

Figure A5. The DEM resulting from Carlotto method. The row 14, is marked.

The contribution to dome height caused by lunar curvature is taken into account (Fig. A6) and is subtracted yielding, for the diameter of 6.5 km, $H_{Carlotto}$=250 m.

Feature dia. (km)	Lunar sphere contribution to feature height
6.5	3.0
6.75	3.3
7	3.5
7.25	3.8
7.5	4.0

Figure A6. The contribution to dome height (3.0 km) caused by lunar curvature is subtracted yielding $H_{Carlotto}$=250 m.

The DEM, as txt format (Fig. A5), is then corrected for lunar curvature using Image J math option, yielding the final DEM derived from the Carlotto method. The graphing function in Excel can be used to generate x, z plots along any desired y row. The x,z plots along row 14 is shown in Fig. A7.

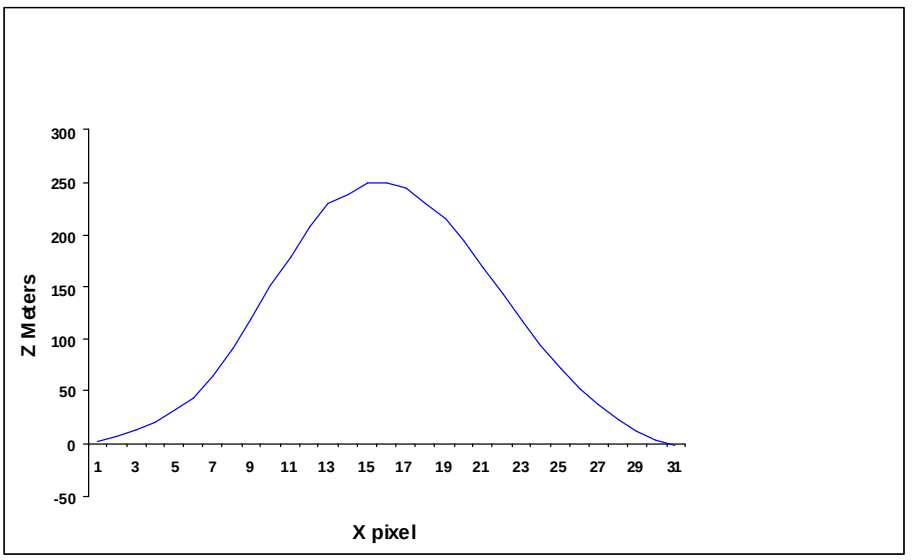

Figure A7. The DEM of Ma27 derived from Carlotto algorithm. The contribution of the lunar curvature is taken into account and it was subtracted.

4) Correction formula: computed height

Assuming L(α)=0.95, for a phase angle of about 26.9°, the empirical formula yields :

- For λ_1 $H_{corrected}$= 356 m
- For λ_2 $H_{corrected}$= 342 m
- For λ_3 $H_{corrected}$= 331 m

The deviation is explained in section 4 and 5. The mean, using the procedure (b) reported in section 7, is calculated as 343 m. Since the standard deviation amounts to σ= 13.0, the true height is comprised at a probability of 95% between the mean value ± 2σ, i. e. in the interval between 316 m and 368 m. Hence the uncertainties are smaller than 10%. Therefore $H_{corrected}$ can be assessed as 343 m.

The average flank slope ξ is thus determined according to:

$$\xi = \arctan 2H/D \qquad (9)$$

The slope amounts to 6.15° using the empirical formula, while with Carlotto algorithm it amounts only to 4.39°.

5) Final DEM and 3D reconstruction

The conversion factor P_c is derived yielding

$P_c = (H_{correction\ formula} / H_{Carlotto}) = 1.33$

The original Carlotto DEM, saved as a txt file, is imported in Image J and then multiplied with the resulting factor P_c, using the math and image calculator features under the Process menu of Image J.

This procedure yields a new DEM, which is compared to initial $DEM_{carlotto}$ (Fig. A8).

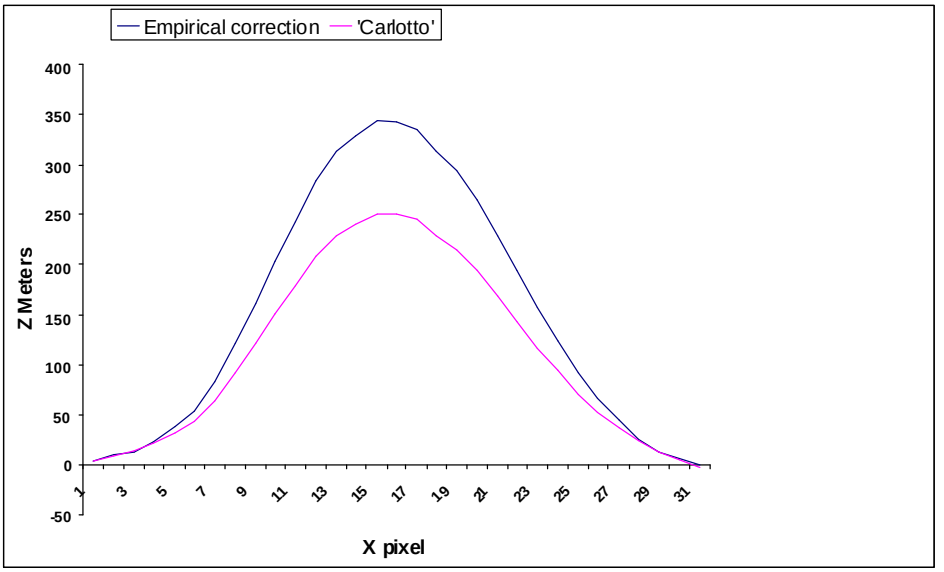

Figure A8. The DEMs of Ma27 for row 14 derived from Carlotto algorithm (red curve) and the empirical formula (blue curve).

Finally, for surface reconstruction the final DEM image, as txt file format, is imported into Image J as a height field map and utilized to generate a three dimensional map of the dome surface (cf. Fig A9).

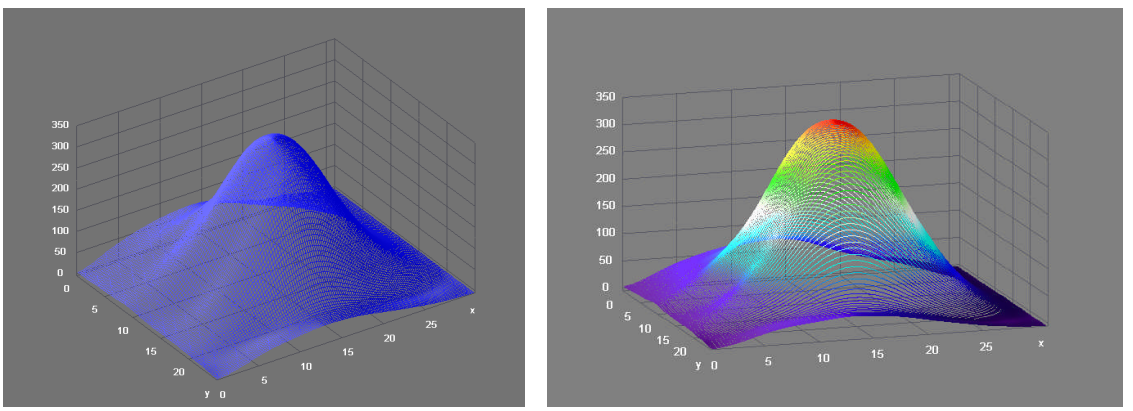

Figure A9.Three dimensional maps of Ma27 dome.

APPENDIX 2

Analysis of Marius 12 (Ma12) dome

As another example of the complex Marius hills dome field an analysis about Marius 12 dome is described.

1) Starting from the lunar image to rectified view

The image was taken by Phillips on April 18, 2008 at 02:05 UT. The image scale, the solar altitude and the selenographic coordinates are computed using the LTVT software package by Mosher and Bondo (2006). The dome is located at longitude -53.88° and latitude 13.13°. The diameter amounts to 6.4 km and the solar altitude was of 5.3°. According to preceding data, reported in Appendix 1, image scale was determined, using LTVT, as 0.270 km per pixel. The Image is thus transformed in rectified view and rotated so that the apparent solar azimuth incidence is 270º (Carlotto 1996), as shown in Fig. A10.

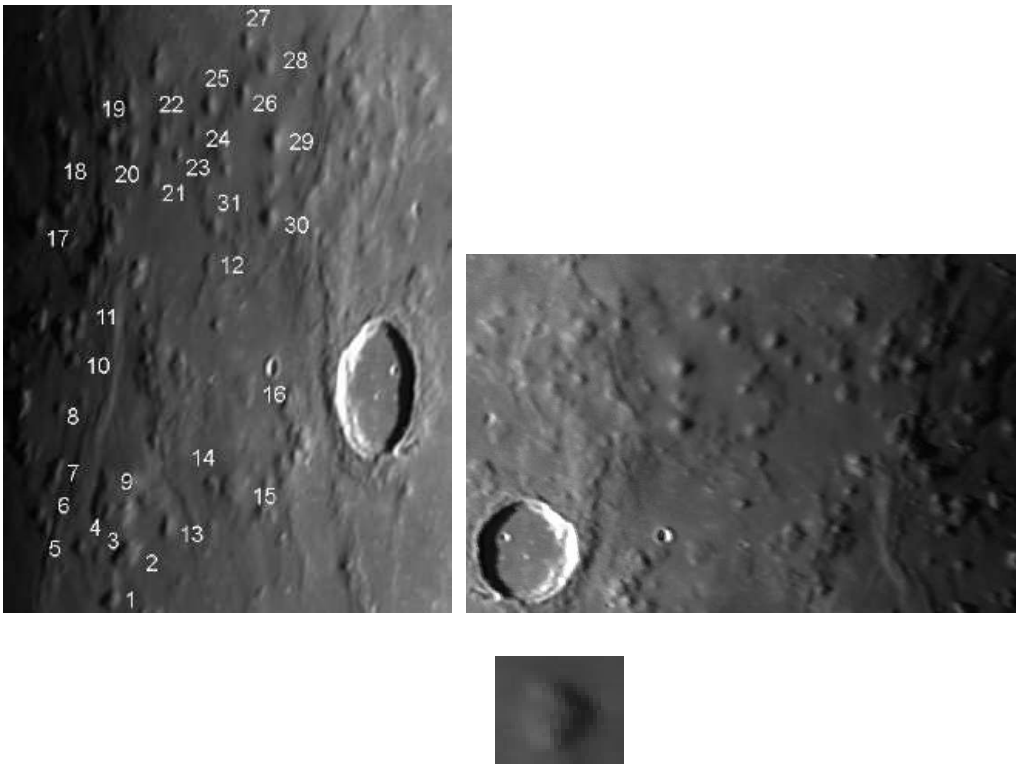

Figure A10. The image taken by Phillips on April 18, 2008 at 02:05 UT. The examined dome is termed as Marius 12 in the above image. To the top the calibrated image based on the UCLN 1994 list of control points. To the centre the rectified view obtained using LTVT software package (the dome is clearly visible to the centre of the image) and to the bottom the ROI of Ma12, here enlarged.

In this case the dome cast a shadow on the soil and the intensity profile observed in the image allows for an estimation of the shadow offset, determined as 29 grey level.

The rectified image was then processed using the math and image calculator features under the Process menu of Image J: thus the corresponding "shadow offset" was subtracted. The resulting image was saved as image txt format and then imported into Excel.

2) DEM corrected for lunar curvature

An automated Excel spreadsheet is used for the computation. The corresponding Image pixel value map, as txt format, is introduced.

The Excel computation, based on Carlotto algorithm, yields H=171 m.

Image scale:	270	meters/px		27	meter/px	uncertainty		
Solar altitude:	5.3	degrees		34.7	Zenith angle degrees			
DEM Max:	171.0	DEM Avg:	42.24248	Eleva-tions	No. rows:	27	No. cols:	32

According with the method described in detail by Evans (2006) and Fisher (2007), the computation yields the gradient elevation maps and the DEM (cf. Appendix 1 for an example of spreadsheet).

The contribution to dome height caused by lunar curvature is taken into account (Fig. A11) and is subtracted yielding, for the diameter of 6.4 km, $H_{Carlotto}$=167 m.

Feature dia. (km)	**Lunar sphere contribution to feature height**
6.4	2.9
6.65	3.2
6.9	3.4

Figure A11. The contribution to dome height (2.9 km) caused by lunar curvature is subtracted yielding $H_{Carlotto}$=167 m.

The DEM, as txt format, is then corrected for lunar curvature using Image J math option, yielding the final DEM derived from the Carlotto method. The graphing function in Excel can be used to generate x, z plots along any desired y row, as described in Appendix 1.

3) Correction formula: computed height

Assuming L(α)=0.95, for a phase angle of about 26.9°, the empirical formula yields :

- For λ_1 $H_{corrected}$= 237.2 m
- For λ_2 $H_{corrected}$= 226.8 m
- For λ_3 $H_{corrected}$= 219.9 m

The deviation is explained in section 4 and 5. The mean, using the procedure (b) reported in section 7, is calculated as 228.0 m. Since the standard deviation amounts to σ= 8.68, the true height is comprised at a probability of 95% between the mean value ± 2σ, i. e. in the interval between 210 m and 245 m. Hence the uncertainties are smaller than 10%. Therefore $H_{corrected}$ can be assessed as 228 m in good agreement with the full lunar Lambert law (220 m).

The average flank slope ξ is thus determined according to:

$\xi = \arctan 2H/D$

The slope amounts to 4.0° using the empirical formula, while with Carlotto algorithm it amounts only to 2.9°.

4) Final DEM and 3D reconstruction

The conversion factor P_c is derived yielding

$P_c = (H_{correction\ formula} / H_{Carlotto}) = 1.36$

The original Carlotto DEM, saved as a txt file, is imported in Image J and then multiplied with the resulting factor P_c, using the math and image calculator features under the Process menu of Image J.

This procedure yields a new DEM, which is compared to initial $DEM_{carlotto}$ (Fig. A12).

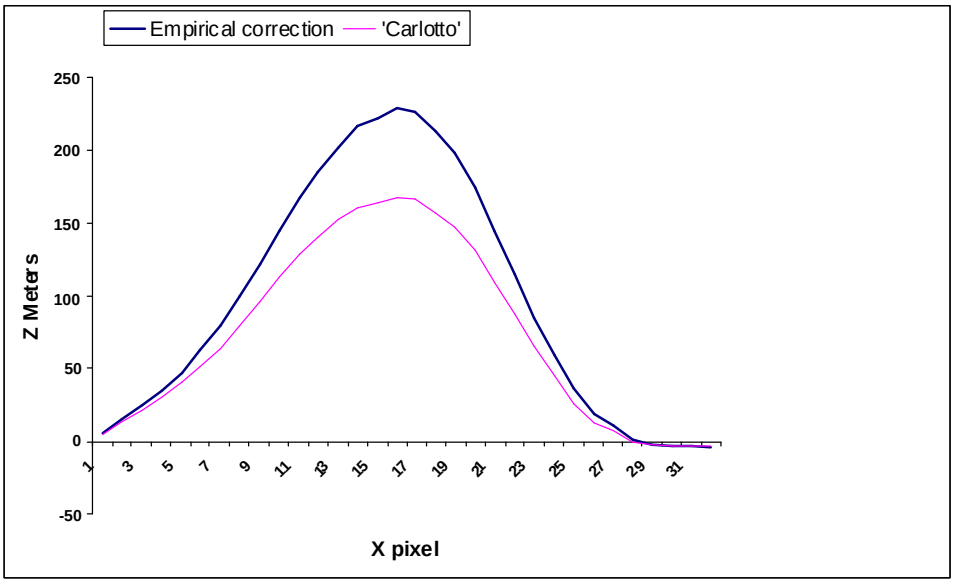

Figure A12. The DEMs of Ma12 for row 17 derived from Carlotto algorithm (red curve) and the empirical formula (blue curve).

Finally, for surface reconstruction the final DEM image, as txt file format, is imported into Image J as a height field map and utilized to generate a three dimensional map of the dome surface (cf. Fig A13).

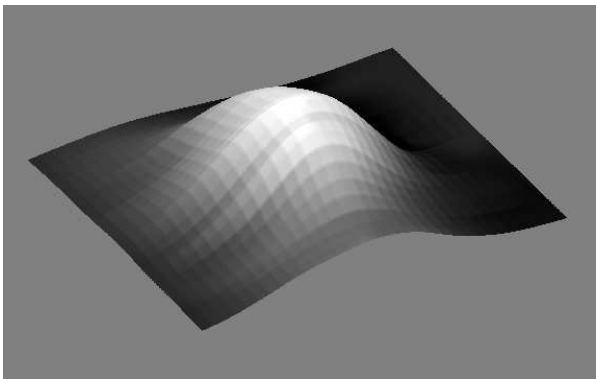

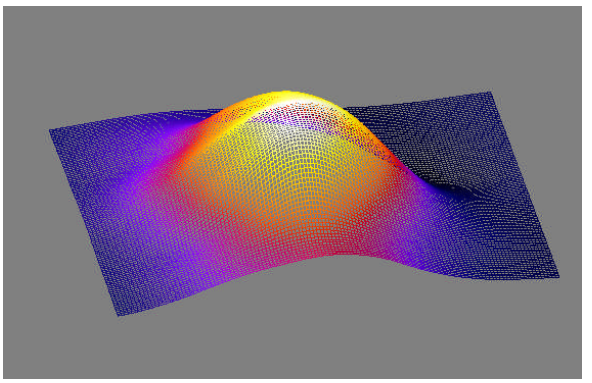

Figure A13.Three dimensional maps of Ma12 dome.

APPENDIX 3

Analysis of Birt 1(Bi1) dome

As another example of the computation steps I describe also the analysis about Birt 1 dome.

1) Starting from the lunar image to rectified view and shadow offset

The image was taken by C. Wöhler on April 25, 2007, at 19:48 UT using a 200 mm Newtonian reflector and a Lumenera LU75M CCD camera.

The dome diameter of Birt 1 amounts to 16.0 ± 0.5 km. The image scale, the solar altitude and the selenographic coordinates are computed using the LTVT software package by Mosher and Bondo (2006).

This calibration is performed based on the UCLN 1994 list of control points. The dome is located at longitude -9.66° and latitude 20.73°. The solar altitude was of 1.48°. Image scale was determined, using LTVT, as 0.450 km per pixel. The Image is thus transformed in rectified view and the corresponding "shadow offset" was subtracted. The resulting image, as described in detail in Appendix 1, was rotated, saved as image txt format and then imported into Excel.

The ROI of Bi1 dome, here enlarged, is shown in Fig A14.

Figure A14. The ROI of Bi1 dome, here enlarged and rotated according to Carlotto method with offset subtraction applied.

2) DEM corrected for lunar curvature

An automated Excel spreadsheet is used for the computation. The corresponding Image pixel value map, as txt format, is introduced and is reported in Fig. A15.

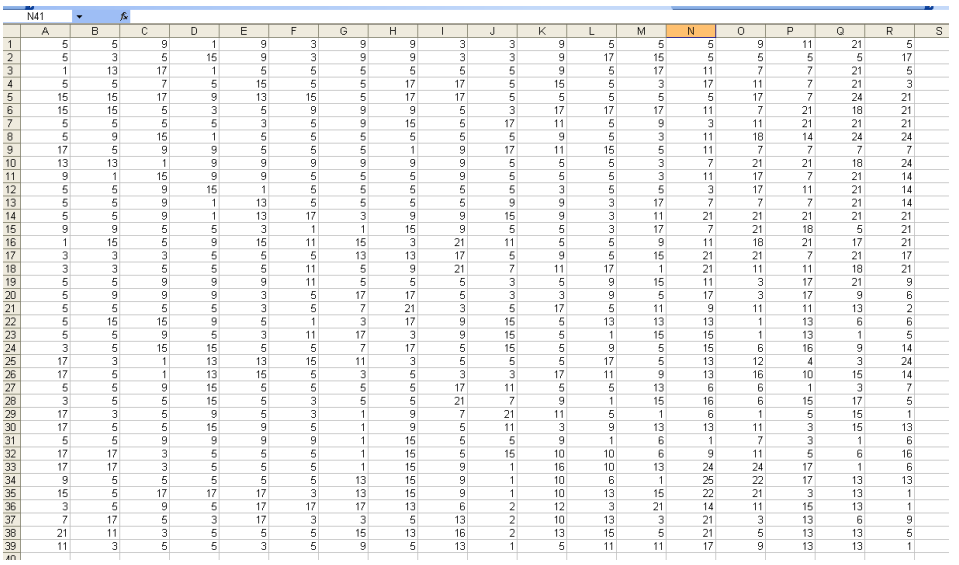

	A	B	C	D	E	F	G	H	I	J	K	L	M	N	O	P	Q	R	S
1	5	5	9	1	9	3	9	9	3	3	9	5	5	5	9	11	21	5	
2	5	3	5	15	9	3	9	9	3	3	9	17	15	5	5	5	5	17	
3	1	13	17	1	5	5	5	5	5	5	9	5	17	11	7	7	21	5	
4	5	5	7	5	15	5	5	17	17	5	15	5	3	17	11	7	21	3	
5	15	15	17	9	13	15	5	17	17	5	5	5	5	5	17	7	24	21	
6	15	15	5	3	5	9	9	9	5	3	17	17	17	11	7	21	18	21	
7	5	5	5	5	3	5	9	15	5	17	11	5	9	3	11	21	21	21	
8	5	9	15	1	5	5	5	5	5	5	9	5	3	11	18	14	24	24	
9	17	5	9	9	5	5	5	1	9	17	11	15	5	11	7	7	7	7	
10	13	13	1	9	9	9	9	9	9	5	5	5	3	7	21	21	18	24	
11	9	1	15	9	9	5	5	5	9	5	5	5	3	11	17	7	21	14	
12	5	5	9	15	1	5	5	5	5	5	3	5	5	3	17	11	21	14	
13	5	5	9	1	13	5	5	5	5	9	9	3	17	7	7	7	21	14	
14	5	5	9	1	13	17	3	9	9	15	9	3	11	21	21	21	21	21	
15	9	9	5	5	3	1	1	15	9	5	5	3	17	7	21	18	5	21	
16	1	15	5	9	15	11	15	3	21	11	5	5	9	11	18	21	17	21	
17	3	3	3	5	5	5	13	13	17	5	9	5	15	21	21	7	21	17	
18	3	3	5	5	5	11	5	9	21	7	11	17	1	21	11	11	18	21	
19	5	5	9	9	9	11	5	5	5	3	5	9	15	11	3	17	21	9	
20	5	9	9	9	3	5	17	17	5	3	3	9	5	17	3	17	9	6	
21	5	5	5	5	3	5	7	21	3	5	17	5	11	9	11	11	13	2	
22	5	15	15	9	5	1	3	17	9	15	5	13	13	13	1	13	6	6	
23	5	5	9	5	3	11	17	3	9	15	5	1	15	15	1	13	1	5	
24	3	5	15	15	5	5	7	17	5	15	5	9	5	15	6	16	9	14	
25	17	3	1	13	13	15	11	3	5	5	5	17	5	13	12	4	3	24	
26	17	5	1	13	15	5	3	5	3	3	17	11	9	13	16	10	15	14	
27	5	5	9	15	5	5	5	5	17	11	5	5	13	6	6	1	3	7	
28	3	5	5	15	5	3	5	5	21	7	9	1	15	16	6	15	17	5	
29	17	3	5	9	5	3	1	9	7	21	11	5	1	6	1	5	15	1	
30	17	5	5	15	9	5	1	9	5	11	3	9	13	13	11	3	15	13	
31	5	5	9	9	9	9	1	15	5	5	9	1	6	1	7	3	1	6	
32	17	17	3	5	5	5	1	15	5	15	10	10	6	9	11	5	6	16	
33	17	17	3	5	5	5	1	15	9	1	16	10	13	24	24	17	1	6	
34	9	5	5	5	5	5	13	15	9	1	10	6	1	25	22	17	13	13	
35	15	5	17	17	17	3	13	15	9	1	10	13	15	22	21	3	13	1	
36	3	5	9	5	17	17	17	13	6	2	12	3	21	14	11	15	13	1	
37	7	17	5	3	17	3	3	5	13	2	10	13	3	21	3	13	6	9	
38	21	11	3	5	5	5	15	13	16	2	13	15	5	21	5	13	13	5	
39	11	3	5	5	3	5	9	5	13	1	5	11	11	17	9	13	13	1	

Figure A15 The Image pixel value map is obtained after subtraction of shadow offset.

The excel spreadsheet is shown in the figure.

The Excel computation, based on Carlotto algorithm, yields H=160.7 m.

Image scale:	450	meters/px		45	meter/px	uncertainty		
Solar altitude:	1.48	degrees		38.52	Zenith angle degrees			
DEM Max:	160.7	DEM Avg:	13.08876	Eleva-tions	No. rows:	39	No. cols:	55

According with the method described in detail by Evans (2006) and Fisher (2007), and reported in Appendix 1, the computation yields the gradient elevation maps and the DEM. The contribution to dome height caused by lunar curvature is taken into account (Fig. A16) and is subtracted yielding, for the diameter of 16 km, $H_{Carlotto}$=142.3 m.

Feature dia. (km)	**Lunar sphere contribution to feature height**
16.0	18.4
16.25	19.0
16.5	19.6

Figure A16. The contribution to dome height caused by lunar curvature is subtracted yielding $H_{Carlotto}$=142.3 m.

The DEM, as txt format is then corrected for lunar curvature using Image J math option, yielding the final DEM derived from the Carlotto method. The graphing function in Excel can be used to generate x, z plots along any desired y row, as described in Appendix 1.

3) Correction formula: computed height

Assuming L(α)=0.75, for a phase angle of about 72°, the empirical formula yields :

- For λ_1 $H_{corrected}$= 169.7 m
- For λ_2 $H_{corrected}$= 175.1 m
- For λ_3 $H_{corrected}$= 169.8 m

The mean, using the procedure (c) in section 7, is calculated as 171.5 m. Since the standard deviation amounts to σ= 3.0, the true height is comprised at a probability of 95% between the mean value ± 2σ, i. e. in the interval between 165 m and 177 m.

Using a value of L(α)=0.8, the derived height as mean yields 172.5 m.

Therefore $H_{corrected}$ for Birt 1 dome can be assessed as 172 m, according to full Lunar Lambert law (170 m).

APPENDIX 4

Analysis of the Valentine dome (V1)

1) Starting from the lunar image to rectified view and shadow offset

The procedure described in detail in Appendix 1 was used. The image was taken by the author on May 1, 2009, at 19:21 UT using a 180 mm Maksutov Cassegrain and a Lumenera LU75M CCD camera (Fig. A17).

The dome diameter amounts to 30 ± 0.5 km. The image scale, the solar altitude and the selenographic coordinates are computed using the LTVT software package by Mosher and Bondo (2006). This calibration is performed based on the UCLN 1994 list of control points.

The dome is located at longitude 10.07° and latitude 30.84°. The solar altitude was of 6.1°. Image scale was determined, using LTVT, as 0.370 km per pixel.

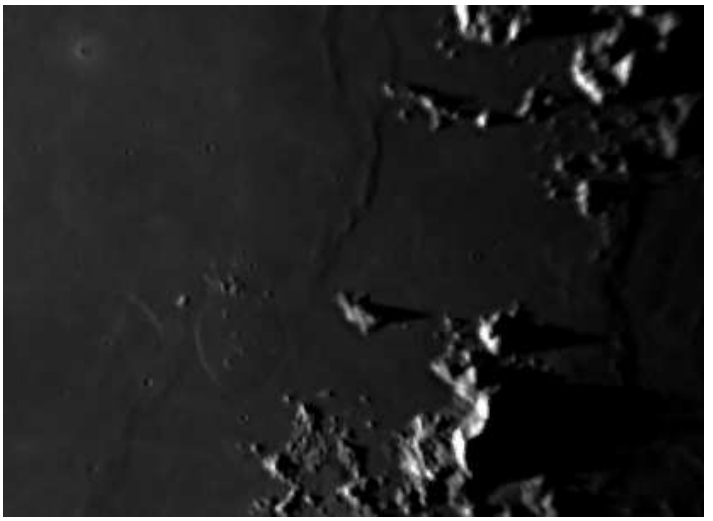

Figure A17. This image was taken by the author on May 1, 2009, at 19:21 UT.

According with the method reported in Appendix 1, the computation yields the gradient elevation maps and the DEM. The contribution to dome height caused by lunar curvature is taken into account (67 km) and is subtracted yielding, for the diameter of 30 km, $H_{Carlotto}$=214 m for all the surface (including the hills located on the summit).

Assuming L(α)=0.75, for a phase angle of about 90°, the empirical formula yields :

H= 270 m, which is referred to the full surface reconstruction.

The conversion factor P_c is derived yielding

$P_c = (H_{correction\ formula} / H_{Carlotto}) = 1.2723$

The original Carlotto DEM, saved as a txt file, is imported in Image J and then multiplied with the resulting factor P_c, using the math and image calculator features under the Process menu of Image J.

This procedure yields a new DEM. For surface reconstruction the final DEM image, as txt file format, can be imported into Image J as a height field map (Tiff image at 32 bit) and utilized to measure the heights for all the surface as shown in the figure A18.

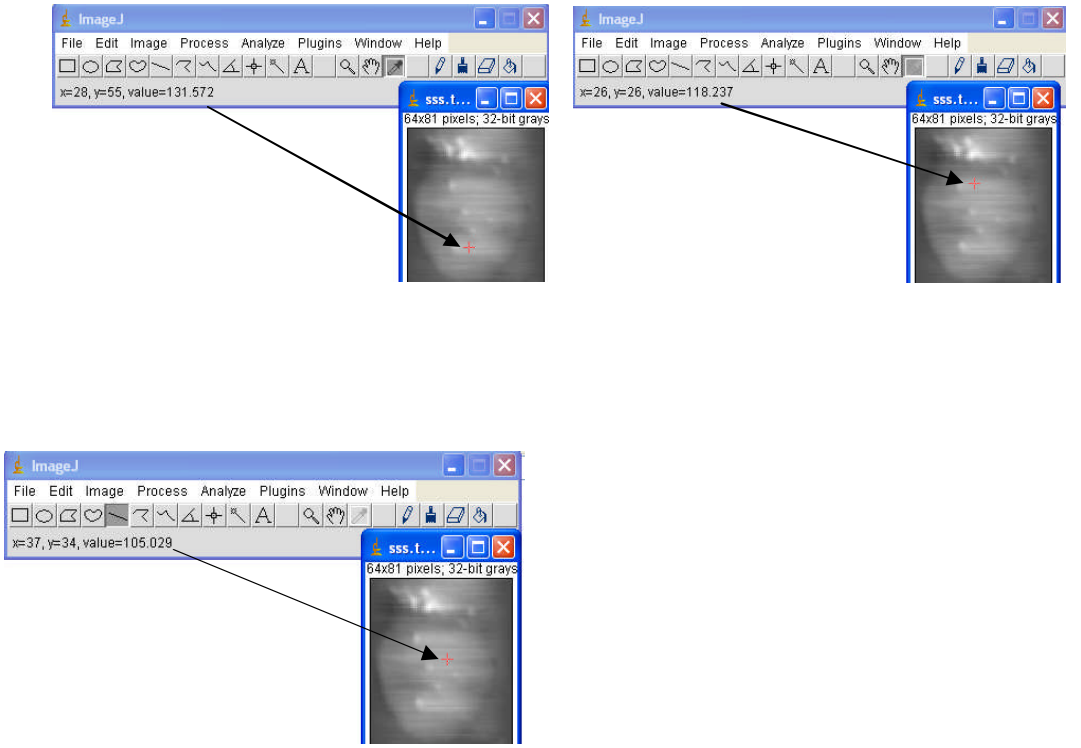

Figure A18. Height field map for several measurements.

Therefore $H_{corrected}$ for Valentine dome is computed as 131 m, excluding the hills located on its summit, according to full Lunar Lambert law (130 m).

Finally, the DEM can be used to generate a three dimensional map of the dome (Fig. A19).

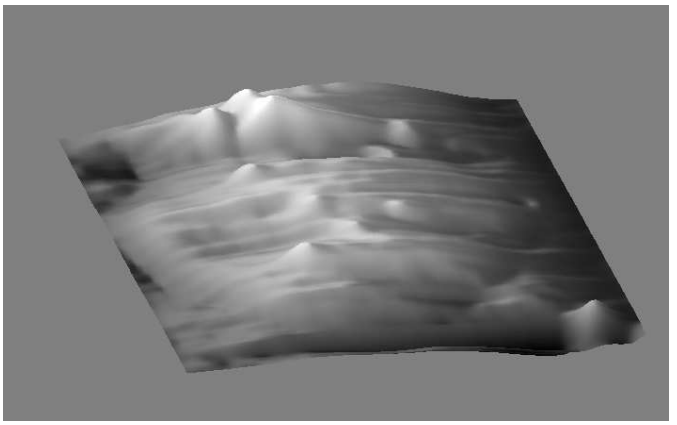

Figure A19.Three dimensional map of Valentine dome.

An Impact on Jupiter and Evolution of the Dark Spot

Report by Raffaello Lena, GLR group

1. Introduction

The lunar surface has been formed by impacts. Since we cannot observe large impacts on the Moon, it is quite illustrative to report on such an impact on another body of our solar system. A celestial body has impacted into Jupiter on July 2009, leaving behind a black spot in the planet's atmosphere. This is the second time such an impact has been observed. The first time was 15 years ago, when more than 20 fragments of the comet Shoemaker-Levy 9 (SL9) collided with Jupiter.

Anthony Wesley from Australia discovered the impact on 19 July, 2009, at 13:30 UT, using an 14.5-inch (36.8 cm) diameter telescope (http://jupiter.samba.org/).

The Alert was sent to NASA Jet Propulsion Laboratory. Infrared observation by Keck

(http://www.berkeley.edu/news/media/releases/2009/07/21_bruise.shtml)

and NASA Infrared Telescope Facility (IRTF) at Mauna Kea

(http://www.jpl.nasa.gov/news/news.cfm?release=2009-112)

showed a bright spot where the impact took place, indicating that the impact warmed a 190 million square km area near Jupiter's south pole. Using near-infrared wavelengths the spot's prominence indicates that it is composed of high-altitude aerosols similar to those seen during the SL9 impact. The spot was captured also by Hubble telescope on July 23:

(http://hubblesite.org/newscenter/archive/releases/2009/23/image/a/).

The combination of the Hubble data with mid-infrared images from ground-based telescopes will give an insight into changes of the vertical structure of Jupiter's atmosphere due to the impact. The object that caused the impact scar could have been a small comet or asteroid. A day after its discovery, the dark spot in Jupiter's cloud was easy to see through small telescopes. Appendix 1 reports images taken by Hubble, Gemini and Keck II telescopes. Appendix 2 describes some data of the Shoemaker-Levy 9 impacts of July 1994 for comparison.

2. Observations

A survey was carried out following a GLR group program of observations, including polar and cylindrical projections. This first note reports the evolution and spreading of the cloud as the Jovian winds smear the spot. Single reports and further data are provided on the following next pages (cf. section “Observations of the impact scar”).

The impact site is the very dark spot at the south of Jupiter's disk, as reported by Antonello Medugno (Italy) on July 20, Zac Pujic (Australia) on July 20 and Jim Phillips (USA) on July 21. Further data were obtained by Raffaello Lena, Paolo Lazzarotti and Carmelo Zannelli (Italy) on July 22 with independent observations, Zac Pujic (Australia) on July 22, Jim Phillips (USA) and George Tarsoudis (Greece) on July 23 and Maurice Collins (New Zealand) on July 25.

The fragment impacted Jupiter at 56.9° southern latitude and 216.0° longitude (System II).

The shape of the feature shows a dark oval nucleus and an arc of ejecta, as also shown by observation made with the Keck telescope and other ground-based telescopes. Turbulence and jet streams in Jupiter's atmosphere caused the dark cloud to spread out.

The core has remained black, and become more elongated. The ejecta arc became blurred, appearing as a small patch following the core. On July 27 the core appeared as two condensed nuclei rather than a single dark spot stretched by the local jet stream (Raffaello Lena and Paolo Lazzarotti Italy). Images taken on July 30 showed that the impact site was spreading out in a rather ” > “ shape (Raffaello Lena and Paolo Lazzarotti Italy).

The black core extended in longitude like a short streak composed of two edges.

The northern edge extended to 54° southern latitude while the southern edge, centred at 202.8 ° longitude (system II), extended to 58.5° southern latitude.

Images taken on August 1 show an evolution: a defragmentation into three parts while the streaks have curved around to enclose a light oval. Another explanation is that this oval could be a transient hole between the independently drifting dark streaks.

However, the black core extended westward while a small patch of dark material was detectable northward and in the opposite direction (Raffaello Lena and Paolo Lazzarotti Italy). Images taken on August 3 (George Tarsoudis) showed four spots: three distinct spots were arranged in a linear formation and another spot appeared just to the north. The image showed them as disconnected features.

3. Evolution of the dark spot

The expansion of the dark spot was obvious, from both the N and S edges.

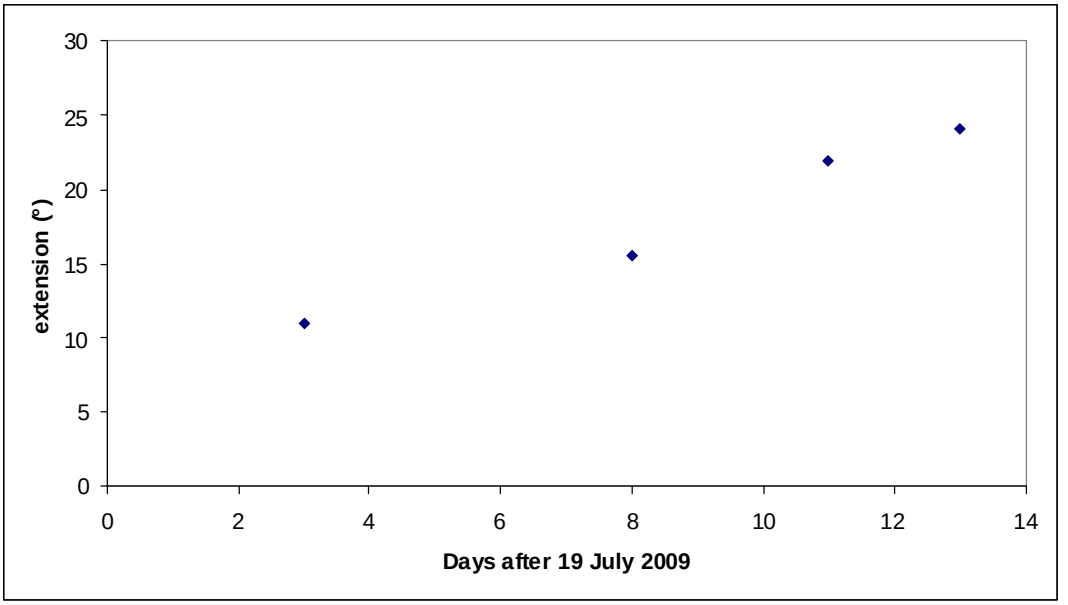

The core of the site has remained almost stationary (with a computed drift of DL2 of about -4 degrees/mouth).

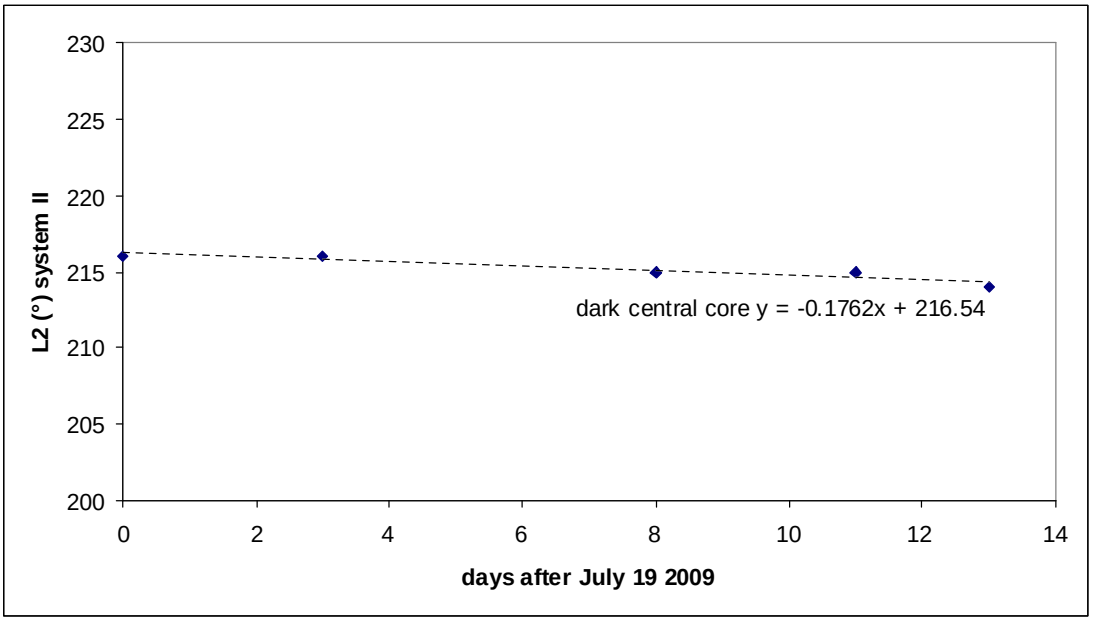

The N and S edges are prograding and, from July 22 to August 1, the complex elongated gradually to the east and west, as visible in the charts below.

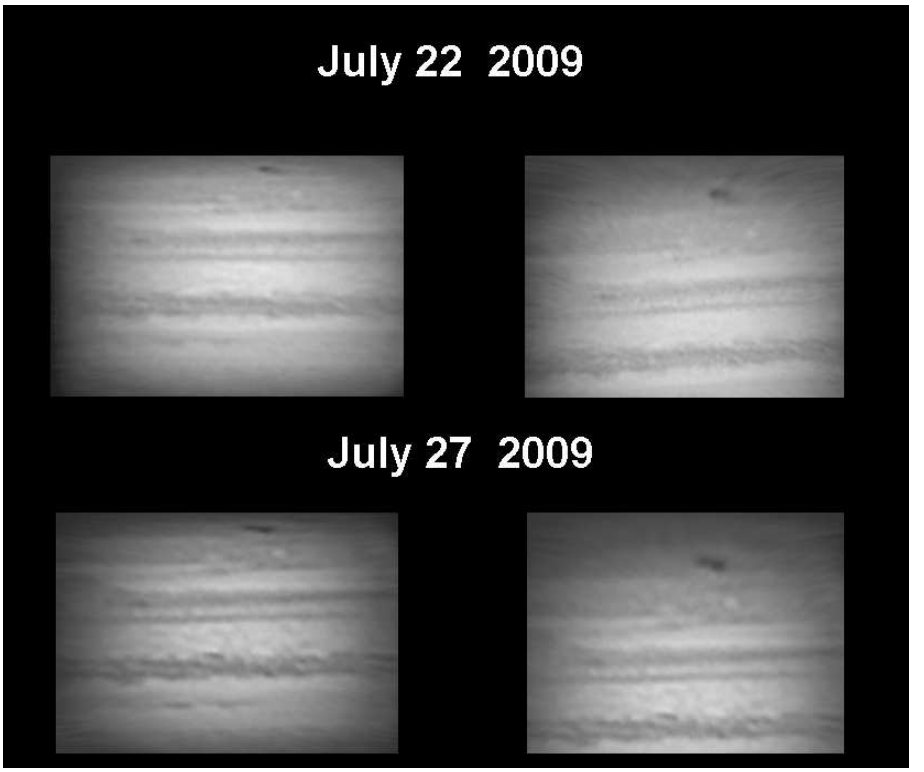

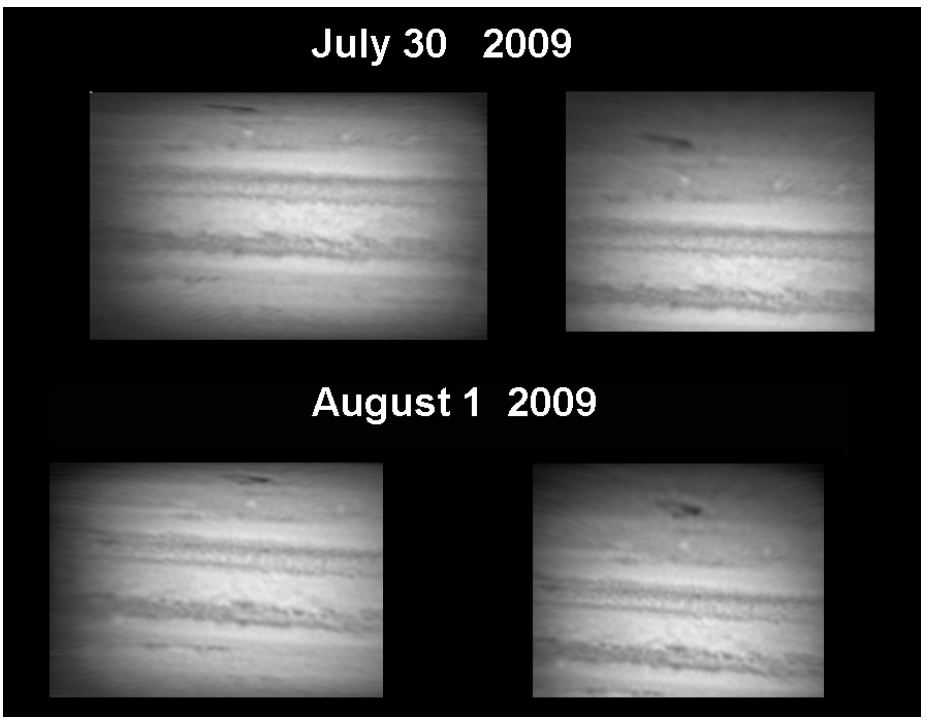

The impact site was still nearly black as on August 1st but became fainter in the following days as it stretched out.

Data from August 15 show evidence that the impact remnant has faded. The pale markings are disappearing.

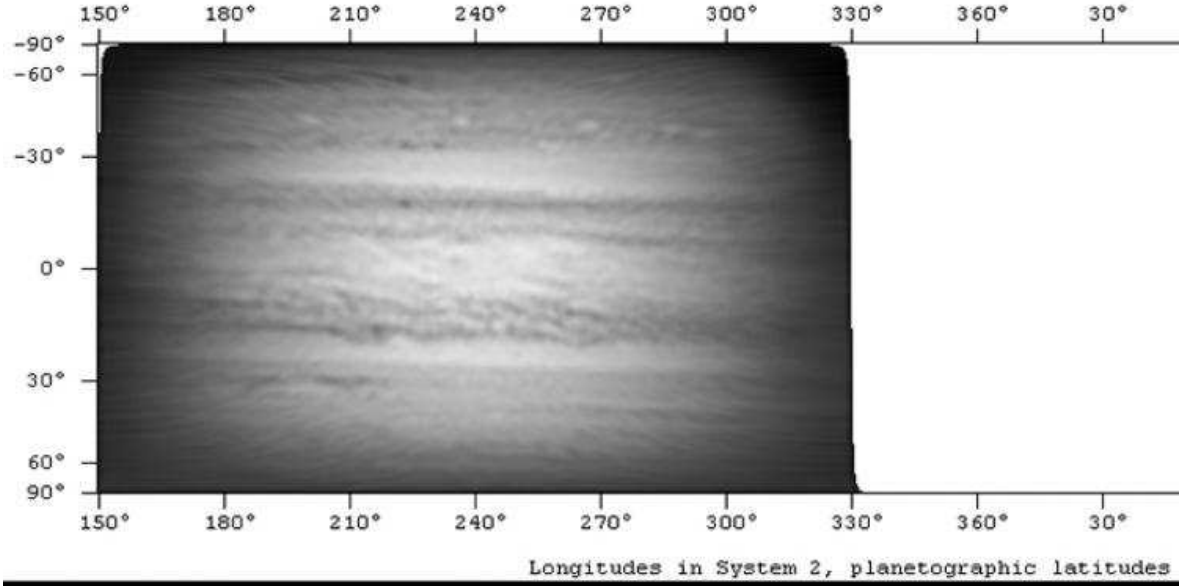

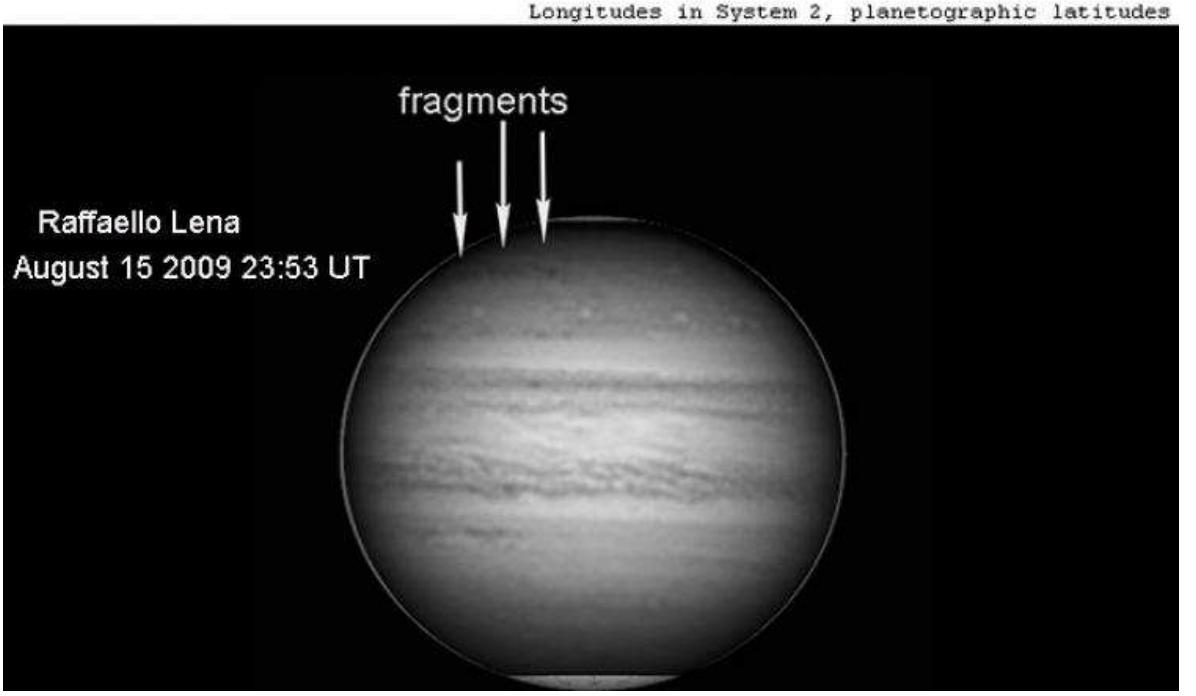

Image above shows the elongated fragments of the impact scare.

Observations of the Impact scar

July 20 2009

by Antonello Medugno (Italy)

Images taken on July 20, 2009 at 01:08 UT (R+Ir), 01:12 UT(RGB) and 02:13 UT (R+Ir) respectively with the impact scar.

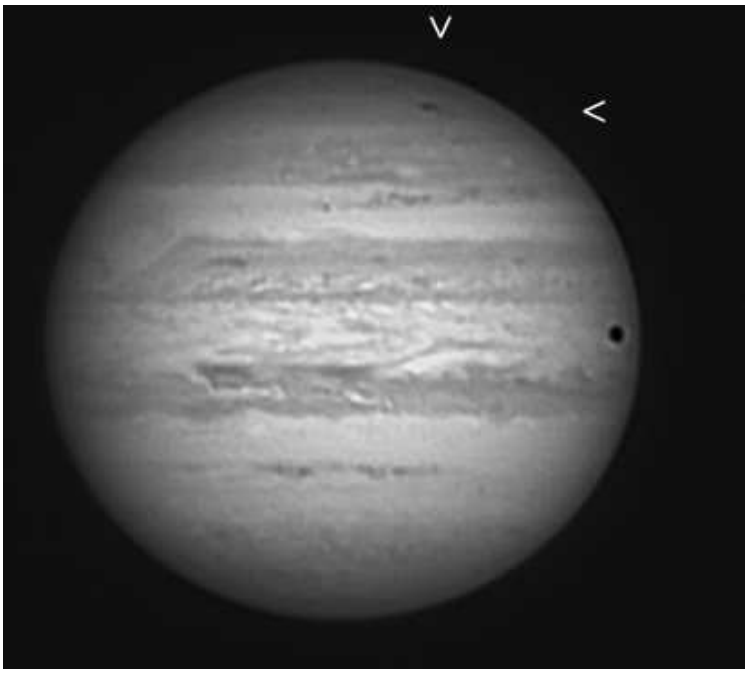

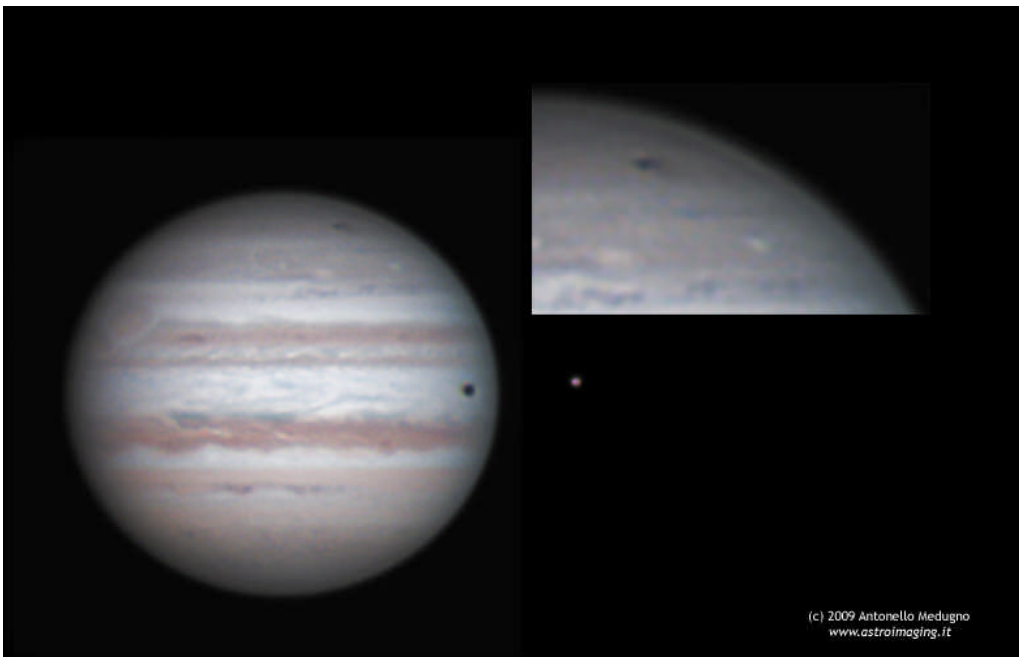

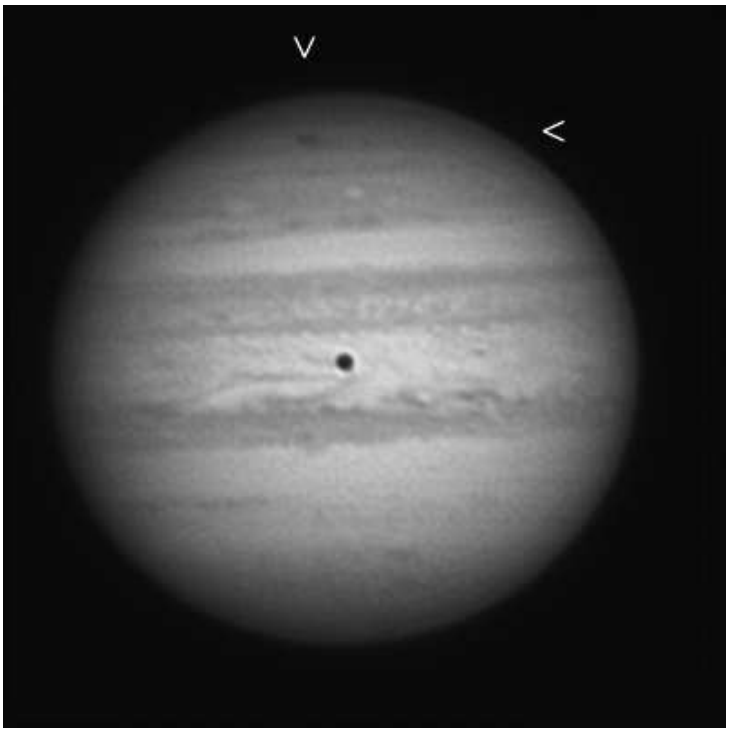

by Zac Pujic (Australia)

Images from July 20, 2009. The impact site is best visible in the RGB and near-infrared images. The methane band image shows the impact site is bright indicating that the debris is at a high elevation in the Jovian atmosphere.

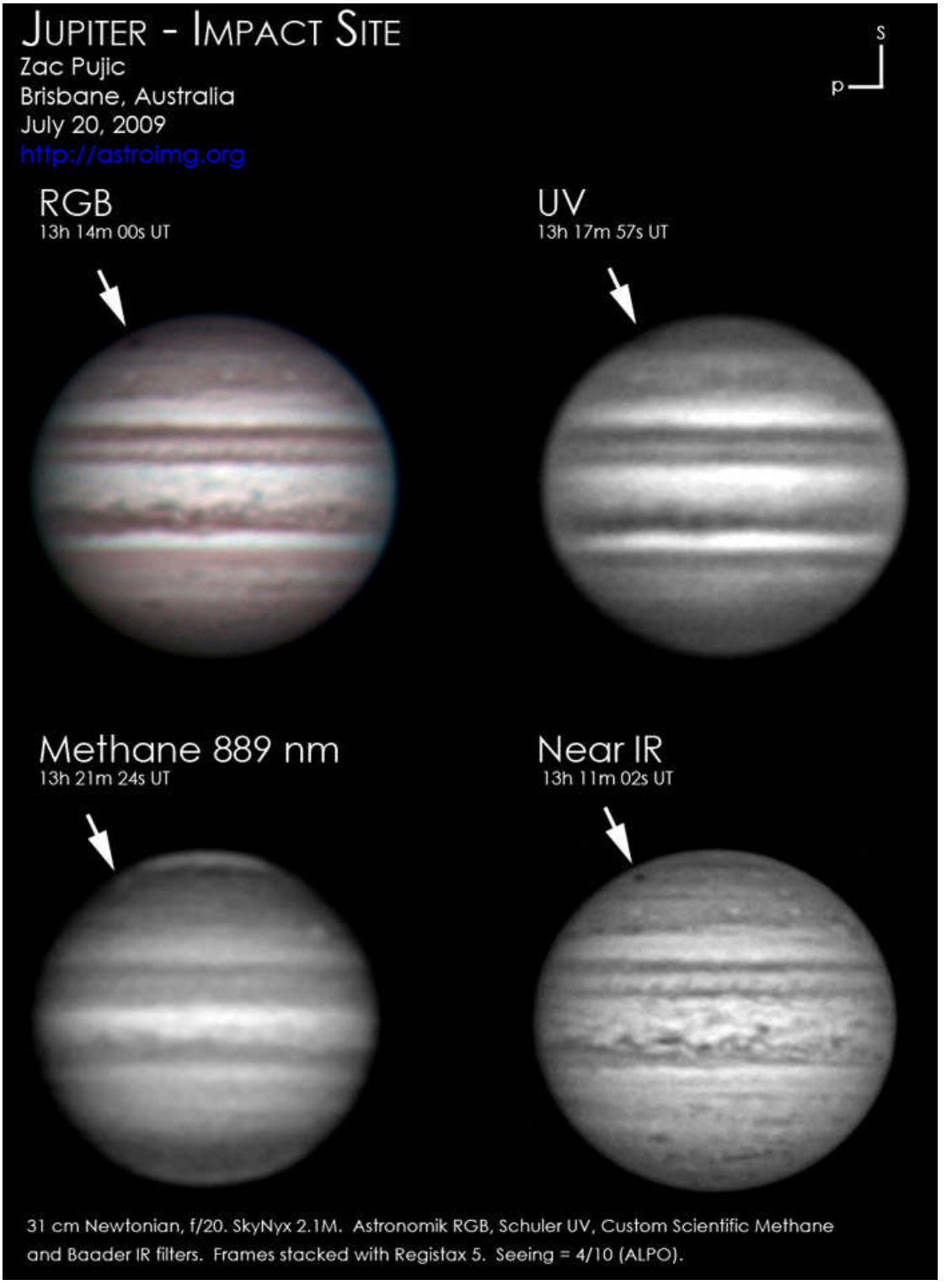
JUPITER - IMPACT SITE
Zac Pujic
Brisbane, Australia
July 20, 2009
http://astroimg.org
S
p
RGB
13h 14m 00s UT
UV
13h 17m 57s UT
Methane 889 nm
13h 21m 24s UT
Near IR
13h 11m 02s UT
31 cm Newtonian, f/20. SkyNyx 2.1M. Astronomik RGB, Schuler UV, Custom Scientific Methane and Baader IR filters. Frames stacked with Registax 5. Seeing = 4/10 (ALPO).

July 21 2009

by Jim Phillips (USA)

Images taken on July 21, 2009 at 01:08 UT.

It is shown the dark spot due to the impact occurred into Jupiter.

July 22 2009

by Raffaello Lena (Italy)

Maksutov Cassegrain 18 cm Lumenera LU075 M, with the impact spot.

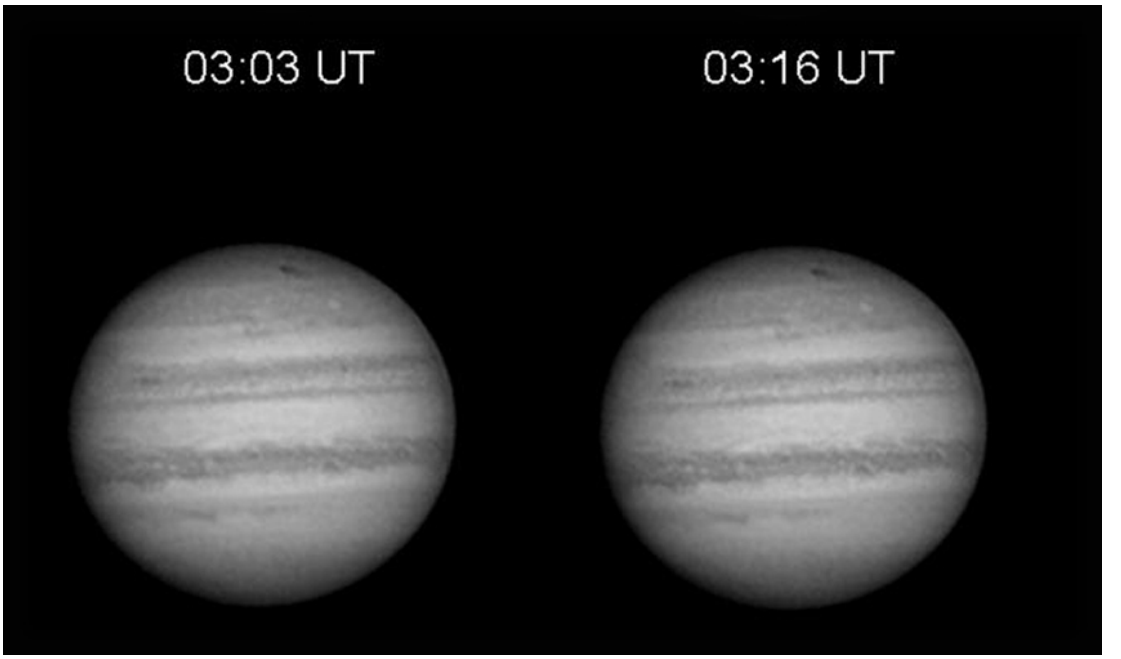

by Paolo Lazzarotti (Italy)

I used a couple of my friends' scopes to grab the dark spot here under very difficult weather conditions, but I feel this image can be of some help nonetheless for the measurement.

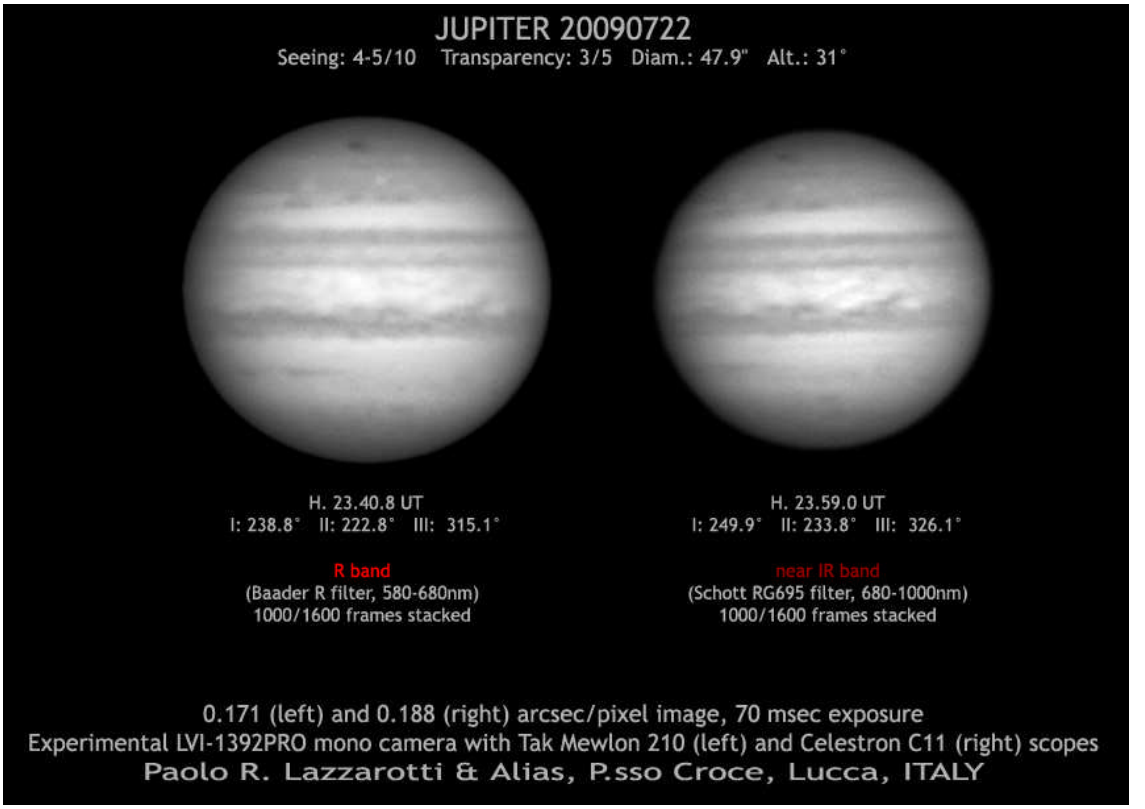

by Carmelo Zannelli (Italy)

My first Jupiter capturing attempt under very poor to poor seeing and transparency conditions.

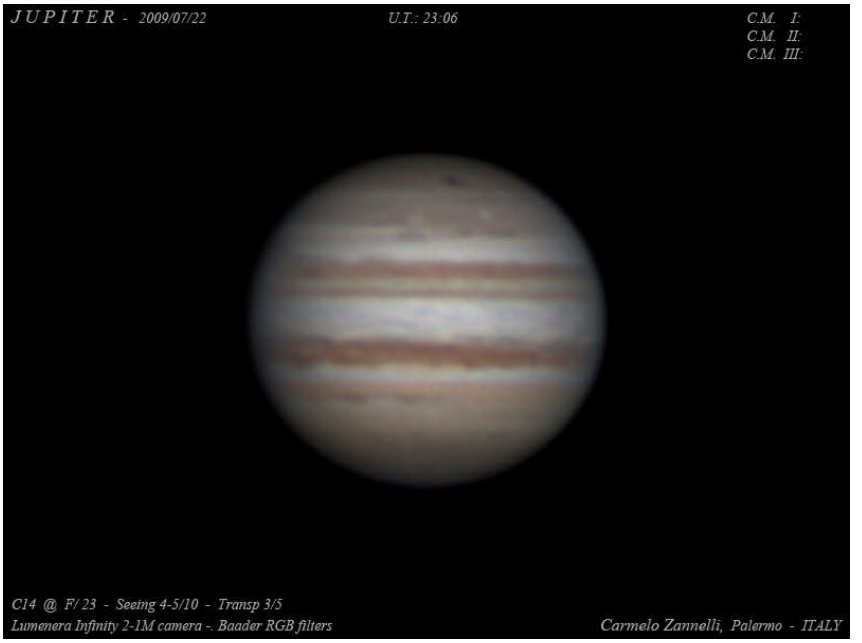

by Zac Pujic (Australia)

Image taken on July 22, 2009, with a polar view.

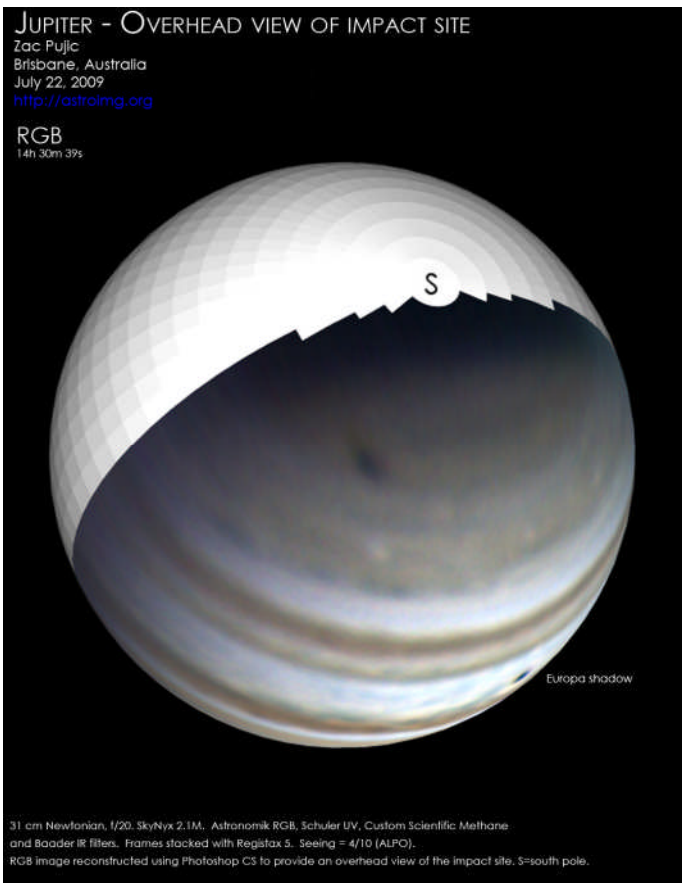

July 23 2009

by Jim Phillips (USA)

I started imaging before the Impact site rotated into view and ended with this one near the CM.

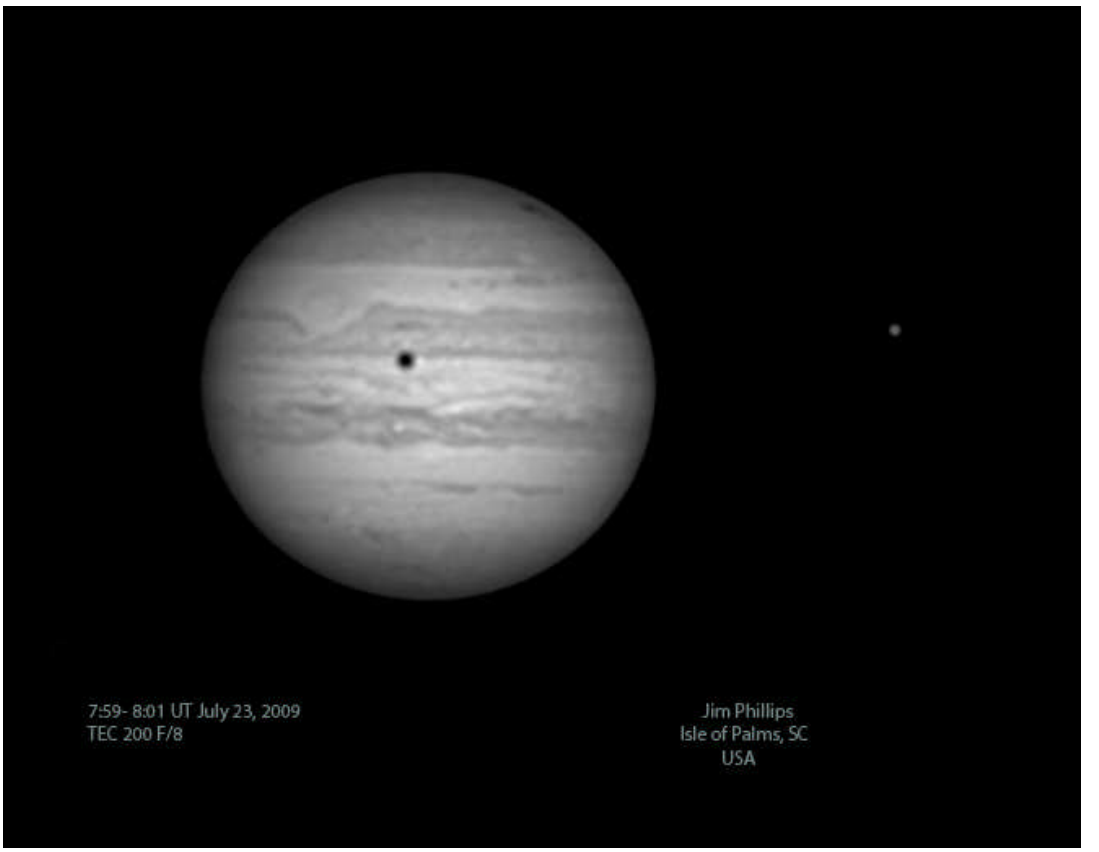

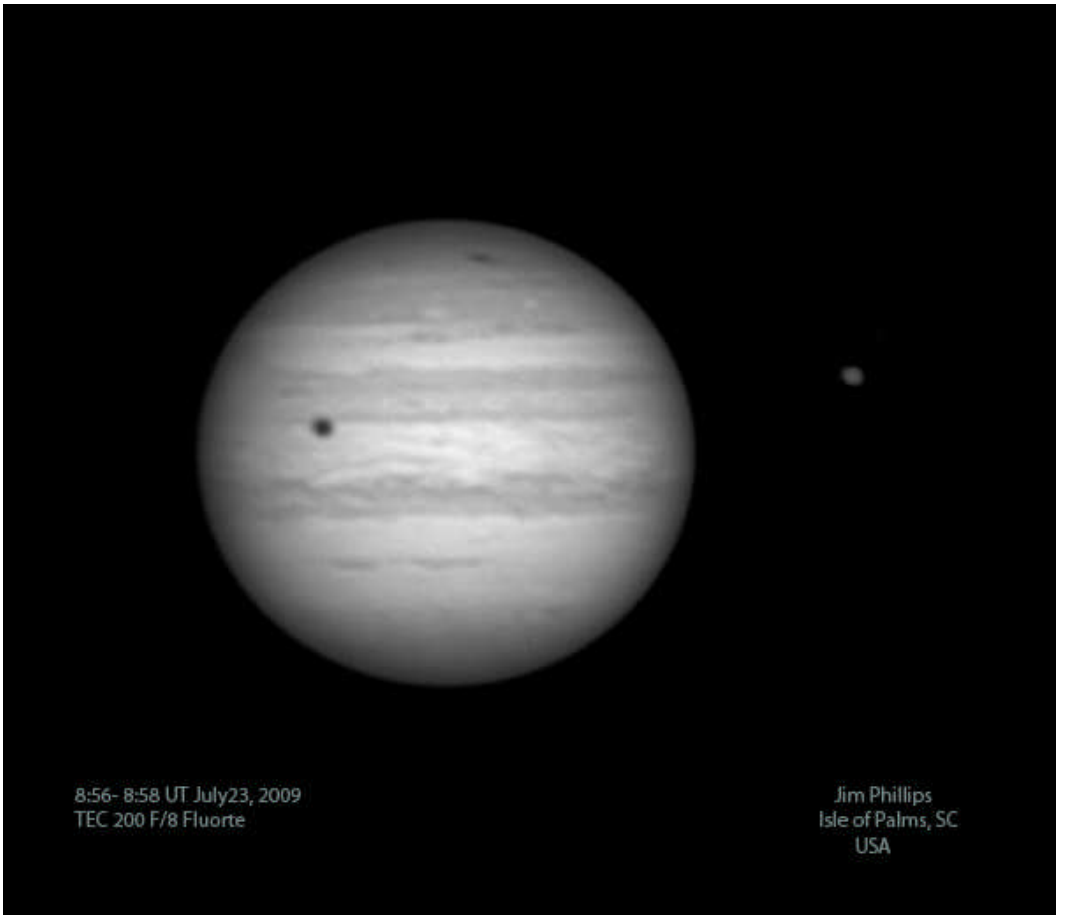

by George Tarsoudis (Greece)

Captures made on July 23, 2009: two hours record of L-RGB videos but with poor seeing.
An animation is linked at

http://astroforum.gr/var/090723_jupiter_tar.gif

Images of the sequence, shown below, were taken at 22:56 UT and 23:41 UT respectively using a Newtonian 250 mm telescope.

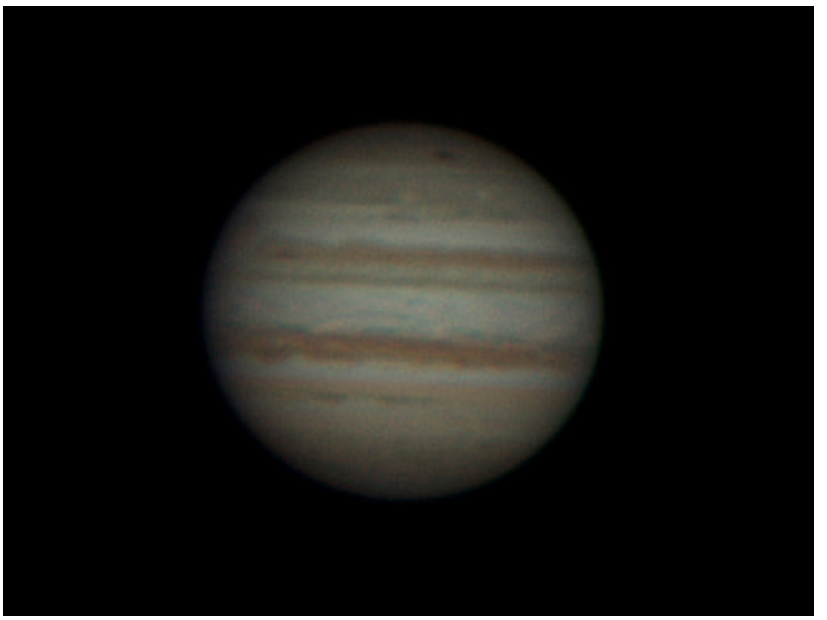

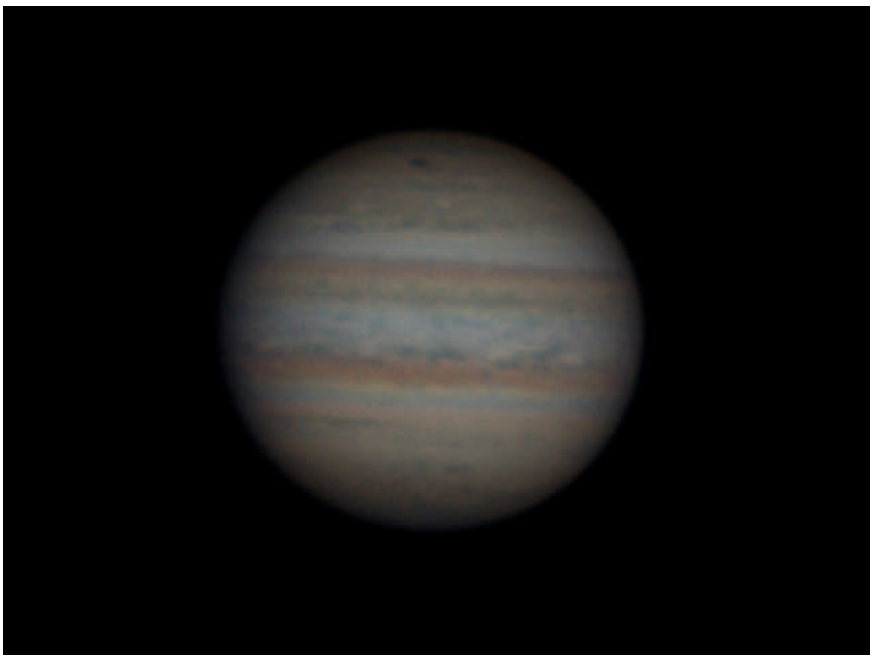

July 25 2009

by Maurice Collins Palmerston North (New Zealand)

Image taken on July 25, 2009.

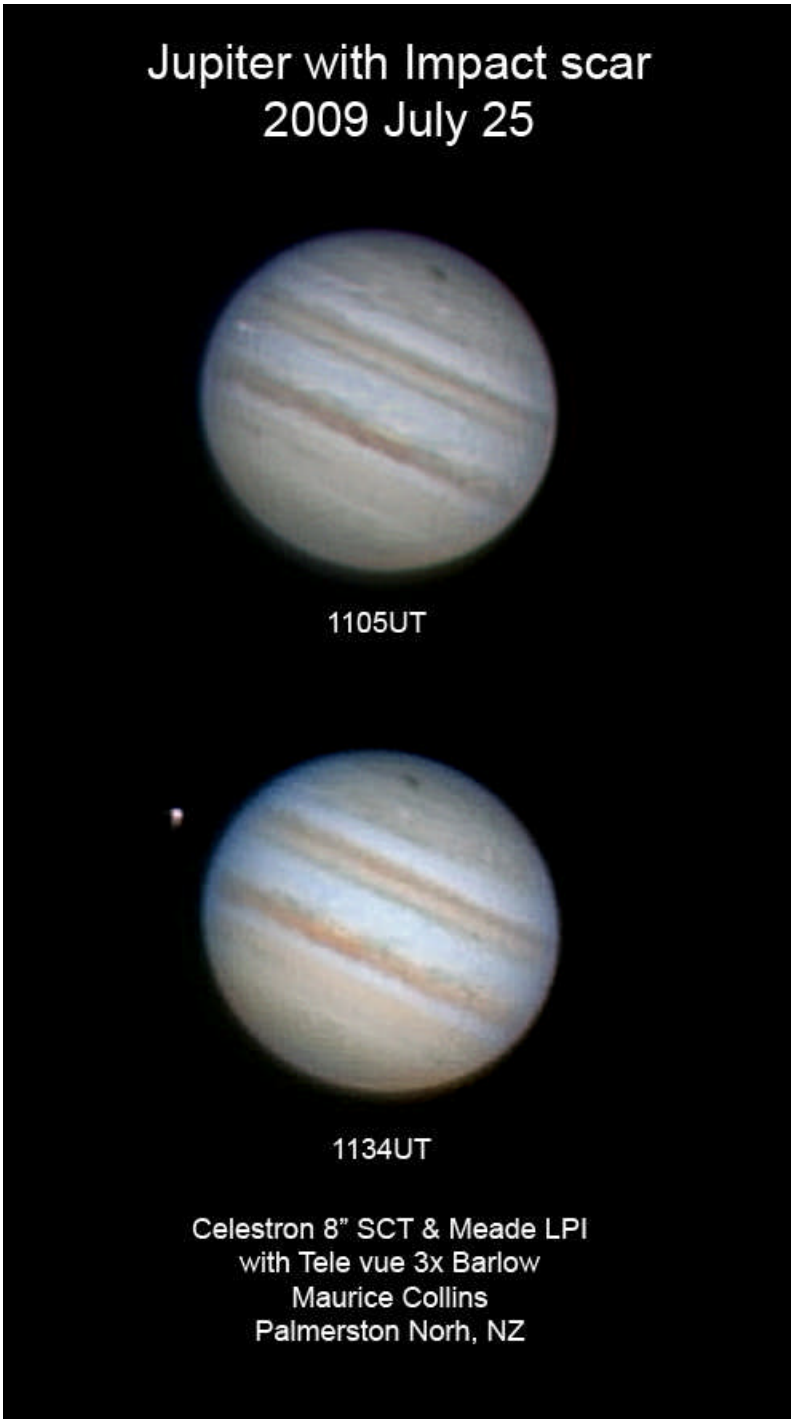

July 27 2009

by Raffaello Lena (Italy)

On July 27th, the Jupiter impact site has evolved and now contained two condensed nuclei. Images taken with a TMB 13 cm refractor and Lumenera LU075 M.

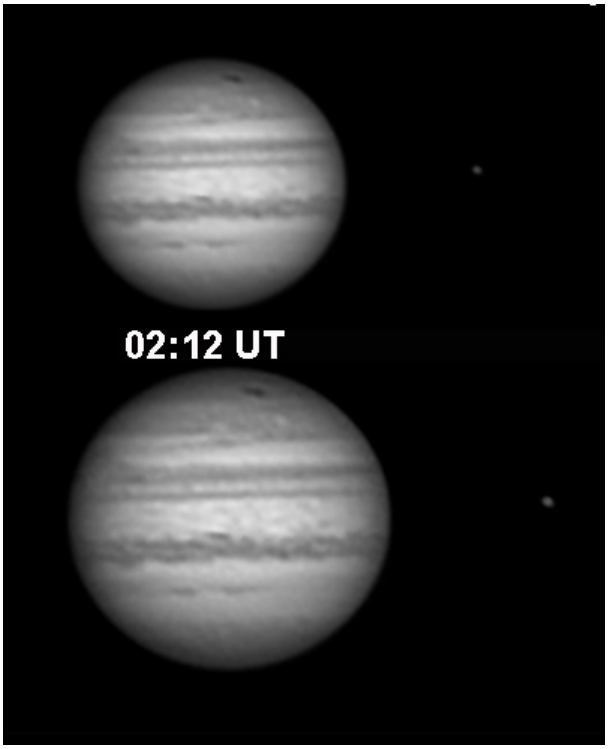
02:12 UT

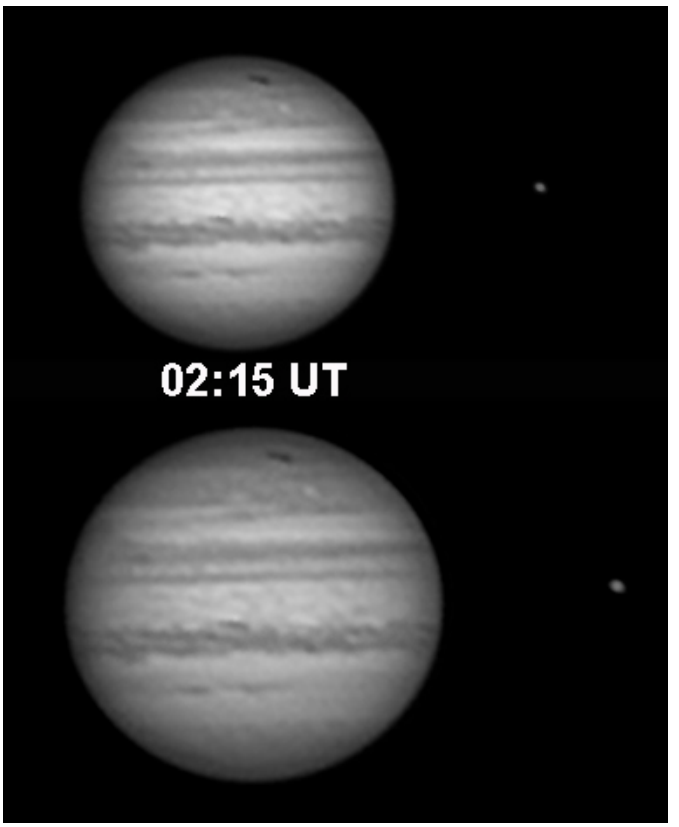
02:15 UT

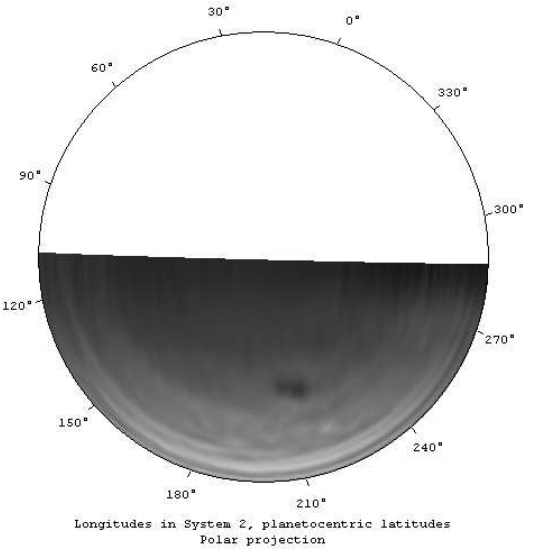

by Paolo Lazzarotti (Italy)

The impact area was very evident at the eyepiece and looks like a solar spot with two well condensed nuclei rather than a single dark spot stretched by the local jet stream.

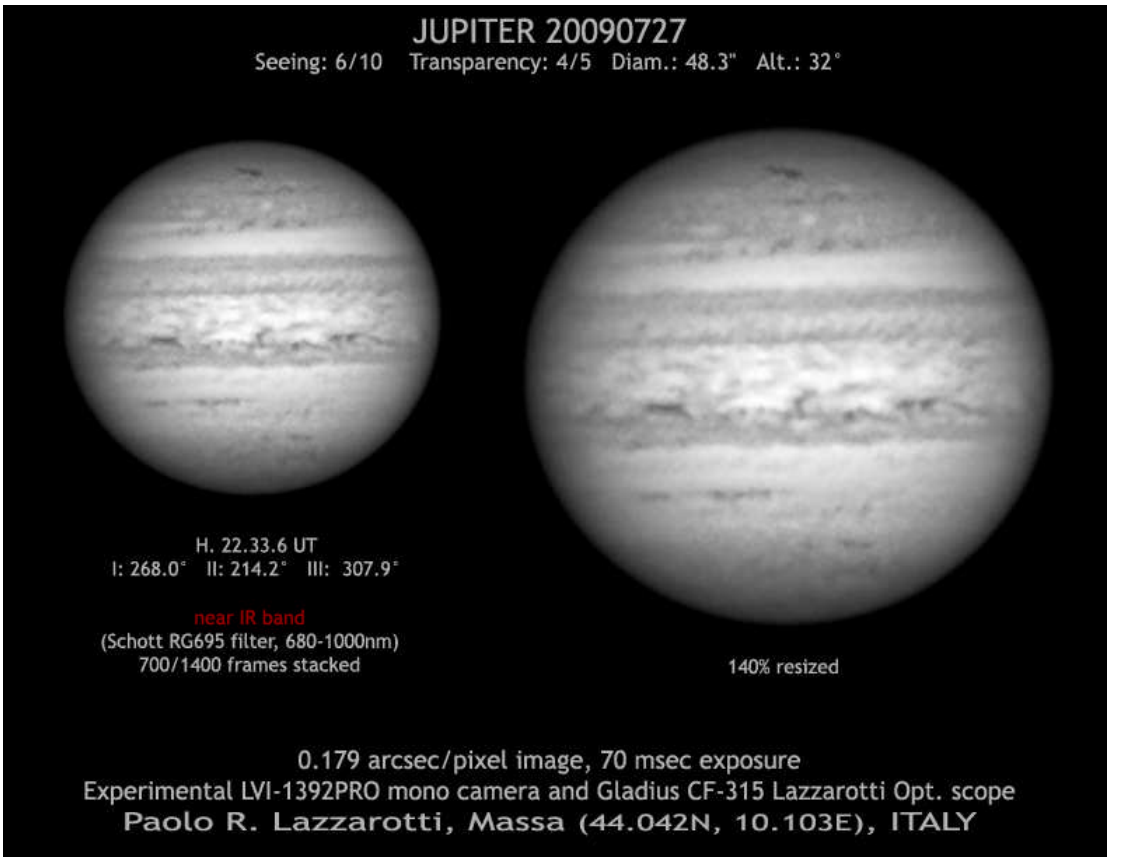

July 29 2009

by Paolo Lazzarotti (Italy)

Image of Jupiter, now showing the impact spot slowly approaching to the GRS.

Shape of the impact site looks like a ">".

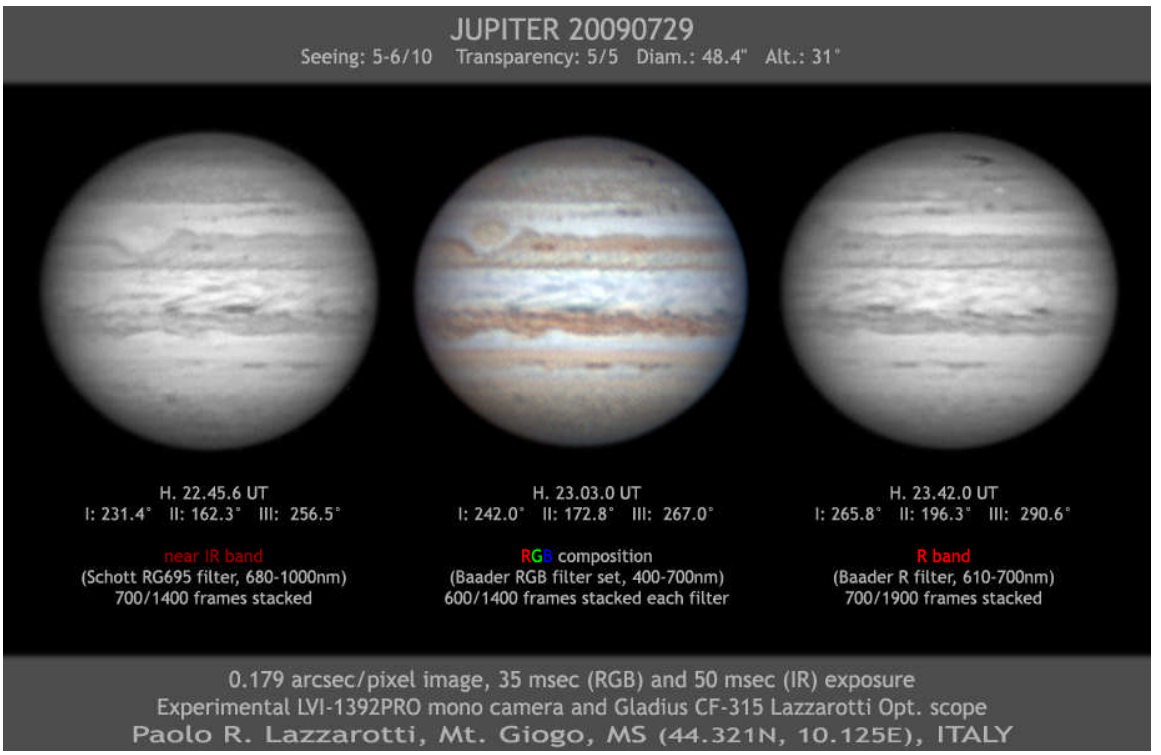

July 30 2009

by Raffaello Lena (Italy)

Impact site is expanding with some subtle features: short segment and shape looks like a ">".

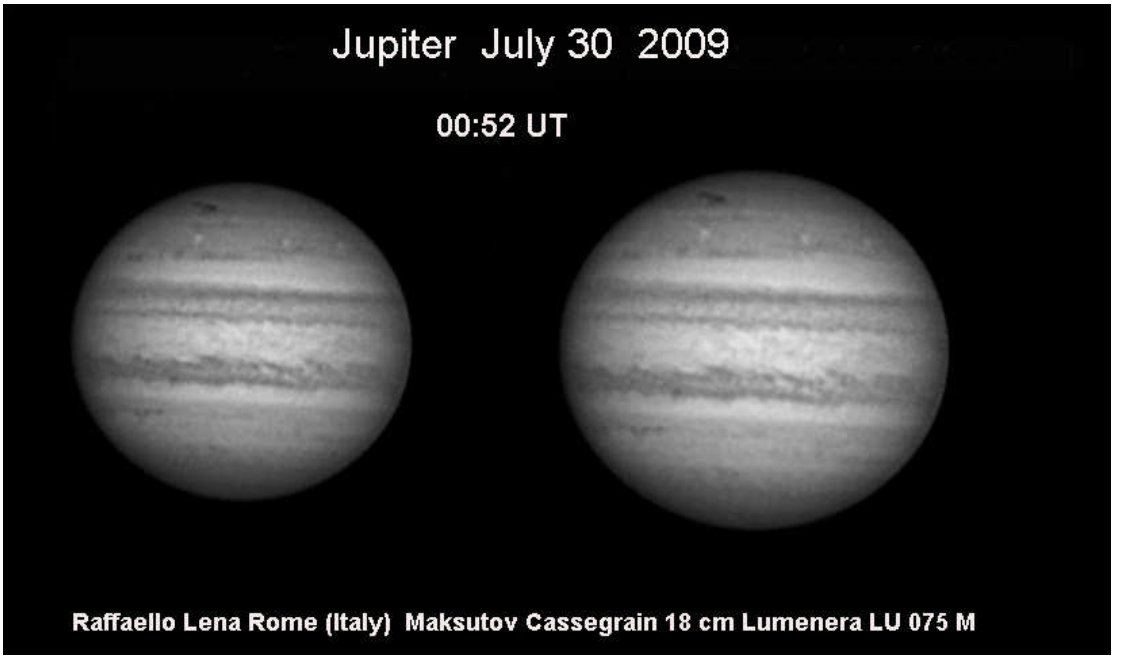
Jupiter July 30 2009
00:52 UT
Raffaello Lena Rome (Italy) Maksutov Cassegrain 18 cm Lumenera LU 075 M

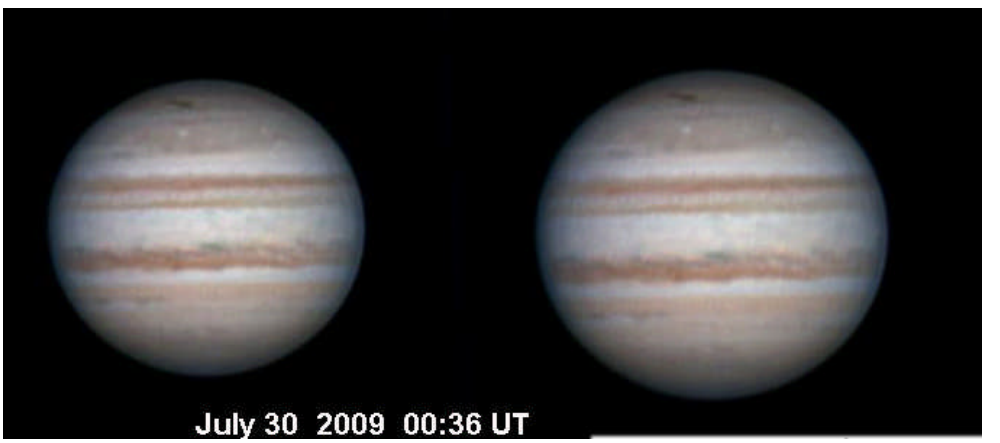
July 30 2009 00:36 UT

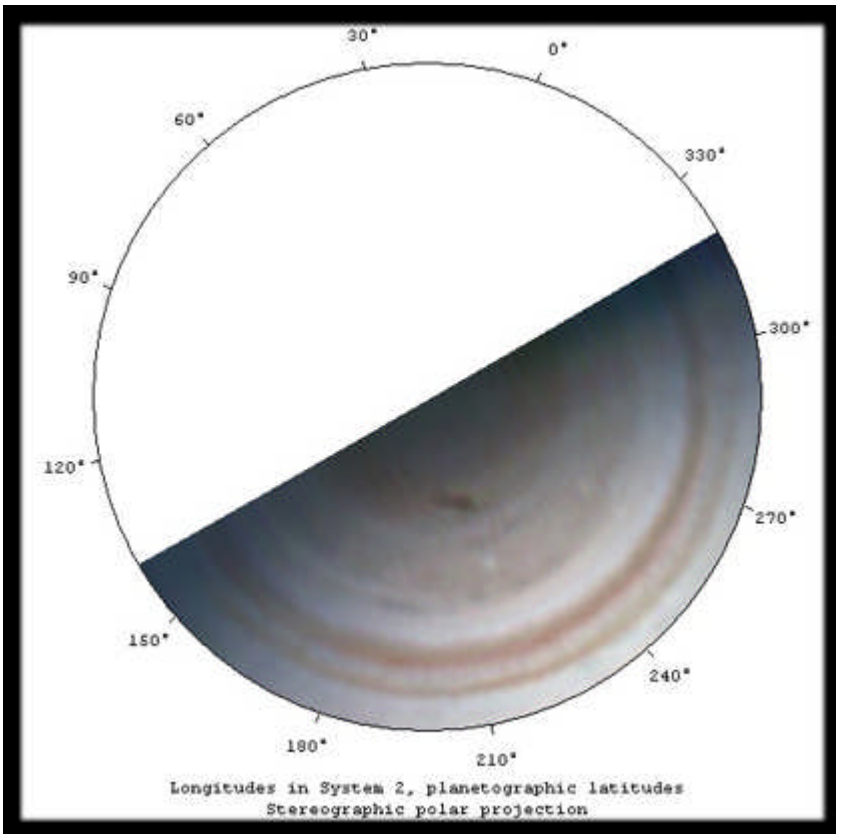

August 1 2009

by Paolo Lazzarotti (Italy)

On August 1st I imaged one among my best ever night on Jupiter. Visually, the impact scar was still obvious (!) as a dark segment parallel to the SPC. The same happened in the visual band (RGB) where the scar is still very prominent respect to the IR, but you can see here a defragmentation into three parts probably due to the interaction with a local oval.

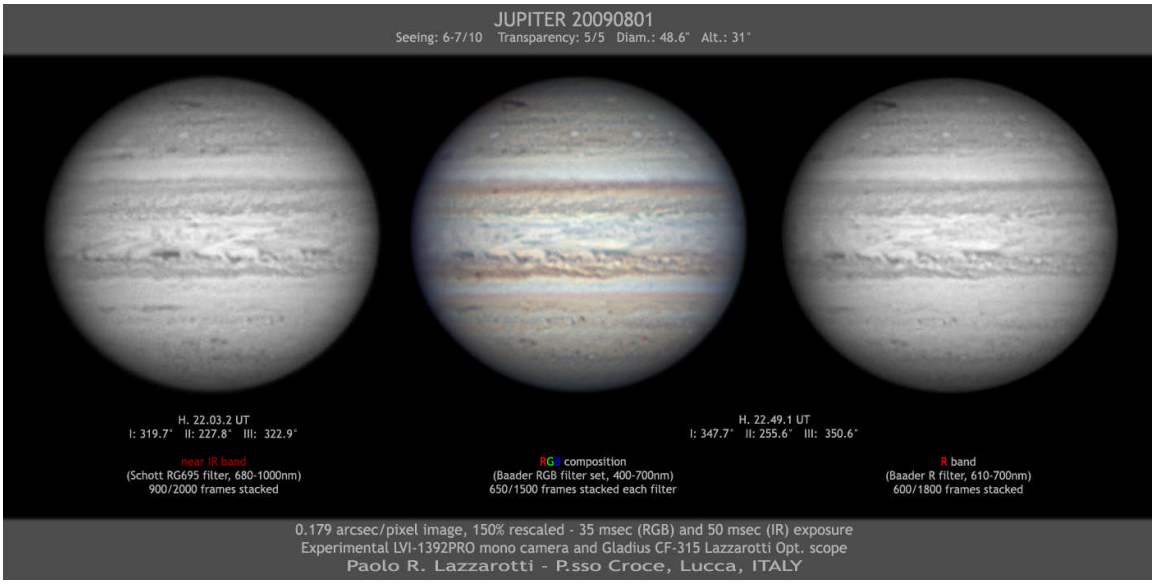

by Raffaello Lena (Italy)

Evolution of the impact scar is present definitively. Before it was like " >". Now the size is assuming, for the expansion of material, a sort of "reversed delta" including an oval. This oval could also be a transient hole between the independently drifting dark streaks.

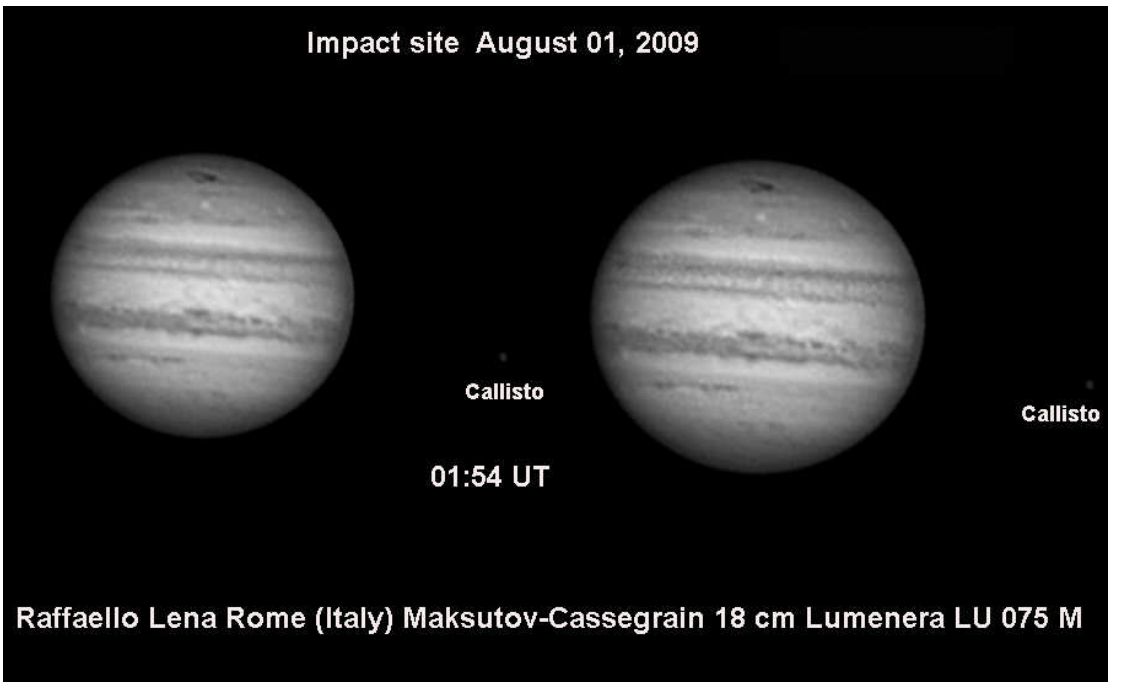

August 3 2009

by George Tarsoudis (Greece)

Fragmentation in four dark spots (DS) from images taken on August 3 2009.

I have included a polar view of the impact area.

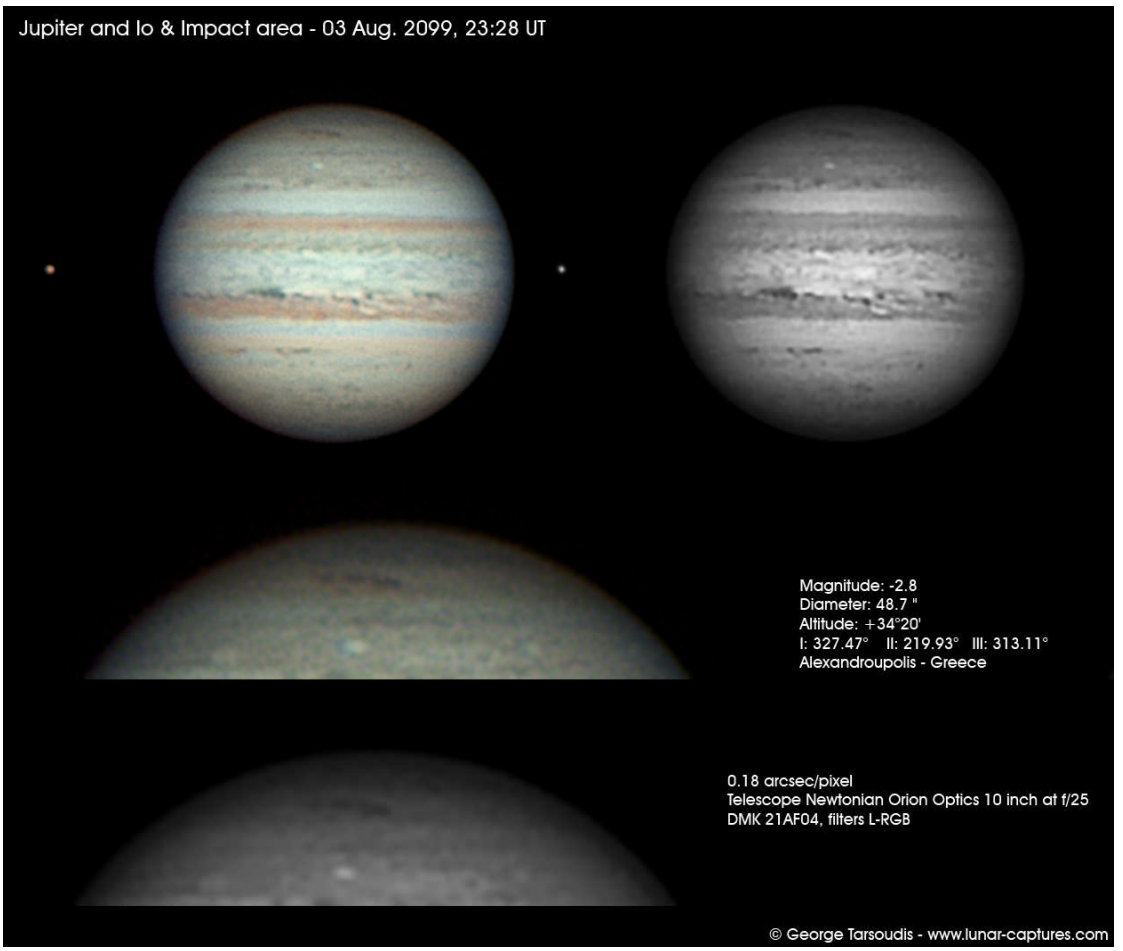

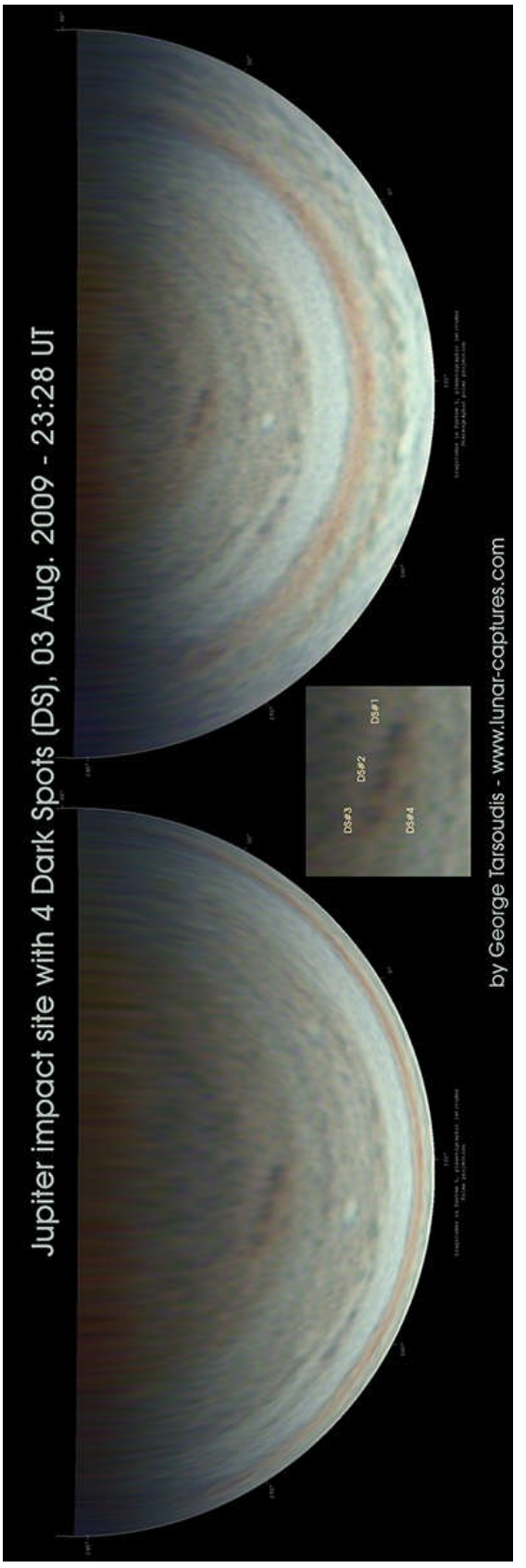
Jupiter impact site with 4 Dark Spots (DS), 03 Aug. 2009 - 23:28 UT
DS#1
DS#2
DS#3
DS#4
by George Tarsoudis - www.lunar-captures.com

August 15 2009

by Raffaello Lena (Italy)

The impact site has another evolution with at least three fragments. They are detectable in the images taken on August 15 2009.

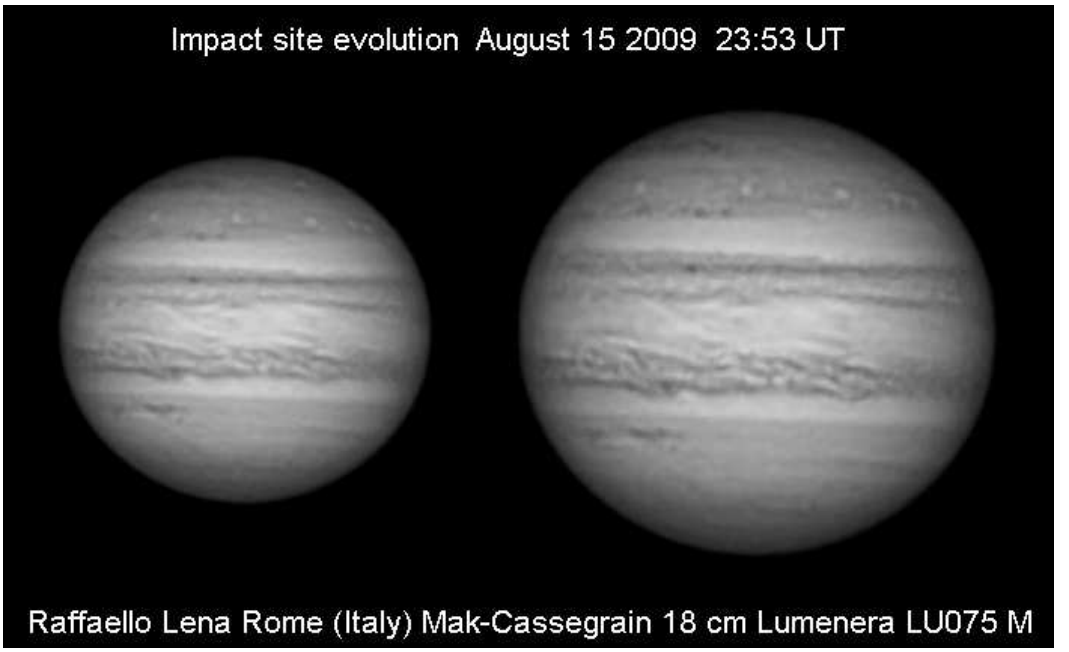

APPENDIX 1

Hubble's new Wide Field Camera 3 was rushed into service to take this closeup view of Jupiter's impact mark on July 23, 2009. *NASA / ESA / Heidi Hammel / Jupiter Impact Team*

This mid-infrared composite image was obtained with the Gemini North telescope on Mauna Kea, Hawai, on 22 July at ~13:30 UT with the MICHELLE mid-infrared spectrograph/imager. The impact site is the bright yellow spot at the center bottom of Jupiter's disk. The image was constructed from two images: one at 8.7 micron (blue) and one at 9.7 micron (yellow). The excellent quality of the Gemini images reveals that the morphology of this new impact bears a striking resemblance to that of the larger impact sites seen after the comet Shoemaker-Levy 9 crashed into Jupiter in 1994.

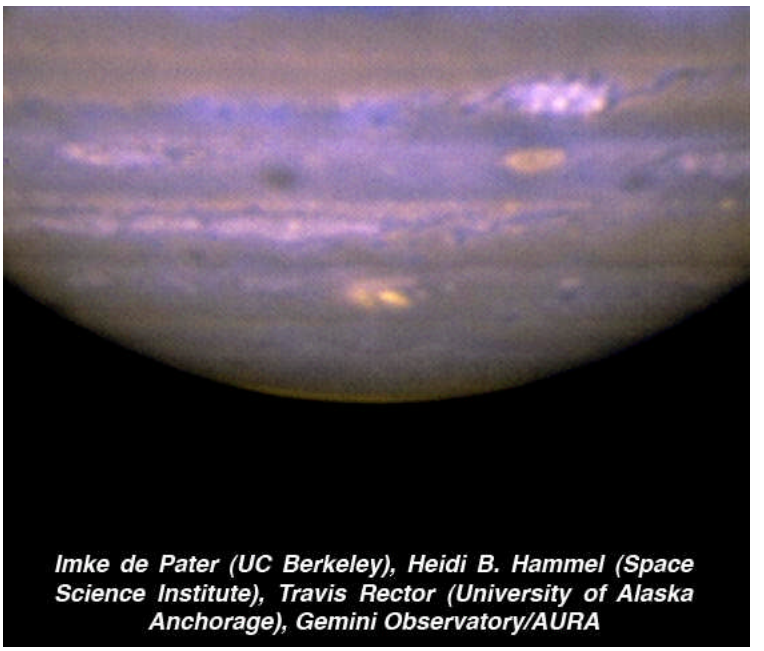

The scar from the impact appeared July 19 in Jupiter's southern hemisphere, and has grown to a size greater than the extent of the Pacific Ocean. This infrared image taken with Keck II on July 20 shows the new feature observed on Jupiter and its relative size compared to Earth. (Paul Kalas ,UCB; Michael Fitzgerald, LLNL/UCLA; Franck Marchis, SETI Institute/UCB; James Graham, UCB).

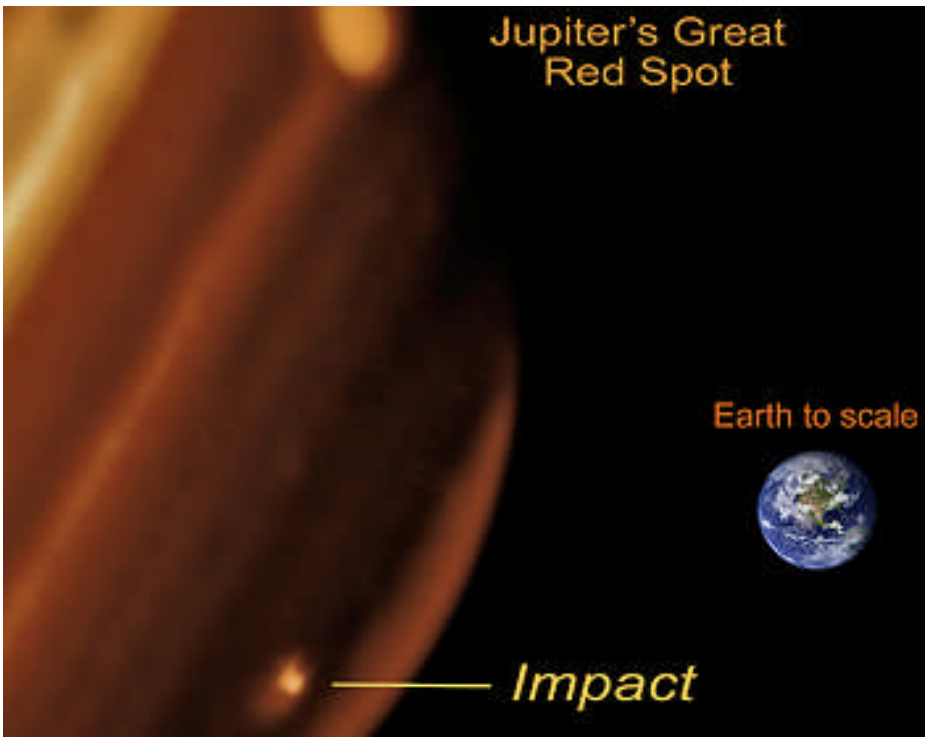

APPENDIX 2

Shoemaker-Levy 9's remains struck Jupiter in July 1994

After Comet Shoemaker-Levy 9's remains struck Jupiter in July 1994, the Hubble Space Telescope captured this double hit: a large multiring spot caused by the G fragment and a small dark spot from the D fragment.

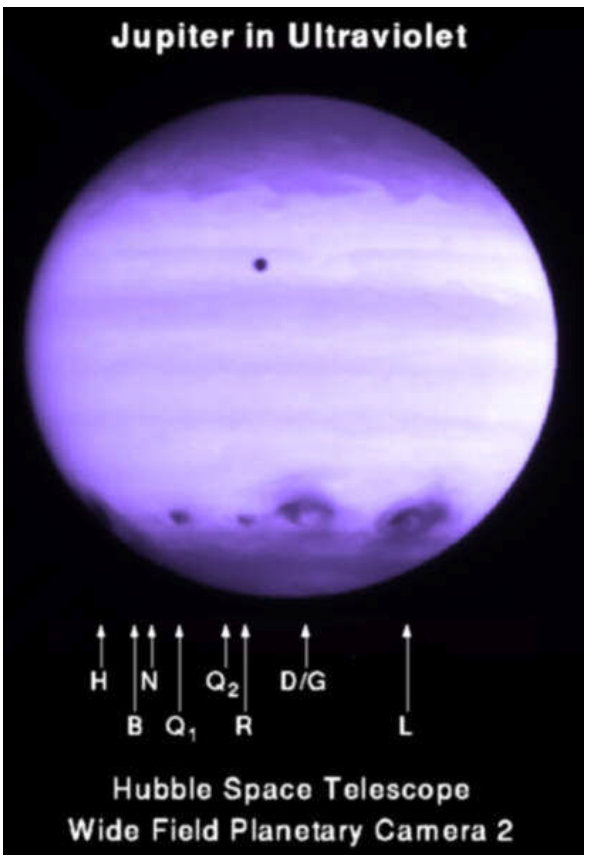

Image taken by Carmelo Zannelli on July 21 1994, using a chemical film and a 13 cm Newtonian telescope.

The resolution and contrast would illustrate advances in amateur imaging after 15 years.